RIP CURRENTS

A LABORATORY STUDY OF A RIP CURRENT IN THE PRESENCE OF A SUBMERGED REEF

Delft University of Technology

M.C.L. POORT
SEPTEMBER 2007
DELFT

RIP CURRENTS

A LABORATORY STUDY OF A RIP CURRENT IN THE PRESENCE OF A SUBMERGED REEF

PROF. DR. IR. M.J.F. STIVE

DR. IR. H.L. FONTIJN

DR. IR. A.J.H.M. RENIERS

DR. IR. W.J.S. UIJTTEWAAL

DR. IR. P.J. VISSER

IR. M. HENRIQUEZ

M.C.L. POORT

SEPTEMBER 2007

DELFT

VOOR MIJN LIEVE VADER DIE ALTIJD ALLES MAKEN KON

Acknowledgements

In this last stage of my studies I encountered many issues of life and found that health is the most important. I am grateful for the support and attention I received, sometimes totally unexpected.

Student counsellors gave support and motivation during the years. I would like to thank specifically Mr. Karsen for providing clearness and solutions in the maze of shifting study program regulations.

For this Master Thesis, a laboratory study of rip currents, I would like to acknowledge my graduation committee for their supervision and support during the whole research.

The committee consists of:

- Prof. Dr. Ir. M.J.F. Stive
- Dr. Ir. H.L. Fontijn
- Dr. Ir. A.J.H.M. Reniers
- Dr. Ir. W.J.S. Uijttewaal
- Dr. Ir. P.J. Visser
- Ir. M. Henriquez

Special thanks goes out to Ad for his angelic patience. Being always at his door (especially during MATLAB programming) eventually resulted in my own desk in his office.

Finally I would like to thank all the members of the support staff of the Fluid Mechanics Laboratory for their help and advice during the experiments.

Maaike Poort
Delft, September 2007

Table of Contents

LIST OF FIGURES

LIST OF TABLES

ABSTRACT

Detailed laboratory measurements of the wave and current field induced by bi-chromatic waves incident on an artificial surfing reef are presented. Strong wave focussing occurs on the surfing reef. Both PTV and in-situ measurements are reported that show the presence of a strong rip current flowing oblique off-shore.

Observed water level set-up and set-down indicate the locations of feeder currents, driving the rip current. Wave-current interaction between the incoming bi-chromatic waves and the outgoing rip-current are apparent in the measurements. The stochastic character of meandering of the rip current is shown by the variance of the low pass filtered time-averaged local velocities.

The vertical velocity distribution could not be determined reliably due to limitations in the test set-up and measurement devices. The dispersion relationship is utilized to connect the PTV surface measurement with the underlying velocity field obtained by in-situ measurements. The total dataset gives a detailed synoptic view of the wave-current field that can be used for model verification and validation.

1 INTRODUCTION

1.1 Rip currents in general

Rip currents are jet-like currents of water that typically extend from near the shoreline out past the line of breaking waves. Rip currents can be caused by several wave phenomena. These include offshore flow through channels in sandbars, natural variability of breaking-wave heights, and longshore current interaction with man-made structures like (submerged) reefs. Rip currents are a natural part of the dynamic nearshore circulation system. A portion of the longshore current enters into "feeder currents," which are the segments on the shore-side of a rip current. A rip current also has a neck across the breaker zone, and a mushrooming head, as illustrated in Figure 1-1. A rip current neck can be very narrow or more than 45 meters in width. The seaward extent of rip currents can vary from just beyond the line of breaking-waves to hundreds of meters offshore, extending up to a maximum of 2.5 times the surf zone width (Haller et al., 1999).

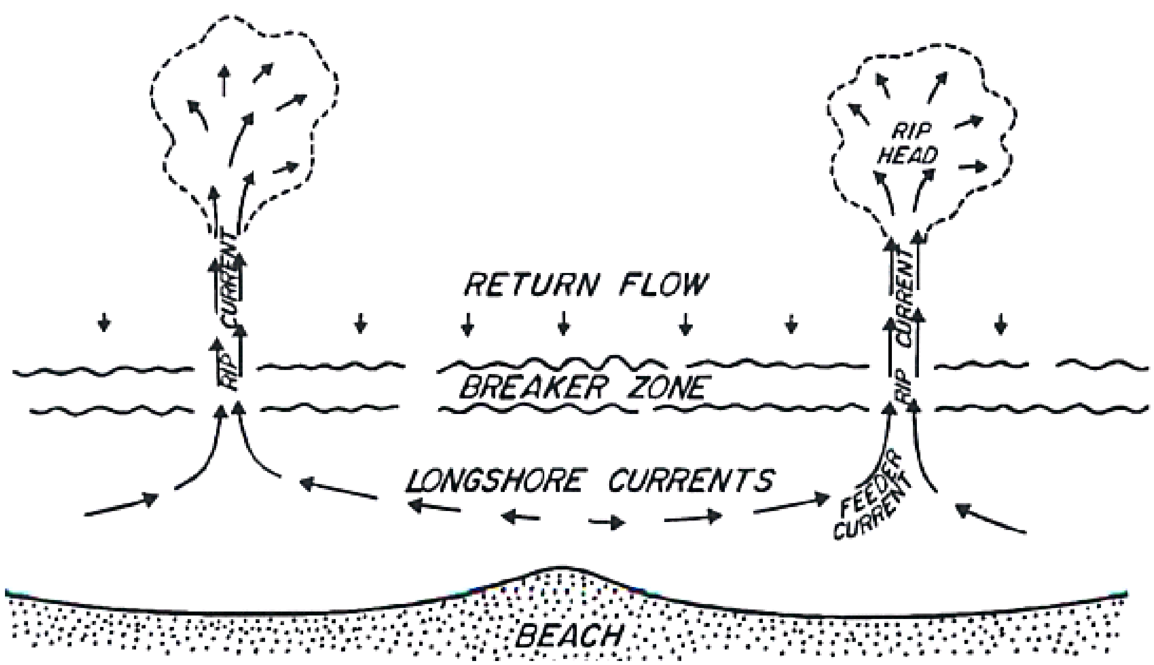

Figure 1-1: Sketch of a rip current (Komar 1976)

Rip currents are dangerous to swimmers and contribute to the erosion of the beach. It is important to be able to predict the development of rip currents. Measurements in the field are rare and expensive.

The pattern of behaviour of a rip current strongly depends on local bathymetry. Above all it is difficult to predict where a rip current will occur. There are already computer models which can predict how a rip current will behave. But in order to validate the model and to get more insight in the physical processes causing rip currents, there is need for measurements, both from the field and from scale models in laboratories (MacMahan et al., 2006).

In this report, the results of a laboratory study on the development of a rip-current are presented. Different from other laboratory studies is that in this case the rip current was not fixed by bathymetry, but could freely develop. Detailed in-situ measurements picture the velocity field of the rip-current. Also, the phenomenon whether offshore from the surf zone rip currents tend to be confined near the surface (Haas et al., 2002), or near the bottom (Drønen et al., 2002) has been investigated.

1.2 State of the art in related research

A recent overview of rip-current research is given by MacMahan, Thornton and Reniers (2006). For the purpose of this report, only a small portion of research into rip-current phenomena is presented. Three main aspects of rip current research are regarded; field observations, laboratory measurements and numerical models.

1.3 Field observations

In this section, a few field observations are presented briefly, since they are essential for understanding the complex character of rip currents. Early field observations (first half of the twentieth century) obtained rough estimations of rip current velocities, ranging from 0-1 m/s. Rip currents shape the sandy shoreline and may be important for transporting sediments offshore. Due to the effort and costs associated with field observations, only a few data collections on rip currents are available.

Using a sector-scanning Doppler sonar, Smith et al.(1995) performed field observations in the surf zone. The scanning Doppler acoustic technique provides information about the radial velocity (depth averaged). It does not provide information about the vertical structure of the velocity field.
Well-defined jets of water extending seaward from the surf zone, identified as rip currents, were observed. Outside the breaker region, 15 min. oscillations of the rip

current were observed. Fluid velocities were estimated from the Doppler shift of the sonar signal, approaching 0.7 m/s in some cases. Furthermore, observations suggest that rip currents could cause significant exchange between nearshore and offshore waters.

A large dataset was collected by MacMahan et al.(2005) in a 44 day field measurement at Monterey Bay. Rip-current kinematics and beach morphodynamics were obtained from instruments composed of co-located velocity and pressure sensors, acoustic Doppler current-profilers and rapid kinematic GPS bathymetric mappings. The morphology consisted of a low-tide terrace with incised quasi-periodic channels, representative of transverse bars. The mean wave direction was consistently near shore normal resulting in rip channel morphology, which evolved in response to the changing wave characteristics. Amongst others, it was observed that the flow field within the surf zone was depth-uniform, except for significant shear occurring near the surface due to Stokes drift.

MacMahan et al.(2006) report that most field observations of rip currents have been coupled to the underlying beach morphology. Rip-current morphology generally consists of a feeder channel that is parallel to the shoreline, which converges to a deeper rip channel that is oriented in an approximately shore-normal direction. Within the last decade, there has been an increasing number (less than ten) of field experiments involving rip currents, which lead to advances in understanding these systems.

1.4 Laboratory measurements

Laboratory measurements provide an environment where, for instance, bathymetry and wave conditions can be controlled, enabling to focus research and collect data in a less complicated way than with field observations. Related to current rip-current research questions, a few laboratory measurements related to aspects of vertical flow velocity distribution and repeatability of the rip current are cited in this section.

Vertical structure of the velocity distribution in the rip current

In research by Haas et al.(2002) into the vertical structure of rip currents, it was observed that rip currents are unstable and appear sporadically at any given location. Furthermore, it was found that the vertical profile of the rip current is depth-uniform inside the channel and depth-varying further offshore. Offshore from the channel the rip has much stronger velocities at the surface than near the bottom. Instantaneous profiles twist rapidly over depth farther offshore and are fairly uniform in the channel.

Additionally, Drønen et al.(2002) performed a laboratory study of the flow over a bar with a single rip channel. One side wall is located in the rip current. This prohibits the rip current to fluctuate in longshore direction. It was stated that 3D-effects play an important role and that a depth-integrated viewpoint may not always be sufficient for predicting the flow in the near-bed region. The offshore-directed rip flow has a tendency to be stronger closer to the bed (contrary to Haas et al., 2002), but as a first approximation the profile is relatively uniform especially around the location where the current is maximum. On the bar crest and around the point where the bar, the trough and the rip channel meet, the orientation of the flow is seen to be very dependent on its vertical position, suggesting that three-dimensional effects like helical motion and/or undertow are important for the dynamics.

Repeatability of the rip current

Haller et al.(2001) observed in laboratory experiments (barred beach) with monochromatic waves normally incident to the shore that rip currents contain energetic low-frequency oscillations in the presence of steady wave forcing. A limited analysis of cross-spectra showed that the rip oscillations are offshore-propagating wavelike motions. The presence of multiple spectral peaks in some tests suggests the presence of multiple unstable modes. Performed model calculations show highly unstable behaviour of rip currents.

Influence of the rip current on the wave-pattern

Haller et al.(2002) presented wave and current measurements from a set of laboratory experiments performed on a fixed barred beach with periodically spaced rip channels using a range of incident wave conditions (monochromatic waves). The presence of gaps dominated the nearshore circulation system for the incident wave conditions considered. The rip current was shown to influence the wave breaking and the wave induced set-up in the rip channel. The strong rip current can weaken the radiation-stress gradient opposing the feeder currents and lead to even stronger feeder currents and rips.

Correlation between PTV-and in-situ measurements

Kennedy et al.(2004) investigated the circulation in a laboratory rip-current system using large numbers of Lagrangian drifters, with supplementary current meters and water level measurements. Drifter and current meter measurements were compared in the rip channel and Stokes drift was found to be a significant component of drifter velocities in this region. Three-dimensional effects were also apparent as the rip travels into deeper water but proved to be difficult to quantify.

1.5 Numerical models

Numerical models prove to be a powerful tool in predicting rip-current behaviour and emphasising specific processes in the rip. In combination with field observations and laboratory measurements, models can be verified and validated. Related to current research questions, a selection of published work is summarized in this section.

Vertical structure of the velocity distribution in the rip current

Zou et al.(2003) made theoretical predictions of the vertical structure of the wave motion over a sloping seabed to compare this to field observations close to the bed in the nearshore zone. Field measurements of near-bed velocity profiles were obtained using a coherent Doppler-profiler. The surface elevation was measured by a co-located, upward-looking acoustic sounder. It was concluded that linear theory appears to adequately describe the transfer function between the surface elevation and the near-bed velocities, not only at peak frequencies but also at their harmonics. Both theory and observations show that skewness and asymmetry of the vertical velocity are subject to significant bottom slope effects, whereas those of horizontal velocity are not.

Repeatability of the rip current

Describing rip-current systems with the quasi-three-dimensional model SHORECIRC and comparing model predictions to laboratory measurements, Haas et al.(2003) found reasonable agreement. From their analysis, it was concluded that higher bottom stress leads to more stable flow where the rip current meanders less and fewer eddies are generated. Three dimensionality was found to be a significant effect on the overall circulation patterns.

Influence of the rip current on the wave pattern

A simplified model describing rip-current behaviour in terms of main-flow parameters such as the current intensity and mean water levels, geometrical parameters and wave characteristics was constructed by Bellotti (2004). The proposed model was validated against laboratory experiments and suggested to be applicable in the preliminary design stages of submerged breakwaters and of potential value in evaluations of hydrodynamics on barred beaches.

Park et al.(2001) describe an adaptive quadtree-based wave-current interaction model evaluating wave-induced currents in the surf zone. The model accounts for wave breaking, shoaling, refraction, diffraction, wave-current interaction, set-up and set-down, turbulent diffusion, bottom frictional effects and movement of the land-water interface at the shoreline. The model is verified using nearshore circulation at an idealised half-sinusoidal beach and compared with experimental laboratory data. At steady-state, the numerically simulated wave-height field and nearshore circulation patterns were in close agreement with the experimental data. It was concluded that, although approximations by the developed model have limited application for certain conditions compared to other models, the adaptive regridding strategy of the model could be a useful approach in describing the complex nearshore flow-physics.

Rip current pulsations are generally associated with wave groups at the infragravity band. Reniers et al.(2006) report on a comparative study on a non-linear shallow-water wave model, operating on the time-scale of wave groups, and rip channel beach measurements of infragravity motions. Field data were obtained in the RIPEX field experiments at Monterey Bay. Overall performance of the present model approach compared with measurements at both the cross-shore and alongshore array are satisfactory, typically explaining up to 80% of the infragravity wave-height and 70% of the infragravity velocities present.

Chen et al.(1999) extended an existing numerical model, based on non-linear Boussinesq equations, to include wave breaking and moving shorelines for simulation of wave transformation and wave-induced nearshore circulation. The current field was obtained by time averaging of the computed fluid particle velocity over two wave periods, while the vorticity field is computed directly from the instantaneous fluid particle velocities. Fairly good agreement is observed between laboratory measurements (Haller et al., 1997) and the computed longshore and cross-shore currents and mean water level. In agreement with the physical experiment and theoretical predictions, the numerical results indicate that the rip current is unstable. The rip instability results in an oscillating rip current and the alongshore movement of vortices associated with the rip current.

2 Research Description

2.1 Introduction

Rip currents are seaward directed flows and can appear near submerged break-waters. Public interest in rip currents is due to beach safety issues and beach erosion. To increase the understanding of rip systems, detailed quantitative measurements are necessary (MacMahan et al., 2006).

This research is focused on the phenomena related to the development of rip currents in the presence of a submerged reef. Series of extensive measurements have been performed in the Fluid Mechanics Laboratory of Delft University of Technology (DUT), Faculty of Civil Engineering and Geosciences.

2.2 Problem definition

In literature few quantitative field and laboratory measurements have been reported. To validate computer-based rip-current models a lack of measurements is observed. Therefore experiments are necessary to provide data for testing these numerical models.

2.3 Objective

The primary objective of this research is to analyse wave and rip-current characteristics in the presence of a submerged reef. Furthermore, the correlation between velocities at the bottom and the water surface is studied. Here fore comprehensive measurements in a laboratory wave-basin were performed. An additional objective of this study is to provide a suitable dataset to validate a computer-based rip-current model.

2.4 Research issues

From the objective, the research issues can be derived with respect to:

- The influence of the rip current on the wave pattern;
- Wave breaking in the presence and absence of a reef;
- Repeatability of the rip current;
- Vertical structure of the velocity distribution in the rip current;
- Correlation between PTV- and in-situ measurements.

2.5 Parameter space and boundary conditions

2.5.1 General

This research is performed at the Fluid Mechanics Laboratory wave-basin.

The wave basin can be characterized by the following parameters, presented in Table 2-1. Figure 2-2 gives a plan view of the wave basin.

Table 2-1: Characteristics of the DUT-laboratory wave basin

parameter	**range**
Water depth (h)	0- 0.40 m
Wave frequency (f)	0.1 – 2 Hz (T: 0.5 – 10 s)
Wave height (H)	maximum 0.10 m
Length of slope	12 m
Steepness of slope	1:20 [-]
Stroke wave-maker	maximum 0.26 m
Waves that can be generated	1st order/2nd order/ monochromatic/ polychromatic/ regular/ irregular
'Reefless-side'	the side where there is no reef
'Reef-side'	the side with the reef

Figure 2-1: Impression of the wave basin

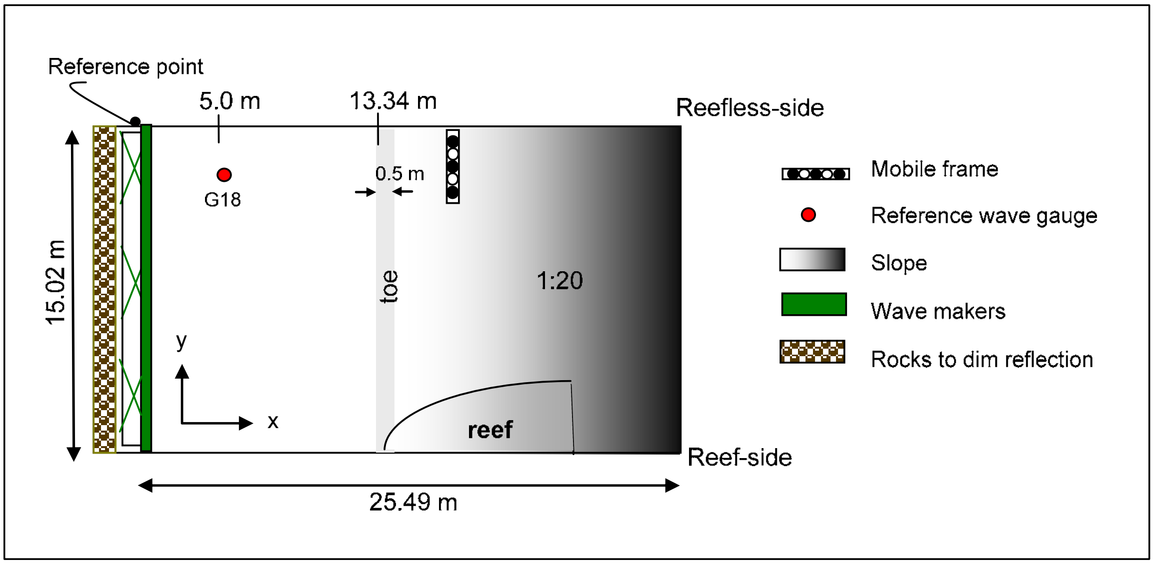

Figure 2-2: Plan view of the basin

Further limitations to the test set-up:

- Behind the reef there is a restricted possibility for measurements, due to the limited water level;
- The applied EMF's should have an immersion depth > 0.01 m and a bottom clearness > 2 [cm]. Measurements in a water depth < 0.03 m are unreliable;
- The relatively short distance between wave maker and toe of the slope,~ 13.5m, can cause interference between the generated wave field and the reflected wave field.

2.5.2 Rip-current characteristics

- The rip current has to show up and must be clearly visible;
- The offshore-directed current influences the incoming wave pattern and the feeder of the rip current;
- Spurious circulation patterns in the wave basin should not dominate over the measured rip-current velocities.

3 LINEAR WAVE THEORY

This section describes shallow-water wave dynamics and associated hydrodynamic processes of wave set-up and set-down and nearshore currents, according to Stokes linear wave theory.

3.1 Shoaling and refraction

The wave height in the surf zone is influenced by both shoaling and refraction which relate as follows in water with straight and parallel bottom contours:

$$H_{\mathbf{1}} = H_{\mathbf{0}} K_s K_r$$

where $[..]_{\mathbf{1},\mathbf{0}}$ denote conditions in limited water depth (*1*) or deep water (*0*), H is the wave height [m], K_s is the shoaling coefficient [-] and K_r is the refraction coefficient [-]

Shoaling effects can be described by the following. Due to decreasing water depth or counter currents, the wave propagation speed reduces. Because of energy conservation, the wave height will change and the following energy balance applies:

$$\frac{\tfrac{1}{8}\rho g H_{\mathbf{1}}^{\mathbf{2}}}{\omega_{\mathbf{1}}}(c_{g\mathbf{1}} + U_{\mathbf{1}}) = \frac{\tfrac{1}{8}\rho g H_{\mathbf{0}}^{\mathbf{2}}}{\omega_{\mathbf{0}}}(c_{g\mathbf{0}} + U_{\mathbf{0}})$$

where ρ is the mass density of water [kg/m^3], g is the gravitational acceleration [m/s^2], ω is the radial frequency $(= \mathbf{2}\pi / T)$ [s^{-1}], c_g is the wave group velocity [m/s] and U is the current speed [m/s]

Shoaling is determined by the ratio between the wave group velocities in deep water and shallow water:

$$\frac{H_{\mathbf{1}}}{H_{\mathbf{0}}} = \sqrt{\frac{\omega_{\mathbf{1}}}{\omega_{\mathbf{0}}} \frac{c_{g\mathbf{0}} + U_{\mathbf{0}}}{c_{g\mathbf{1}} + U_{\mathbf{1}}}} = K_s$$

where c_g is determined by:

$$c_g = n\frac{\omega}{k}$$

$$n = \tfrac{1}{2}\left(1 + \frac{2kh}{\sinh(2kh)}\right)$$

where k is the wave number ($= 2\pi / L = 2\pi / cT$) [m^{-1}], L is the wavelength [m], T is the wave period [s] and c is the phase velocity or wave celerity [m/s].

$\omega' = \omega + kU_{//} =$ constant (conservation of waves)

ω' = absolute frequency

Refraction of waves is the change in wave propagation direction due to variations in phase speed along the wave crest as a result of non-uniform depths (bottom refraction) or currents (current refraction). Change in propagation direction results in a redistribution of wave energy, focusing in areas where wave rays converge and defocusing where wave rays diverge.

The refraction coefficient in absence of a current can be described by:

$$K_r = \sqrt{\frac{b_0}{b_1}} = \sqrt{\frac{\cos\theta_0}{\cos\theta_1}}$$

Where b is the distance between two wave rays and θ is the angle between wave crests and depth contour lines.

The mechanism of refraction due to bottom morphology is illustrated in Figure 3-1.

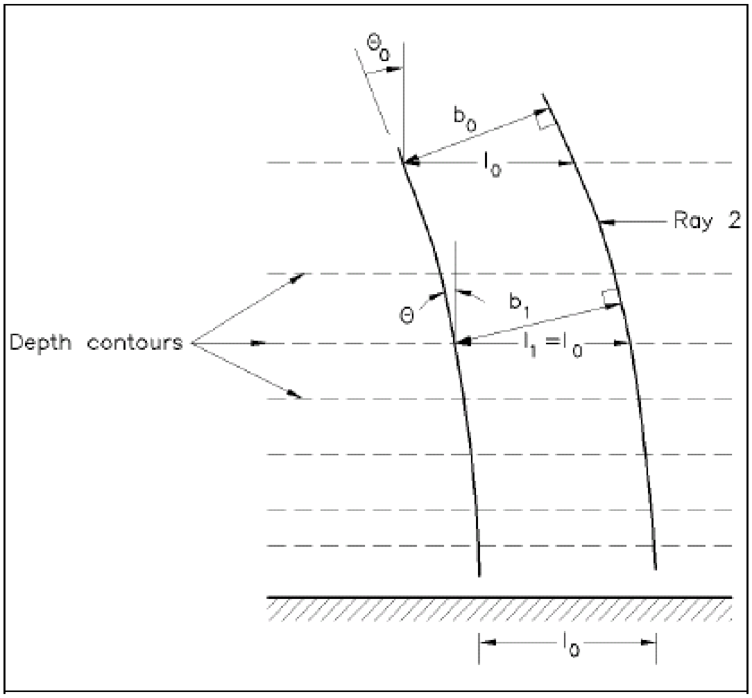

Figure 3-1: Wave-height variation along a wave ray, l_0=distance between two wave rays. (figure courtesy of Coastal Engineering Manual EM 1110-2-1100)

Refraction in presence of an alongshore uniform current can be described by:

$$\frac{\sin\theta_0}{\sin\theta} = \frac{c_0 + U_0}{c + U}$$

(Snel's law)

With a counter current U, the wave celerity decreases resulting in bending wave rays into the current. The mechanism of current refraction is illustrated in Figure 3-2. From the relationship for current refraction it can be derived that, for instance in the situation of a gradient in counter current, waves will converge (Figure 3-2).

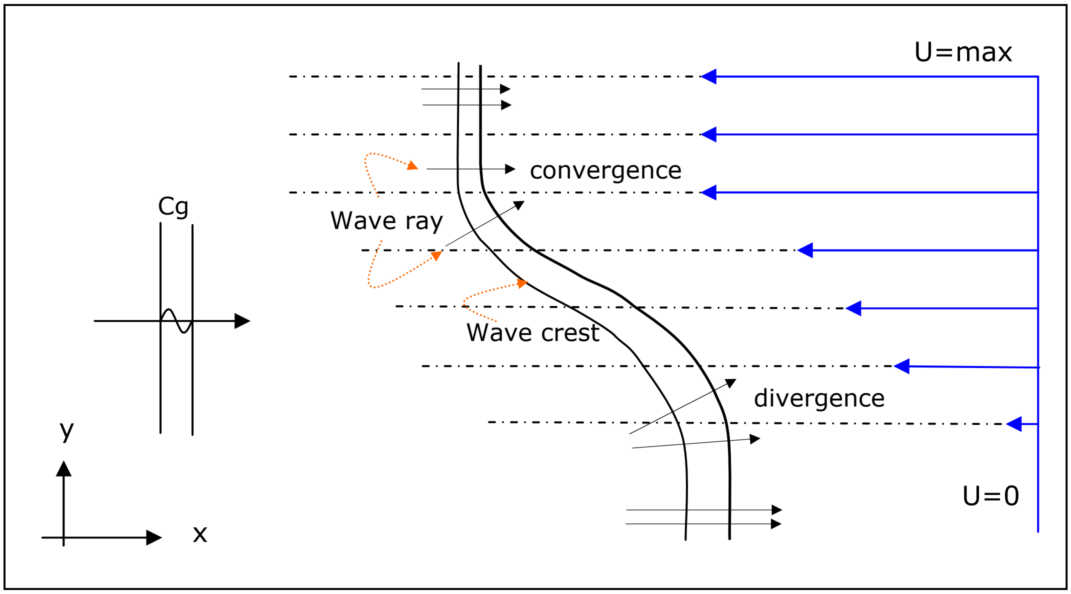

Figure 3-2: Top view of refraction of waves due to varying velocities (U). blue arrows denote velocity-magnitude and direction. The wave direction is indicated by black arrows, wave crests are indicated by black solid lines

3.2 Wave breaking

When the wave reaches a limiting steepness, the wave breaks. The manner in which a wave breaks against a shore is determined by the steepness of the incident wave, the water depth and also the gradient of the shore. The breaker type (Battjes, 1974) is correlated to the dimensionless Iribarren number of surf-similarity parameter ξ.

$$\xi = \frac{\tan\alpha}{\sqrt{H_b / L_{\mathbf{0}}}}$$

where α is the slope angle [-], H_b is the waveheight at breakpoint [m] and $L_{\mathbf{0}}$ is the deep water wave length [m]

The breaker type can be classified into spilling, plunging, collapsing and surging.

Spilling breakers tend to characterise shores with low-angled gradient, regardless of wave steepness, where water from the wave crest spills or cascades down the wave front producing lots of foam.

Plunging breakers occur on steeper beaches and are steep fronted waves that tend to curl over and crash down on the shore, also producing lots of foam.

Collapsing breakers are similar to plunging breakers, but instead of the crest curling over, it collapses.

Surging breakers are low waves from which the crests remain relatively unbroken as the waves slide up the steep beach.

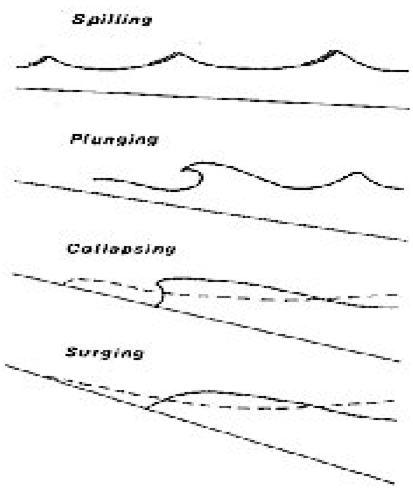

Spilling: $\xi<0.5$

Plunging: $0.5\leq\xi\leq3$

Collapsing: $2.5\leq\xi\leq3$

Surging: $3\leq\xi\leq5$

Figure 3-3: Schematic representation of wave breaker types

3.3 Set-down and set-up

Longshore currents can theoretically be described through consideration of the concept of radiation stress. Radiation stress both raises (*set-up*) and lowers *(set-down)* the mean water level across shore in the nearshore region.

If the x-axis is placed in the direction of wave advance and the y-axis parallel to the wave crests, then there are two components to the radiation stress. The radiation stress in the direction of the waves is given by:

$$S_{xx} = E\left(\frac{2kh}{\sinh(2kh)} + \tfrac{1}{2}\right) = E\left(2n - \tfrac{1}{2}\right)$$

where the wave energy E is given by: $E = \tfrac{1}{8}\rho g H^2$ and $n = \tfrac{1}{2}\left(1 + \frac{2kh}{\sinh(2kh)}\right)$

The radiation stress perpendicular to the wave propagation direction is given by:

$$S_{yy} = E\left(\frac{kh}{\sinh(2kh)}\right)$$

The onshore momentum flux must be balanced by an opposing force, which is manifested as a water slope, so that the pressure gradient of the sloping water surface balances the change (spatial gradient) in the incoming momentum:

$$\frac{dS_{xx}}{dx} + \rho g(h+\eta)\frac{d\eta}{dx} = 0$$

where h is the still-water depth and η_s is the mean water surface elevation with respect to still-water level (SWL). η_s is known as the set-up or set-down due to the waves. α is the slope angle.

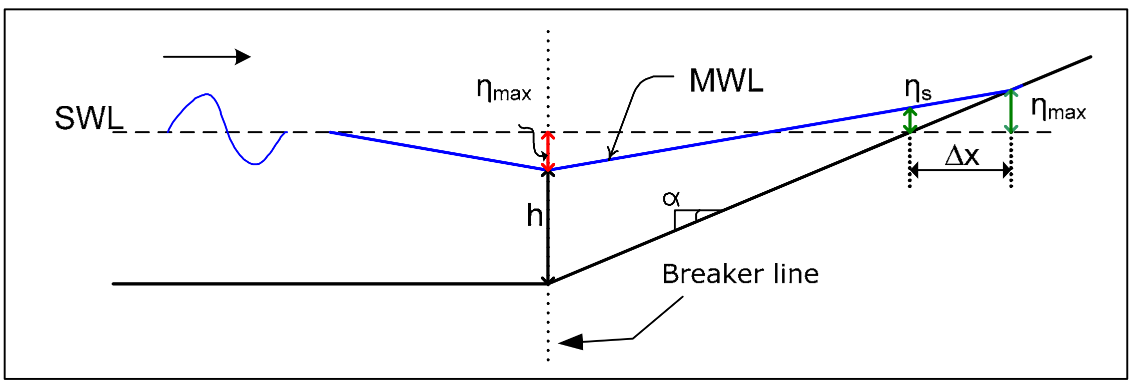

Figure 3-4: Definition sketch for wave set-up

3.4 Stokes

In the surf zone the waves cause an onshore directed flow due to two mechanisms, the wave drift and the surface rollers carrying water shore wards (Svendsen, 1984)

Wave drift, or Stokes drift, is caused by the fact that the fluid particles do not describe exactly closed orbital trajectories in case of small-amplitude (sinusoidal) surface waves propagating in perfect non-viscous (irrotational) oscillatory flow (Figure 3-5 and Figure 3-6) (Phillips, 1977; Van Rijn, 1990).

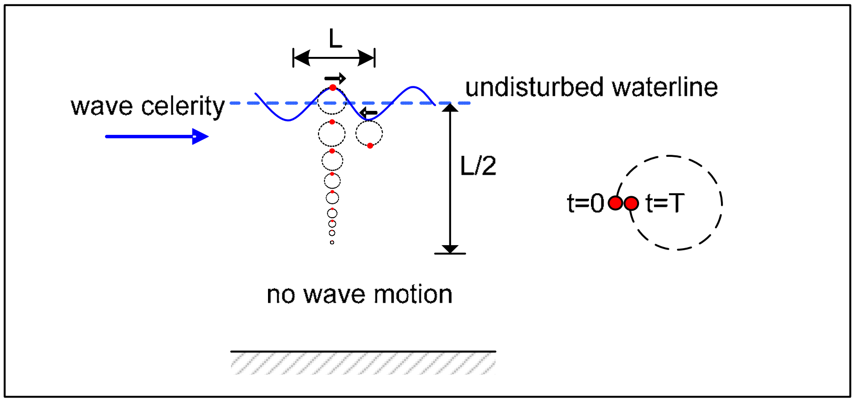

Figure 3-5: Orbital motion in deep water (T= wave period= $2\pi/\omega$ **)**

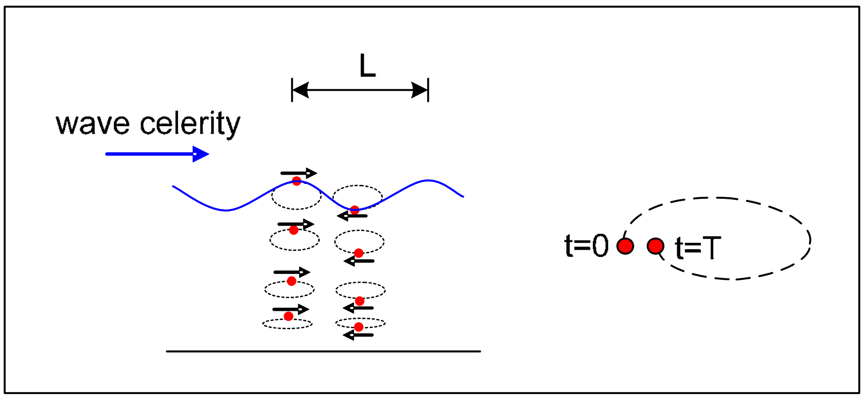

Figure 3-6: Orbital motion in shallow water (T= wave period= $2\pi/\omega$ **)**

In a non-closed particle orbit, a particle at the top of an orbit beneath a wave crest moves faster in the forward direction than it does in the backward direction at the bottom of the orbit beneath a wave trough.

The increase of the horizontal orbital velocity with height above the bed, results in a particle velocity in the direction of the wave propagation (Stokes drift). By definition the lagrangian Stokes drift cannot be detected by taking measurements at a fixed point (Phillips, 1977; Van Rijn, 1990).

In a two-dimensional situation, the shore-normal discharge is zero. Therefore the shoreward discharge caused by the waves must be compensated by a current in the offshore direction (Dyhr-Nielsen, 1970).

The generation of a positive mass flux (in the wave direction) near the surface and a negative flux (against wave direction) near the bottom requires the presence of a horizontal pressure gradient caused by set-up by the free surface towards the coast.

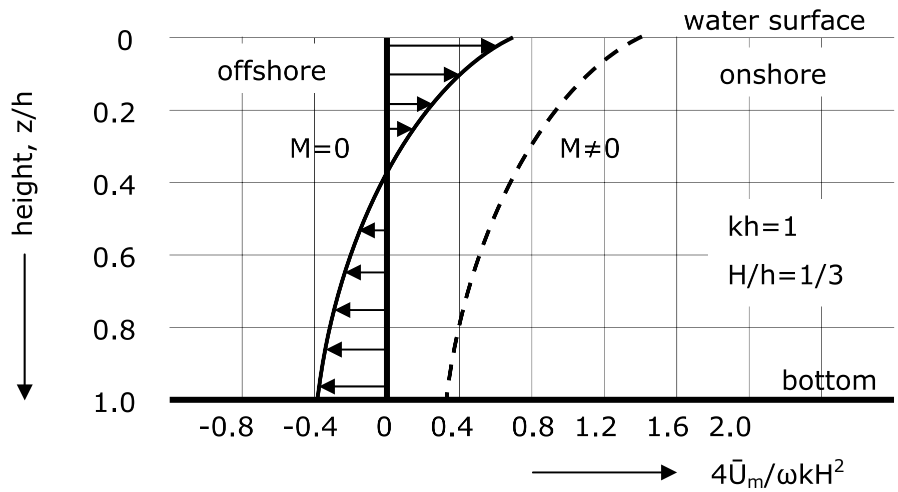

Figure 3-7: Stokes drift velocity profiles

While the shoreward discharge lies near the mean water surface (rollers and Eulerian drift), the return current has its maximum near the bed. This circulating current with its offshore directed flow near the bed, is called the undertow.

The undertow is limited to the surf zone, partly because outside the surf zone no surface rollers transport water towards the coast, and partly because the energy dissipation occurring mainly in the near-bed wave boundary layer is weak and does not cause shear stresses outside the wave boundary layer.

4 EXPERIMENTAL SET-UP

4.1 Introduction

The experimental set-up is designed to provide data to address the research questions. First, the research questions are described and related to measurements. In section 4.4, the applied instruments are described. Sections 4.5 and 4.6 present details with respect to the in-situ and PTV measurements.

The influence of the rip current on the wave pattern

To be able to analyze the influence of a rip current on a wave field, first an image of the undisturbed wave-breaking-field behaviour is needed. How does a wave break on a slope without a rip current present. Therefore measurements are taken where the influence of the rip current is minor, at the reefless side. Another point of attention is the presence of spurious circulation patterns in the wave basin. This in order to be certain that the measured velocities are caused by the rip current and not, for instance, by circulation patterns.

Wave breaking in the presence and absence of a reef

How does a wave break on a normal slope and how does it break in the presence of the reef. Measurements in the breaker area are performed at both sides of the basin to assess the differences.

Repeatability of the rip current

Is there a repeatable pattern in the meandering of the rip current? The assumption is, that close to the reef the path of the rip current is restricted and farther away the meandering increases and is less predictable.

Vertical structure of the velocity distribution in the rip current

What is the vertical structure of the velocity distribution in the rip current? The assumption is, that close to the reef the vertical distribution is depth-uniform and farther offshore the highest velocities are close to the surface (Haas et al., 2002). So velocity measurements at different distances from the bottom, following the flow of the rip current are performed.

Correlation between PTV-and in-situ measurements

What is the correlation between velocity at the surface and velocity at the bottom? In general, field data monitoring the surface is more available than in-situ measurements at the bottom. If a (strong) correlation between surface velocity and bottom velocity can be established, labour-intensive in-situ measurements can be replaced by monitoring the surface velocity with remote-sensing techniques such as video and radar.

4.2 Characteristics of the wave basin

The experiments were performed in the Fluid-Mechanics-Laboratory wave basin. Figure 4-1 presents an overview of the basin including reef, slope and wave maker.

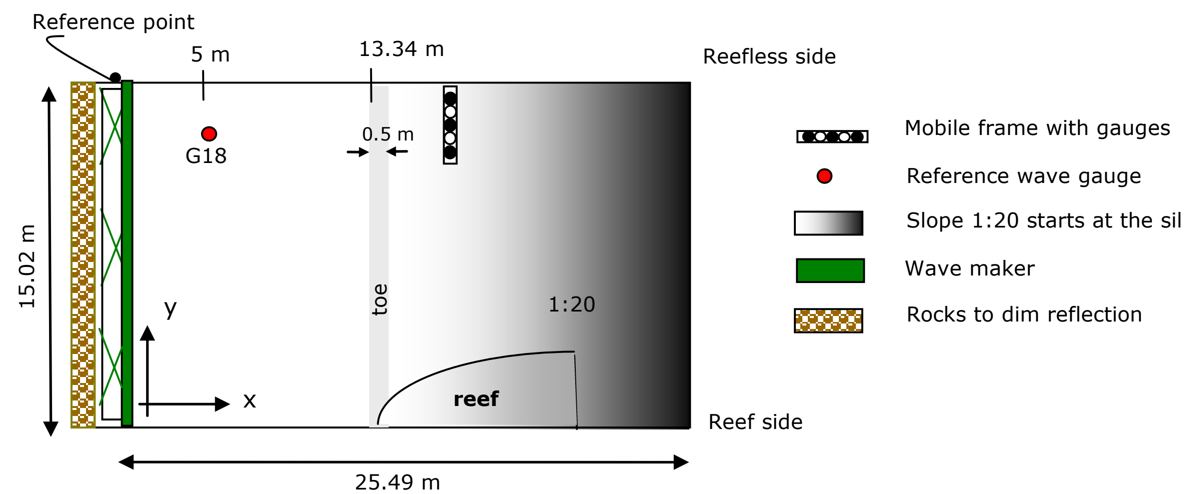

Figure 4-1: Wave basin with coordinate system

One half of a symmetrical reef is located at one side of the basin, so the wall acts as a mirror. The reef is superimposed on the main slope, which has a gradient of 1:20. The reef itself has a 'basic shape' (Henriquez, 2004) with a bed slope of 1:6 normal to the depth contours, and a reef angle of 60 degrees with respect to the x-axis (Figure 4-2).

The reef is submerged and its crest level is at 8 cm below still-water level. The main slope is preceded by a horizontal plane with a water depth of 40 cm. The reef and main slope have similar roughness.

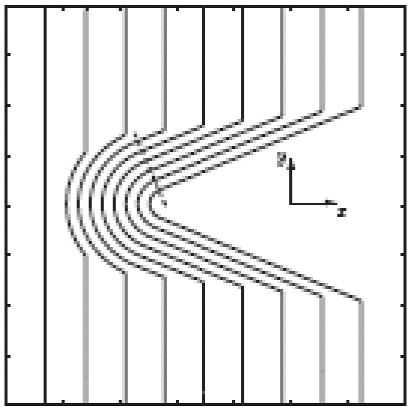

Figure 4-2: Basic shape reef (Henriquez, 2005)

All locations in the basin are given in a local coordinate system. The origin of the coordinate system is located at the 'reference point' which is placed on the wall at the reefless-side, in line with the wave makers, see Figure 4-1. The x-as is directed towards the beach and the y-as is directed towards the reefless side, parallel to the wave maker.

The toe of the slope is at x=13.34 m, parallel to the wave makers. To determine the location of the instruments on the mobile frame a line has been tied parallel to the beach from the reefless side to the reef-side, at a certain distance from the reference point.

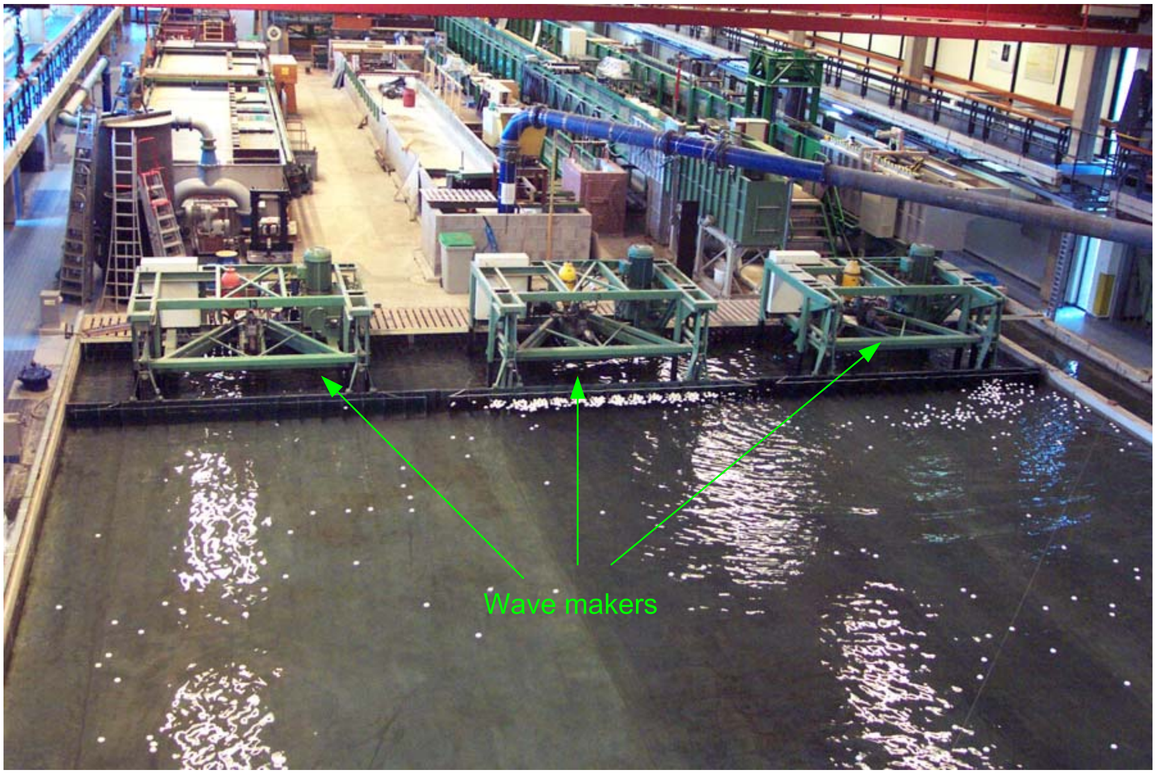

Figure 4-3: Applied piston-type wave makers

Three piston type wave makers, generating uni-directional shore normal incident waves, are placed in one line and are linked to operate synchronously. From now on these three wave makers are referred to as one wave maker. For the wave maker there is a second-order wave paddle steering system with no reflection compensation. Behind the wave maker porous rocks are present to dim reflection of the generated waves.

4.3 Wave conditions

Before starting the experiments it needed to be determined which wave conditions were most suitable. This means that the wave field must be smooth with little interference, disturbance and spurious circulations. The rip current has to show up and must be clearly visible. The waves should be able to occur in nature, so they should have a specific steepness. In addition there are some practical restrictions of the wave maker itself.

Steepness

To determine which wave height and length should be used in the basin, waves in the Netherlands have been taken as an example. Waves with the following deep-water steepness appeared to be realistic:

$$0.01 < \frac{H_0}{L_0} < 0.025$$

In which $L_0 = \frac{gT^2}{2\pi}$, H_0 = deep water wave height [m], L_0 = deep water wavelength [m], T = wave period [s] = $\frac{\mathbf{1}}{f}$ and f = frequency [Hz]

Ursell

Stokes second-order wave theory should be valid at the wave maker. Stokes' second order theory is valid for

$$Ur = \frac{HL^2}{h^3} \lesssim 25$$

Where Ur = the Ursell number[-], H = wave height [m], L = wavelength [m] at the paddle and h = water depth [m]

Paddle restrictions

On top of the theoretical limits, there are some practical restrictions of the wave maker.

- Because of the limited height of the wave board, the water level in the basin is kept at h= 40 cm
- Maximum stroke: 26 cm
- Frequency: 0.1 Hz < f < 2.0 Hz

Application of the CACR Wave maker Calculator made it possible to check the feasibility to make a certain wave (Internet reference 2 and 3)

Applicable waves

Limitations to the wave characteristics:

- All experiments are performed with one type of wave;
- The generated waves are uni-directional normally incident waves;
- A suitable wave is determined prior to starting the experiment;

Different combinations of wave heights and wave periods fit:

- 0.05 m ≤ H ≤ 0.09 m
- 1 s ≤ T ≤ 2.5 s (0.4 Hz ≤ f ≤ 1 Hz)
- Paddle restrictions: H ≤ 0.1 m; period (0.5 s ≤ T ≤ 10 s)

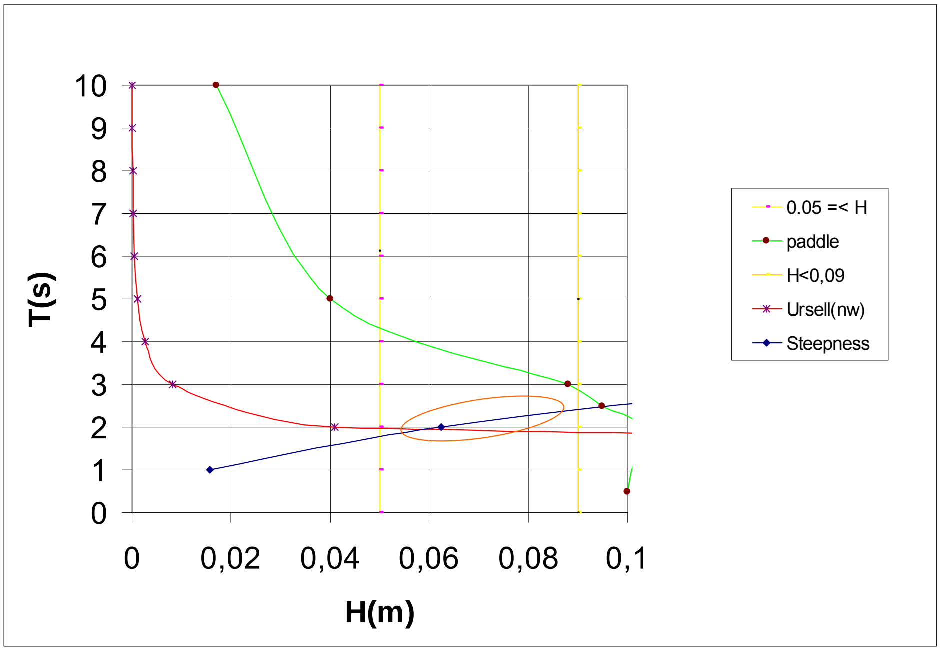

Figure 4-4: Wave conditions, determining suitable waves

Conditions of the wave field

At first, a monochromatic wave field was generated. By means of floating parts (globular-shaped candles), circulation patterns were visualized. Visual inspection showed that for monochromatic wave conditions two strong spurious circulation patterns in the basin arose.

Mechanisms responsible for circulation are bottom geometry plus wave-induced currents and finiteness of the basin. Spurious circulation in this experiment is attributed to the finiteness of the wave basin.

Continuous forcing of a monochromatic wave field increases the circulation effects. For a bi-chromatic wave field this does not occur because of extinguishing effects. Note that a bi-chromatic wave field generates less large-scale currents.

It was concluded that a monochromatic wave field was not feasible. Instead, a bi-chromatic wave field was generated, made of two components with the same wave height and almost the same frequency. The frequency-difference was chosen to have 7 waves in a group (appearance of seven waves in a group is quite common in nature).

When waves were generated with mean frequencies of $f_1 = 0.5357$ Hz, $f_2 = 0.4643$ Hz, the difference-frequency of this combination seemed to be the 'eigen frequency' of the basin, resulting in a strong amplification of the surface elevation. Obviously, this combination of frequencies was not applied.

For the in-situ experiment, several wave fields were assessed, resulting in, a bi-chromatic wave field with the following wave conditions:

- Mean frequency: 0.44 Hz
- Water level: 0.4 m
- H_1=H_2= 0.04 m (minimum wave height in a wave group is 0.0 m, maximum wave height in a wave group is 0.08 m), 7 waves in a group, second-order
- f_1= 0.4714 Hz
- f_2= 0.4086 Hz

To verify that the generated waves during the experiment were similar, one wave gauge(G18) was permanently located offshore (x=5 m, y=13.52 m).

4.4 Applied instruments

This section specifies the applied instruments. A distinction is made between the in-situ measurements and video observations.

In-situ measurements

All gauges are placed on a mobile frame in order to move the instruments simultaneously in a certain direction in a restricted way. The sampling rate of the applied gauges is 50 Hz and 100 Hz, signals of the measuring devices are in Volts. Dedicated computers with data collection software are used.

To determine the location of the mobile frame with the instruments, a line was tied parallel to the wave makers from the reefless-side to the reef-side, the ‘perpendicular line’ (see Figure 4-5).

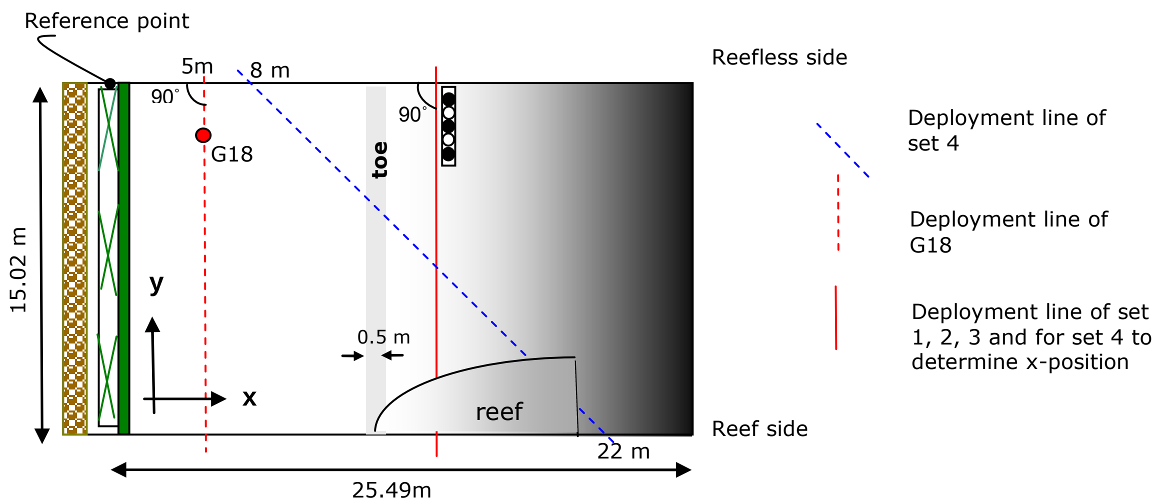

Figure 4-5: Determining the position of the gauges

In order to be able to place the instruments at an exact position in the direction of the rip current, a second line was tied diagonally across the wave basin from (x; y) = (8;0) to (22; 15.02). The mobile frame was repeatedly moved along this line. The intersection of the perpendicular and diagonal line provides the coordinates of the mobile frame.

For the in-situ measurements, three types of gauges were used.

- resistance type wave gauges: wave height meter (WHM, or GHM in Annex 1)
- pressure-type wave gauges (=pressure meters): pr
- electromagnetic flow velocity meters: EMF (or EMS in Annex 1)

Figure 4-6: Wave gauge (left) and velocity gauge with pressure meter (right)

During the in-situ measurements, different combinations and numbers of gauges were used. The used gauges were fixed on a mobile frame at certain distances from each other. When pressure meters were used, they were fixed to the EMF's. For a plan view of the mobile frame, see Figure 4-7.

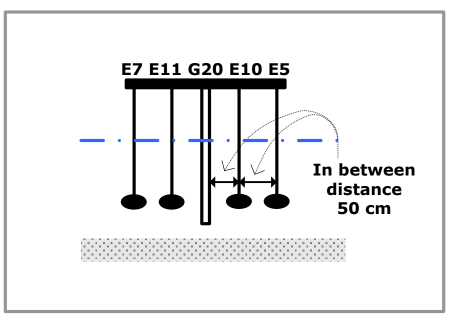

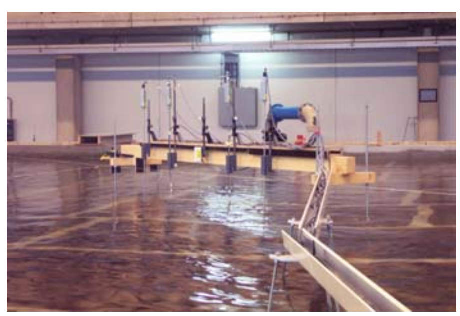

Figure 4-7: Mobile frame with gauges, 4 EMF's (Enn) and 1 WHM (Gmm)

Four EMF's were placed in line with one wave gauge in the middle and two pressure meters fixed at the velocity meters on both sides of the wave gauge.

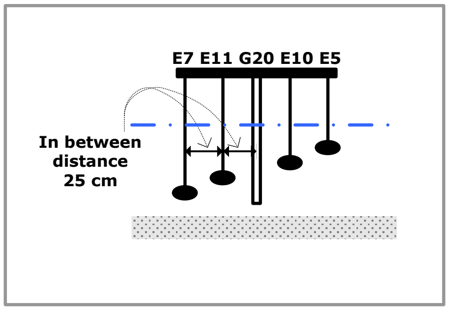

Figure 4-8: Gauges placed at variable distances from the bottom

In order to obtain a vertical profile of the rip current, measurements at different heights in the vertical were needed. The EMF's were placed at ¼, ⅓, ½ and ¾ times the undisturbed water depth in vertical direction, relative to the bottom. To prevent interference in horizontal direction, the minimum in-between distance of the EMF's on the frame is 25 cm. Initially, the velocity gauges were placed with only 15 cm in between. It appeared that they influenced each other. It was also observed that, in this framing, the pressure meters disturbed the EMS's. Hence the pressure meters were removed.

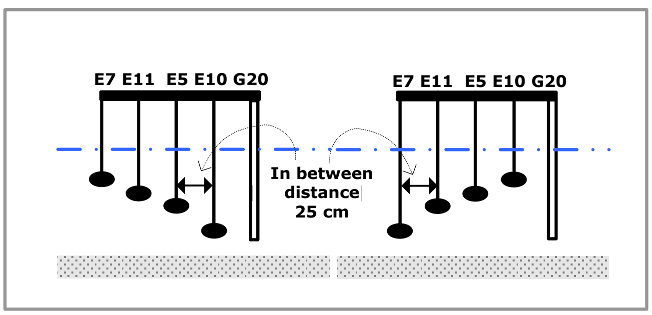

Figure 4-9: Wave gauge placed at the end in order to restrict slipstream - effects

Moving into the direction of the rip-current, the best way to place the gauges is from large distance from the bottom, to close to the bottom. This way gauge deployment is called: HL (from high to low), see Figure 4-8.

To verify this set-up, the gauges were placed in reverse order: small distance from the bottom to large distance from the bottom, LH (from low to high). The successive gauge stood in the slip-stream of the previous one.

Based on test measurements, it was confirmed that the preferable order of the gauges was HL. The wave gauge (G20), which stands as near as possible to the bottom, was placed at the end.

The applied EMF's, had already been calibrated. In the calibration forms, a relationship between Volt and velocity is presented for each individual EMF. Analyses with MATLAB showed that a calibration factor of 1 [Volt] equals 10 [cm/s] could be applied for all EMF's. Results of these analyses for EMF5 are summarized in Figure 4-10.

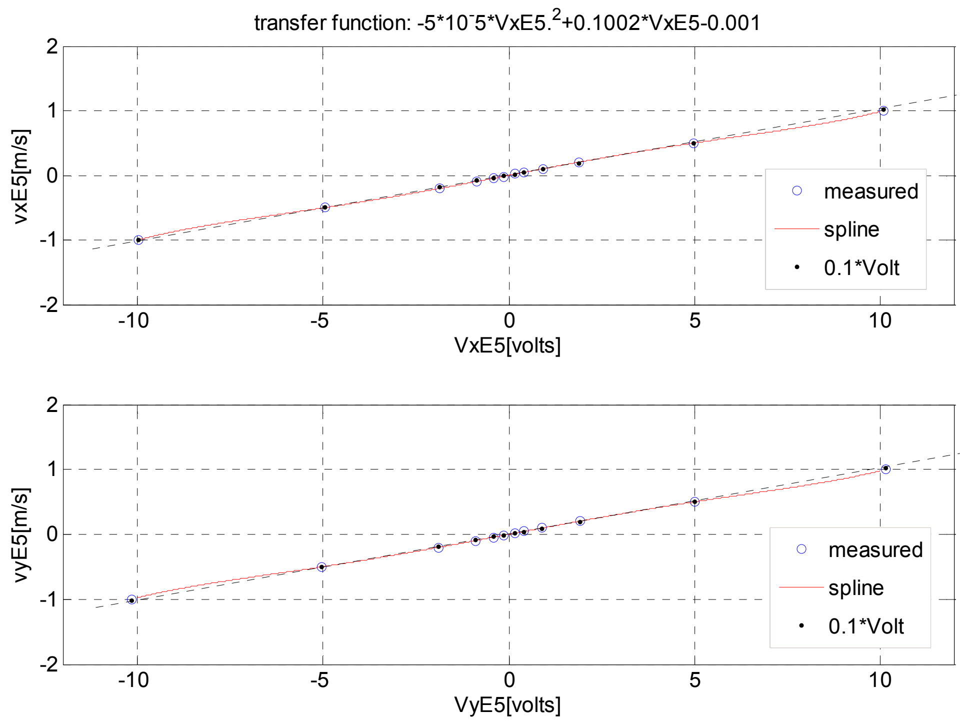

Figure 4-10: Calibration EMF5 (MATLAB)

For the conversion of the Volt signals into velocity, in this research the linear relationship 1 [V] = 10 [cm/s] is applied.

To calibrate the wave gauges (WHM), differences in Voltage were compared with beforehand stipulated differences in height; so, for each WHM a specific ΔV/ΔH was known. Table 4-1 presents a selection of the calibration measurements.

Table 4-1: Calibration measurement WHM (wk 37_test.asc)

	ΔV [Volt]	Δx [cm]	ΔV/Δx
G19	3,08	7	0,44
	2,21	5	0,442
G20	2,08	5	0,416
	2,9	7	0,414
G21	2,08	5	0,416
	2,91	7	0,416
G18	1,28	3,1	0,413

video observations

The video observations were made with a Sony digital video camera recorder DCR-VX700E with the following characteristics:

- frame size: 768h, 576v, 4:3 aspect ratio
- frame rate: 25 Hz
- pixel aspect ratio: square pixels (1.0)

As particles, white globular-shaped candles with a 6 cm diameter were used.

Before recording, a calibration of the recording area was made. The boundaries of the recording area were marked by five fixed points, so potential distortion of the image could be checked. With those markings it was also possible to scale from pixel to world-coordinates.

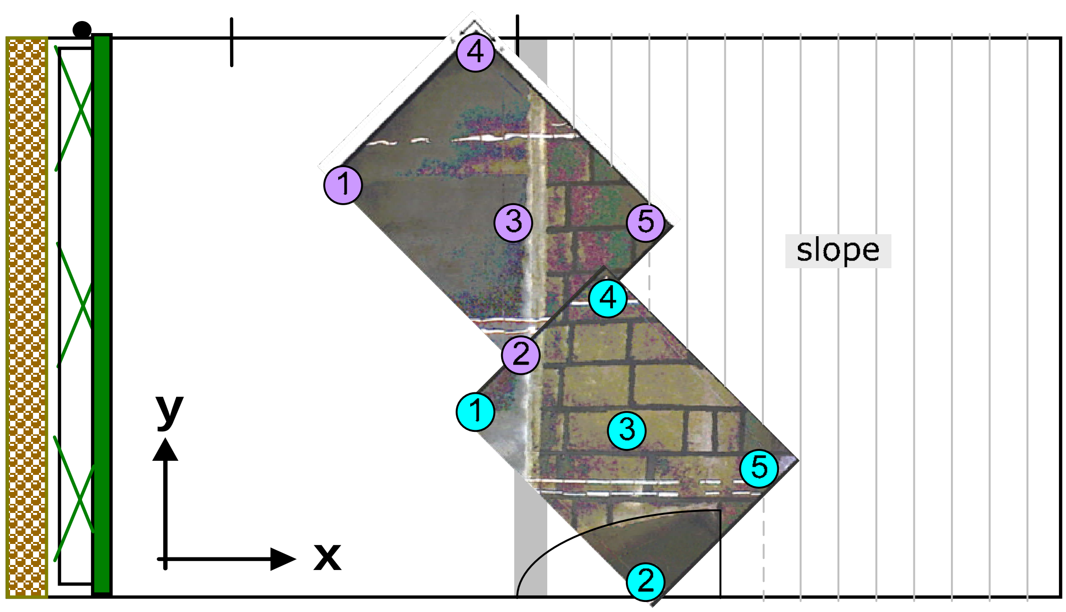

Figure 4-11: Overview of recording area's: blue= recording area(1) and purple= recording area(2)

Previous in-situ measurements made it possible to estimate the approximate path of the rip current. Additionally, the approximate path of the rip current was visualized by supplying the wave basin with a few floats.

Because of the size of the rip current, it was not possible to cover the whole field in one recording. For this, the field was divided into two areas, recording area (1) and recording area (2) (see Figure 4-11). Consequently, the camera was attached to the ceiling of the laboratory above the basin at two different locations.

4.5 In-situ measurements

The in-situ measurements are divided into four sets, each set including several realizations. The first set was to find the undisturbed wave transformation. To that end measurements were taken at the reefless-side. The second set was at the reef side, so differences between the two parts of the basin could be visualized. The third set was to identify the path of the rip current and potential spurious circulations. In set four measurements in the rip current are taken to establish a vertical flow velocity distribution.

For the in-situ measurements, three time-scales are important:

- the frequencies of the two individual waves (mean frequency 0.44Hz)
- the frequency of the wave group (0.06Hz)
- the frequency of the meandering of the rip current (0.01Hz)

Duration of a realization varies from 10 minutes to 30 minutes. This includes all time-scales. A new realization starts from a still-water situation. When two successive realizations are done without waiting until the water level is still again, this is called a ‘hotstart’.

Set one: reefless-side (How does a wave break on a normal slope)
Three resistance-type wave gauges (WHM) and 2 electromagnetic velocity meters (EMF) were placed on a mobile frame (see Figure 4-12). One end of the mobile frame was placed with a fixed angle of 90^{o} at the wall at the reefless-side of the basin. The other end stood on two supports in the basin.

During set one, the mobile frame has only been moved in x-direction, starting at x=5 m. Offshore, approaching the slope, the measurement grid was refined from 4 m (offshore) to 0.125 m (on the slope). Detailed information about the applied grid is presented in Annex 1.

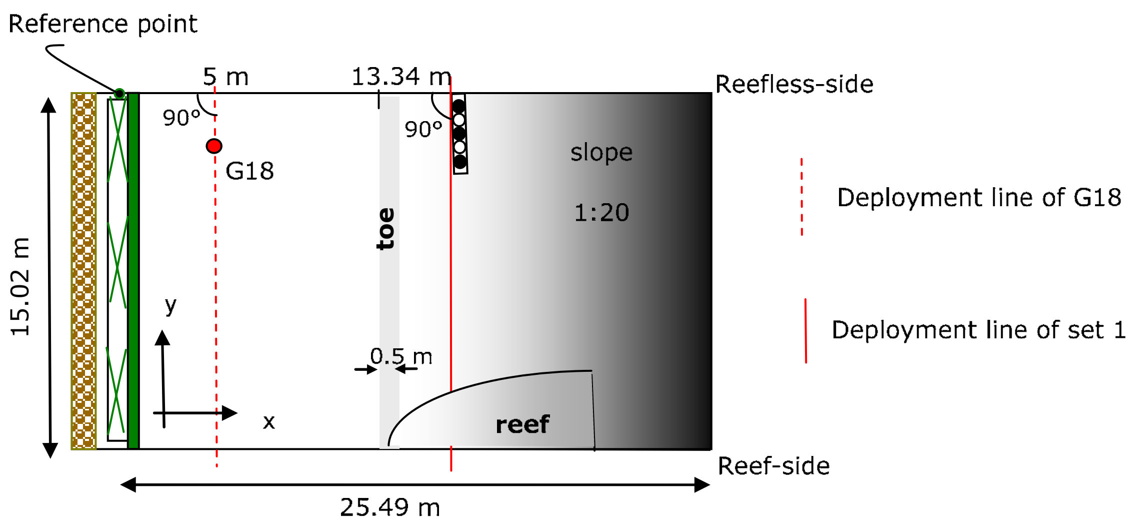

Figure 4-12: Set one, measurements at the reefless-side

Set two: reef-side (breaking waves on a slope with reef)

For set two, the mobile frame is placed next to the wave-basin wall at the reef-side, normal to the wall. For this set the gauges were mirrored in the y-direction with respect to the deployment during set one. The mobile frame was, similar to set one, moved in x-direction exclusively. During set two, two pressure gauges were included. The pressure gauges attached to velocity meter EMF10 and EMF11, respectively recorded the wave height and the velocity simultaneously at the same location to study wave-current interaction.

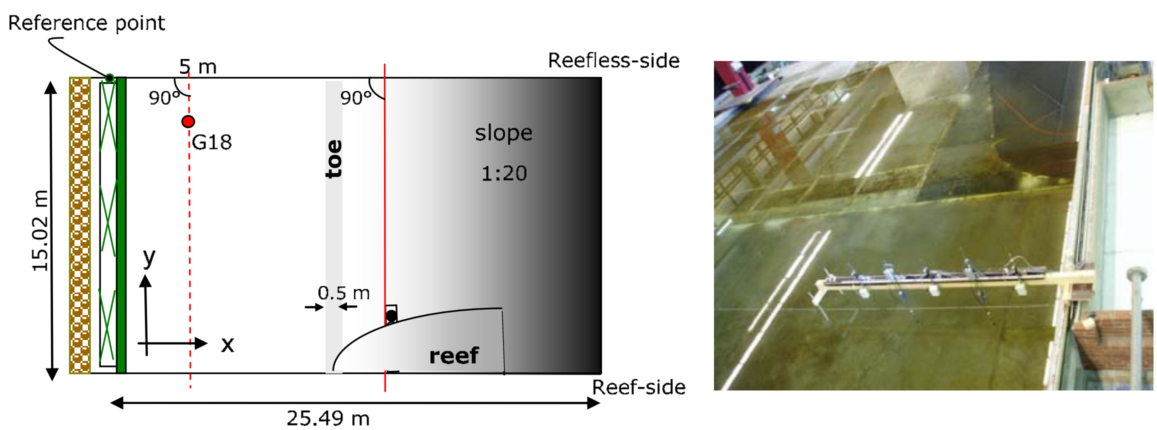

Figure 4-13: Set two, measurements at the reef-side

Set three: measurements all through the basin

In set three, the location of the rip current is identified. Additional purpose of this set is to determine to what extent the rip current influences the wave pattern

In this set, the mobile frame has the same configuration as used for set two (the reef-side measurements). For stability reasons, the construction of the mobile frame was modified marginally by adding two extra legs.

The mobile frame is moved through the wave basin, parallel to the wave maker, starting at x=10 m. A narrow grid of measurement points is collected. In the wave basin on the slope and the reef, a measurement grid with intervals in x- and y-direction of 50 cm was applied. Offshore, in the section between the wave maker and the toe, larger intervals in x-direction have been applied. The interval in y-direction remained 50 cm. Detailed information on the applied measurement positions is given in Annex 1.

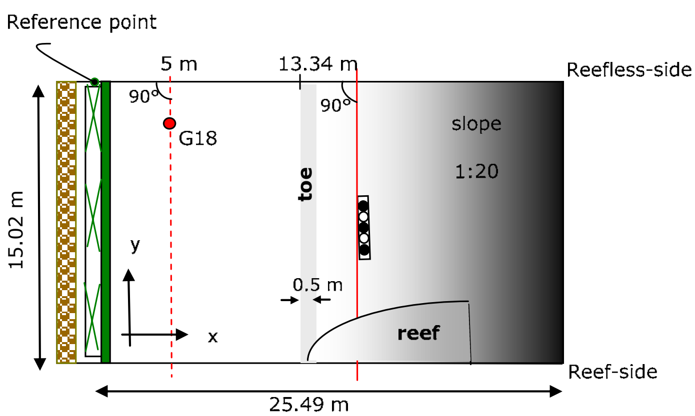

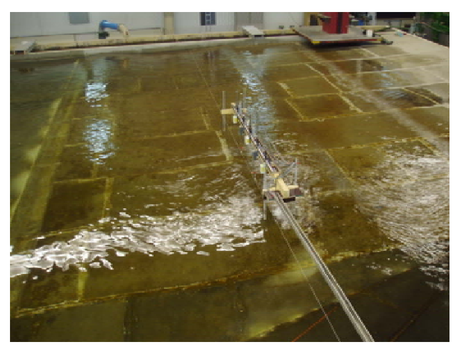

Figure 4-14: Set three, measurements all through the basin

Set four: in the rip current

In set four, measurements were taken to establish vertical flow velocity distributions along the rip current. To cover the vertical profile of the rip current, measurements are taken on the slope and offshore. For this, the mobile frame had to be repositioned several times. In the direction of the expected path of the rip current, sequential measurements at three (Figure 4-7) and four (Figure 4-8) discrete vertical positions were performed.

The expected path of the rip current was identified by the measurements of set three. To confirm the expected location of the rip current visually, floats are supplied to the wave basin. To mark the expected path of the rip current, a line was tied diagonally over the basin (see Figure 4-5 and Figure 4-15) at coordinates (x, y) = (8.0, 15.02) to (x, y)=(22.0, 0.0).

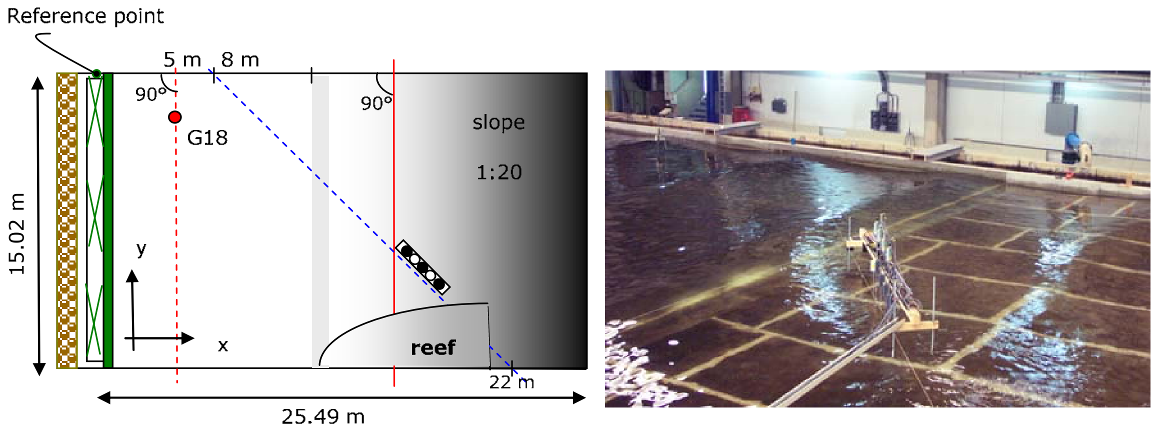

Figure 4-15: Set four, measurements in the rip current

4.6 Video observations

The recordings were divided into two series (one for each recording area). For each series there are three specific time-scenarios:

- recording starts simultaneously with the wave generator (to see the evolution of the rip current)
- recording starts after five minutes of generating waves
- recording starts twenty minutes after generating waves

Before recording, the recording area had to be seeded with particles. To make sure that there were enough particles in the recording area during recording, the recording area had to be filled up with particles from outside, next to the recording area. Here fore it was important to mark the recording area by means of lines over the basin.

Figure 4-16: Seeding the recording area in the wave basin with floats

Now the people who were supplying the recording area with particles were able to see where they had to put the particles (before recording in the recording-area between the lines and during recording outside the recording-area lines).

Note that inhomogeneous distribution of particles contributes to a bias in the velocity statistics with a dominant contribution by high-concentration regions

4.7 Documentation of the measurement data

Annex 1 presents an overview of the in-situ measurement data. Measurements are organized per week number, starting in week 30 until week 52 (
Table 4-2).

Table 4-2: Overview data points

	Week number	Data points	Description
Set one	30	90	Reefless-side
Set two	37; 38; 39; 40; 43	380	Reef-side
Set three	44; 45; 46; 47; 48; 49	460	Detecting the rip current

Set four	51; 52	240	In the rip current

Per data point, the position relative to the reference point, according to a local coordinate system is given. For the MATLAB data-processing, these positions have been transformed into Cartesian coordinates.

Annex 1 contains a brief log, covering issues as duration of the measurement, operational aspects related to the wave basin, calibration of the gauges, identification of data channels and deployment of the instrument frame.

The log of the video observations is presented in Annex 2. The obtained data of the video observation is only analysed for one measurement. All video data is archived at the Delft University of Technology, Ad Reniers or Martijn Henriquez.

5 RESULTS AND ANALYSES

5.1 Introduction

In this chapter, results of the experiment are presented. The experiment can be divided into two parts: in-situ measurements and PTV measurements. The analyses of the measured data will be performed according to the outline of the research issues, presented in section 2.4 of this report. First, the repeatability of the wave generation will be assessed.

5.2 Comparability of wave generation

In order to be able to compare different sets of measurements, the generated waves have to be similar. To that end a reference gauge (G18) was placed just in front of the wave maker at x=1.5 m, y=5.0 m. The repeatability will be assessed by inter-comparing the offshore wave heights at G18 for the different sets. Because of the bi-chromatic character of the generated waves, it is not sufficient to use the mean wave amplitude. In addition the standard deviation (σ_A) of the wave group envelope, responsible for the forcing of the long waves, has to be taken into account.

Figure 5-1: Reference WHM (G18)

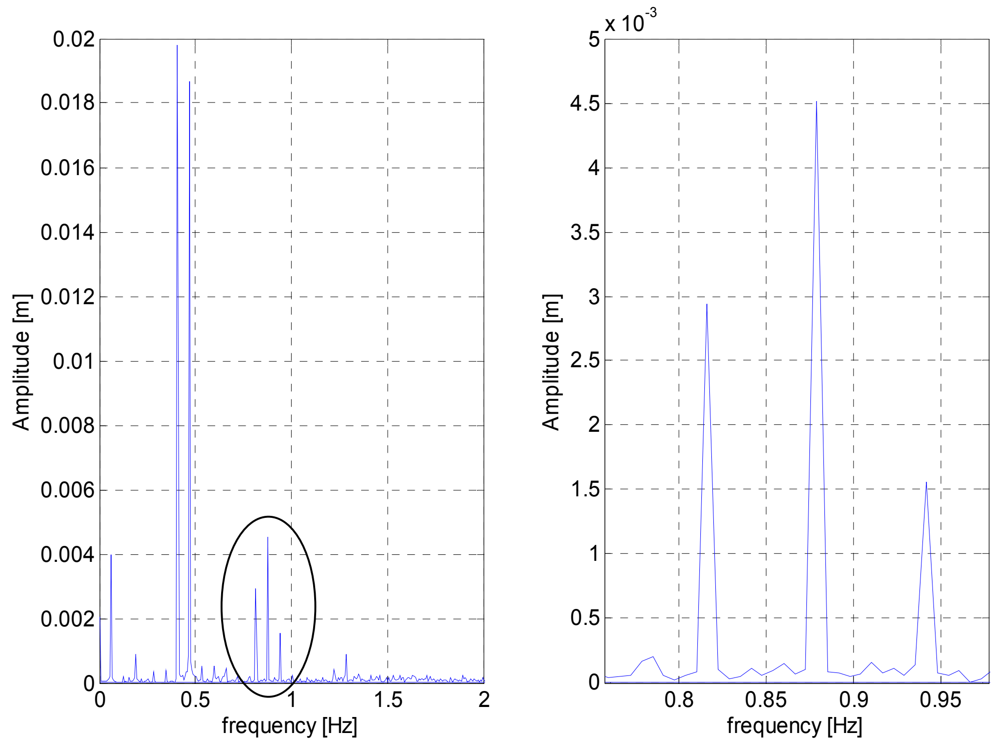

Figure 5-2: Example of amplitude spectrum: left panel. Right panel: detailed view of super harmonic amplitude-spectrum indicated by the circle in the left panel.

The signal contains different frequencies. Figure 5-2 shows peak frequencies at f1=0.4081 Hz, f2=0.4709 Hz corresponding to the input 'short wave' components. The small frequency difference results in a groupy signal.

The difference frequency of f1 and f2 at f=0.0628 Hz is called f_lob and corresponds to the frequency at which the long waves are forced by the wave groups. Each wave group with frequency f_lob contains 7 'short waves'.

For input frequencies, f1 and f2, the first super harmonic frequencies are visible for which

f = 0.8162 Hz = 2*f1

f = 0.9418 Hz = 2*f2

f = 0.879 Hz is the sum frequency of f1+f2

resulting in a non-linear wave shape.

The third-order higher harmonic frequencies have small amplitudes suggesting that second-order wave steering is adequate to generate the desired surface elevation.

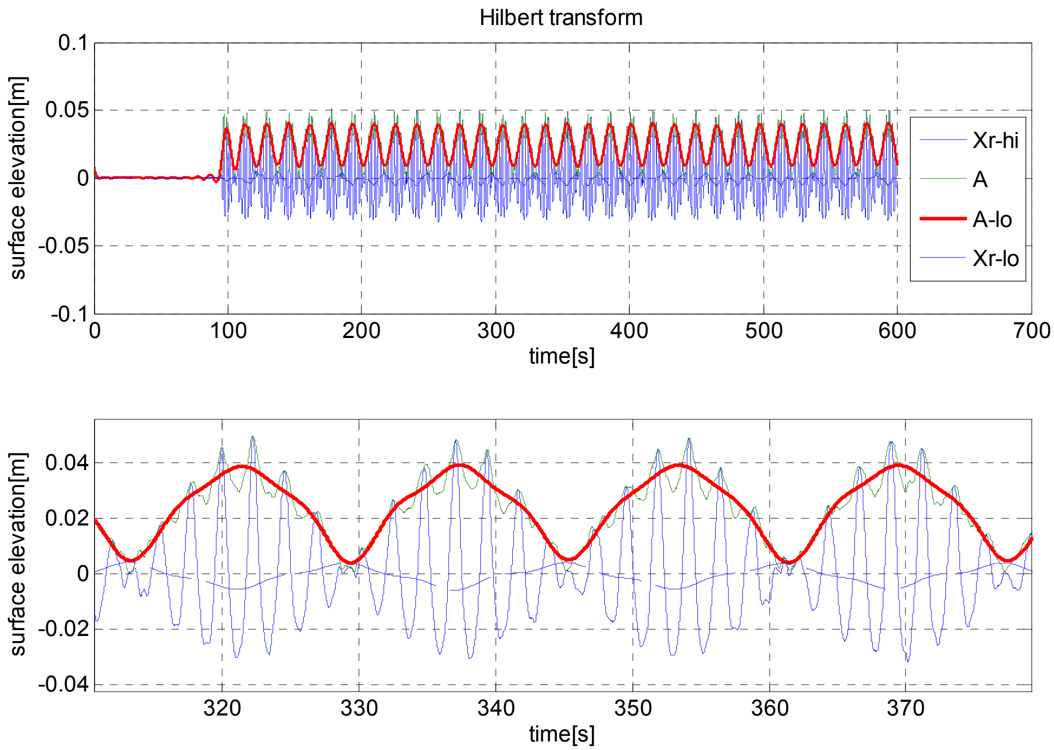

Figure 5-3: Measured surface elevation for the short waves (solid blue line) and long waves (blue dashed line), corresponding wave envelope (green line) and low-pass filtered envelope (red line). Bottom panel: similar, but zoomed in.

An example of the results of the data processing of a single realization of the measured surface elevation to determine the repeatability of the wave generation is shown in Figure 5-3.

The wave envelope has been calculated with the Hilbert transform of the short wave surface-elevation time series in the interval between 300 s < t < 600 s. The short wave surface-elevation time series have been obtained by high-pass filtering of the measured surface-elevation.

The cut-off frequency was set at 0.22 Hz (corresponding to half the mean frequency of the bi-chromatic short wave signal). The resulting time series show flat troughs and sharp crests consistent with non-linear waves (lower panel of Figure 5-3).

Secondary maxima are absent in the troughs indicating that Stokes second-order wave theory, used for the wave generation, is applicable. To delete high-frequency variation (Figure 5-3: lower panel), the wave envelope has been low-pass filtered at 0.22 Hz. Additionally the mean and the standard deviation of the low-pass filtered wave envelope have been calculated. This analysis has been applied on all sets of measurements.

For the wave-group-envelope analysis, as presented in Figure 5-3, the mean wave height, M_{G18} and standard deviation of the wave height, σ_{G18} have been determined for all tests and have been summarized in Figure 5-4.

The mean wave height averaged over all sets ($M_{G18\ tot}$) was found to be 0.0494 m (marked 'test-averaged wave height') with a standard deviation σ $M_{G18\ tot}$ of 0.0008 m (dashed red lines in Figure 5-4). Allowing an error of +/- 2*σ (less than 5%) in the mean wave height (dotted blue lines) shows that the mean wave height at the wave generators is well reproduced for realizations 1,3, 4, 6 and 7. Realizations 2, 5 and 8 that do not comply, have to be verified.

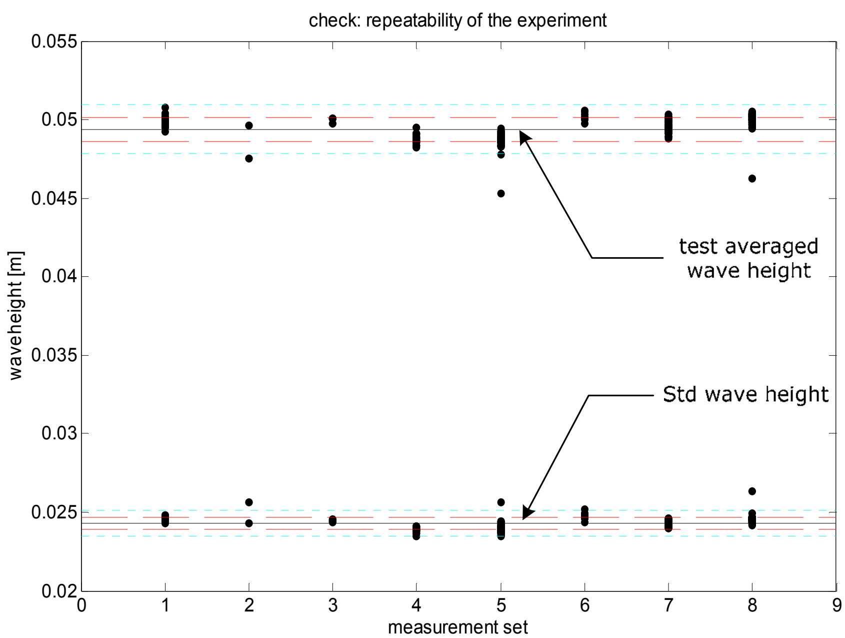

Figure 5-4: Mean wave height and standard deviation of wave height computed from Hilbert transform at the offshore reference gauge (G18). The black lines indicate the mean value of test-averaged and Std wave height. The red dashed lines indicate 1*σ. The blue dotted lines indicate 2*σ.

The standard deviation of the wave envelope ($\sigma_{G18\ tot}$) was determined for all realizations (0.0024 m marked 'STD wave height') and presented in Figure 5-4. The standard deviation of the STD wave height ($\sigma\ \sigma_{G18\ tot}$) was found to be 0.0004 m (red dashed lines).

Allowing an error of +/- 2*σ (less than 5%) in the $\sigma_{G18\ tot}$ (dotted blue lines) shows that 'STD wave height' at the wave generators is well reproduced for the different realizations. Similar to the mean-wave-height analysis, realizations 2, 5 and 8 do not comply and have to be verified.

Table 5-1 summarizes for each measurement realization (Figure 5-4) the mean wave height (M_{G18}), the STD wave height (σ_{G18}), the allowed error (+/- 2*σ) and the variations for the mean wave height and the STD wave height. Realizations 2, 5 and 8 that did not comply with the applied criterion for repeatability (error < 2*σ), are highlighted in Table 5-1.

Table 5-1: Repeatability experiment

x	**n**	**Realization identification**	**M_{G18} (cm)**	**2*σM_{G18} (cm)**	**σ_{G18} (cm)**	**2*σσ_{G18} (cm)**	**VarM %**	**Varσ %**
1	18	G_{18_1}	4.99	0.08	2.46	0.03	1.6	1.2
2	2	G_{18_2}	4.86	0.30	2.50	0.19	6	7.6
3	4	G_{18_3}	5.00	0.03	2.45	0.02	0.6	0.8
4	16	G_{18_30},	4.88	0.07	2.39	0.04	1.4	1.7
5	51	$G_{18\_37\_43}$	4.87	0.12	2.40	0.07	2.5	2.9
6	8	G_{18_4}	5.02	0.05	2.48	0.05	1	2
7	39	$G_{18\_44\_46}$	4.96	0.08	2.43	0.03	1.6	1.2
8	37	$G_{18\_47\_49}$	5.00	0.14	2.46	0.07	2.8	2.8
	175	*G_{18tot}*	*4.94*	*0.15*	*2.43*	*0.08*	*3*	*3.3*

n: number of measurements in a realization

M_{G18}: mean of the wave height envelopes in a realization

σ_{G18}: STD wave height

2*σ M_{G18}: allowed error for M_{G18}

2*σ σ_{G18}: allowed error for σ_{G18}

VarM: procentual variability per realization (2*σ M_{G18}/ M_{G18}*100%)

Varσ: procentual variability per realization (2*σ σ_{G18}/ σ_{G18}*100%)

Low variability for M_{G18} and σ_{G18} indicates good repeatability of the measurements within one realization. Only realization G_{18_2} shows an unexpected high variation, probably due to the low number of measurements (n=2) within this realization.

From the mean-wave-height and STD-wave-height analyses, presented in Figure 5-4, it was identified that within realization $G_{18\_37\_43}$ and $G_{18\_47\_49}$ one measurement did not comply the 2* σ criterion. Due to the relatively large number of measurements within these realizations, the variation is minor (Table 5-1). The deviating measurements have been identified in the database. The coordinates of the EMF's, as well as the coordinates of the EMF's for the deviating measurement in realization G_{18_2}, are presented below.

$G_{18\_37\_43}$ → 'f38','C:\maaike\data\wk43\7bc_209.asc',
x= [18.320 18.320]
y = [1.0050 1.9950]

$G_{18\_47\_49}$ → 'f3','C:\maaike\data\wk49\H197_131.asc'
x = [**18.620** 18.620]
y = [**9.0580** 8.0685]

test G_{18_2} → 'f1','C:\maaike\data\wk52\muir14_66V.asc':
x = [14.7700   15.6900   15.7900   14.6700]
y = [7.6100   6.6200   6.5100   7.7200]

These measurements have been used in the data analysis but are clearly marked by red dots in Figure 5-9. It was found that the measured velocities at these locations corresponded to adjacent velocities, except for x=18.62 y=9.058 where the mean velocity is large compared to adjacent velocities.

Overall conclusion on repeatability of the wave generation: The generated waves are comparable for different sets. The way in which mean flow and rip current, driven by this comparable wave generation, will develop will be discussed in the following paragraphs.

5.3 Wave breaking through bathymetry

A driving force for the occurrence of a rip current is the existence of gradients in water level. These gradients are due to differences in water-level set-up induced by wave breaking differences. This mechanism is considered the main driving force for flow circulation in this study.

Description of the measurements at the reefless-side and the reef-side

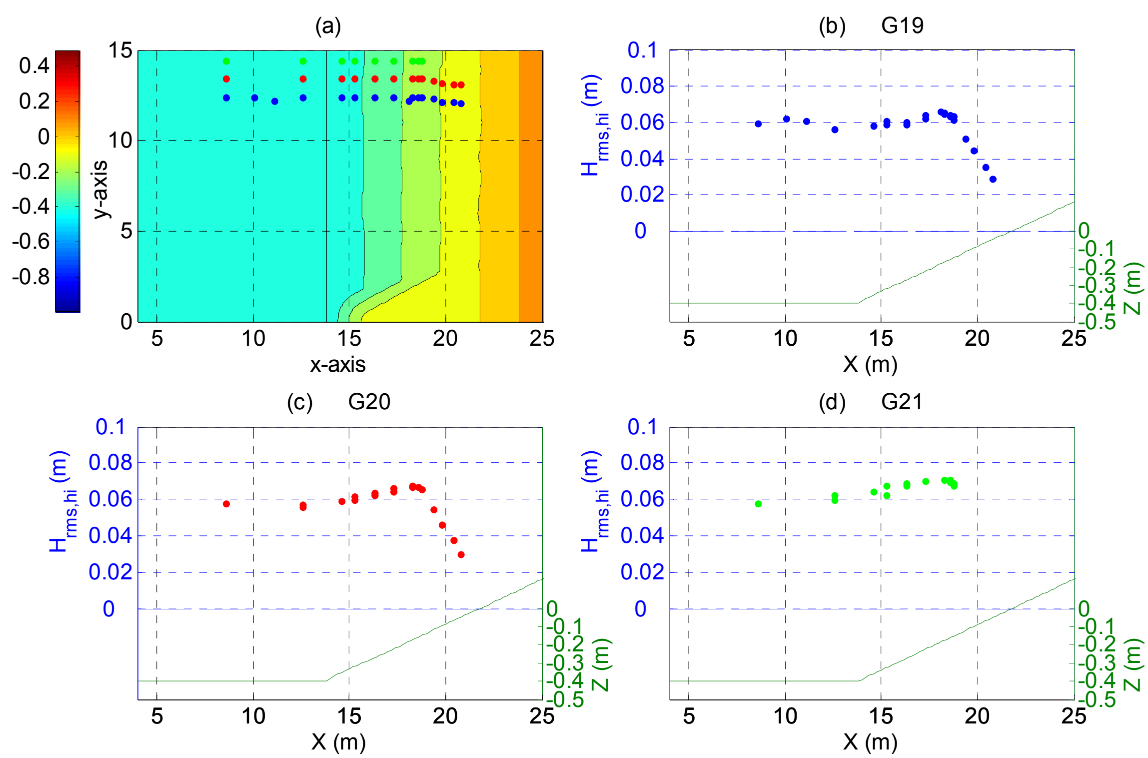

Figure 5-5: Wave breaking at the undisturbed side of the basin. Panel a: top view of the basin with location of wave gauges G19(blue), G20(red) and G21(green). Panel b: Cross-shore distribution of $H_{rms,hi}$ at Y=12.383m. Panel c and d, idem for Y = 13.378 m and 14.383 m, respectively. Mean water level (dashed line) and local bottom profile (solid line) given as a reference

Waves break differently through bottom topography. Figure 5-5 -(a) presents the top view of the basin. The reef is located in the lower right corner and is constructed in such way that surfing wave conditions are created (Henriquez, 2005).

In three parallel cross-sections along the basin (blue, red and green dots), the root-mean-square short wave heights ($H_{rms,hi}$) were measured. In Figure 5-6 - (a) the location of the realizations are presented as blue, red and green dots in a vertical cross-section. The duration of each realization was ten minutes.

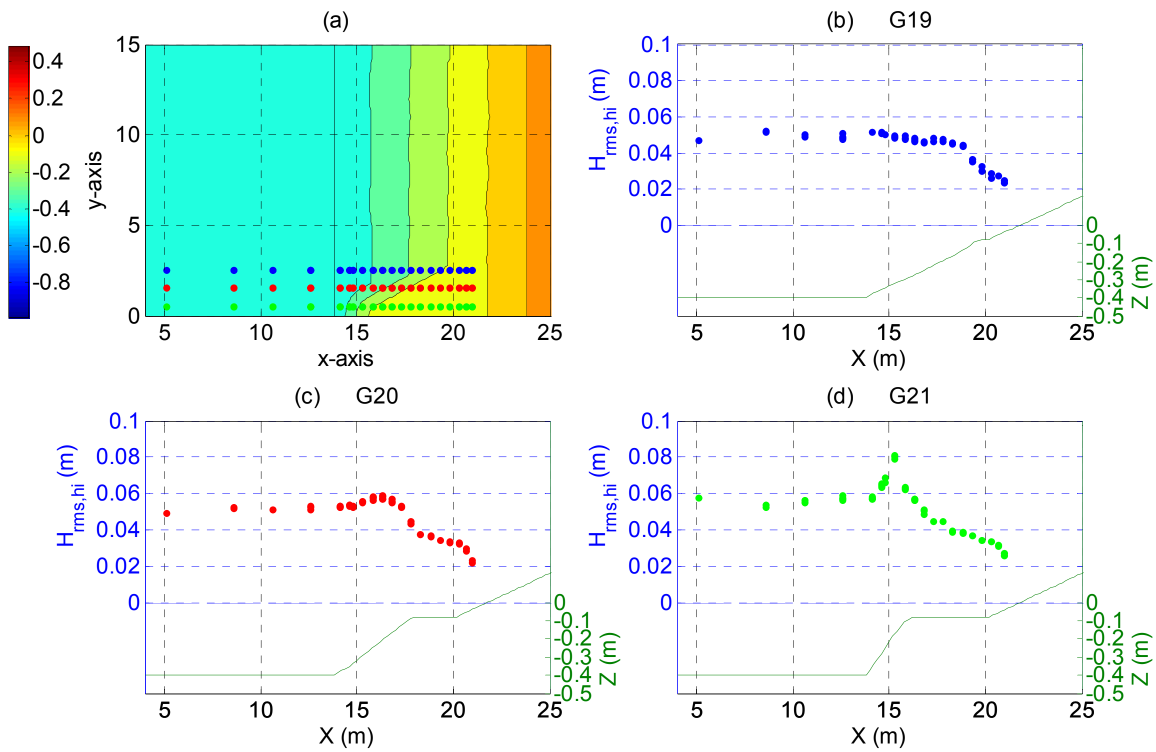

Figure 5-6: Wave breaking through bathymetry. Panel a: plan view of bathymetry with locations of WHM. Panel b: Cross-shore distribution of $H_{rms,hi}$ at Y= 2.5m. Panel c and d, idem for Y = 1.505 m and 0.5 m respectively. Mean water level (dashed line) and local bottom profile (solid line) given as a reference.

Figure 5-6:-(b),-(c) and –(d) present the realizations per cross section. The secondary (right-hand) y-axis Z (m) presents the bottom level; the primary (left-hand) y-axis the wave height. Both y-axes are relative to still water level. The x-axis represents the position in the basin relative to the wave maker.

Breaker type at the reefless-side and the reef-side

In the basin section with the horizontal bottom, the wave height is nearly constant. With decreasing water depth, wave heights increase because of shoaling. This causes increasing wave steepness. When the wave reaches its maximum steepness, the wave breaks. This causes energy dissipation resulting in a decreased wave height after breaking.

In all three panels (b, c and d), the bathymetry is represented by the green line. It can be observed that the bathymetry for the three cross-sections is not uniform, resulting in different wave-breaking behaviour (Figure 5-6). This can be calculated via: $\xi = \frac{\tan\alpha}{\sqrt{H_b / L_0}}$ for which α = slope angle and $L_0 = \frac{gT^2}{2\pi}$ in which T is the mean wave period and H_b is the breaker-wave-height.

Table 5-2: Determination input parameters breaker type reefless-side

Gauge number	H_b [m]	L_0 [m]	$\tan\alpha$ [-]
G19	0.065	8.06	0.05
G20	0.07	8.06	0.05
G21	0.075	8.06	0.05

Table 5-3: Breaker type at the reefless-side

Gauge number	Irribarren parameter (ξ)	Type of breaking
G19	0.56	Spilling / plunging
G20	0.54	Spilling / plunging
G21	0.52	Spilling / plunging

Table 5-4: Determination input parameters breaker type reef-side

Gauge number	H_b [m]	L_0 [m]	$\tan\alpha$ [-]
G19	0.05	8.06	0.05
G20	0.06	8.06	0.09
G21	0.082	8.06	0.15

Table 5-5: Breaker type at the reef-side

Gauge number	Irribarren parameter (ξ)	Type of breaking
G19	0.7	Plunging
G20	1.0	Plunging
G21	1.5	Plunging

With increasing steepness of the bottom slope, the wave steepness just before breaking increases as well. The type of breaking shifts from spilling to plunging (see Table 5-3 and Table 5-5).

Observations at the reef-side, cross section G19

Observations at gauge G19 indicate the onset of wave breaking at X=15 m and a second, more pronounced wave breaking at X=18 m. Given the limited wave-height variations at X=15 m, no significant level set-up is expected at this coordinate.

At X=18 m, only a slight increase of wave height is observed before wave breaking. This is different with respect to the wave breaking at the reef-less side of the basin. The waves are less high at this end, probably because of refraction effects of the reef (see Figure 5-10). The refraction effect is stronger than the shoaling effect. The wave height pattern after wave breaking implies a water level set-up in the section X=18-20 m.

Observations at the reef-side, cross section G20

At gauge G20, increasing wave heights are observed in the section X=15-16 m. Wave breaking occurs at X=16 m and at X=20 m.
Water level set-up can be expected at X=17-18 m.

Observations at the reef-side, cross section G21

Gauge G21 presents a sharp crest at X=15 m, followed by significantly decreased wave heights between X=16-18 m. At x=15 m, there is a combination of strong refraction and also shoaling, causing the waves to increase (These effects are caused by the form and shape of the reef, designed to create high / surfable waves (Henriquez, 2005). A water level set-up is expected in the section X=16-18 m.

Differences in wave breaking at the reefless-side relative to the reef-side

Combining the individual observations per gauge, the development of an alongshore water-level gradient is expected starting from X=16 m onwards. The most pronounced alongshore gradient is expected between gauge G20 and gauge G21, based on the observed wave height variation.

On the bed slope away from the reef the wave height increases due to a decreasing water depth until the waves get unstable and subsequently break. The waves are higher than on the reef-side due to refraction effects and probably due to a small difference in the wave generation (Carceres et al., 2007).

As a result of gradients in the cross-shore radiation stress the mean water level rises (water level set-up). On the reef, the angle of the bed slope is significantly steeper. Therefore the waves on the reef break differently from those on the slope adjacent to the reef. This difference in wave breaking in combination with the wave (de-)focusing due to refraction results in a water level set-up gradient, the driving force for the development of the current.

5.4 Set-up and set-down

In this section, the observed mean water levels during the generated wave conditions is presented. Based on these measurements, set-up and set-down phenomena will be discussed.

Approaching the reef or the plane slope, the wave height increases (Figure 5-5 and Figure 5-6) and subsequently the mean water level decreases associated with the set-down (dark blue in Figure 5-7 and Figure 5-8). At breaking the decrease in wave related momentum (radiation stress) pushes the water level up resulting in a set-up of the mean water level (yellow, red in Figure 5-7 and Figure 5-8).

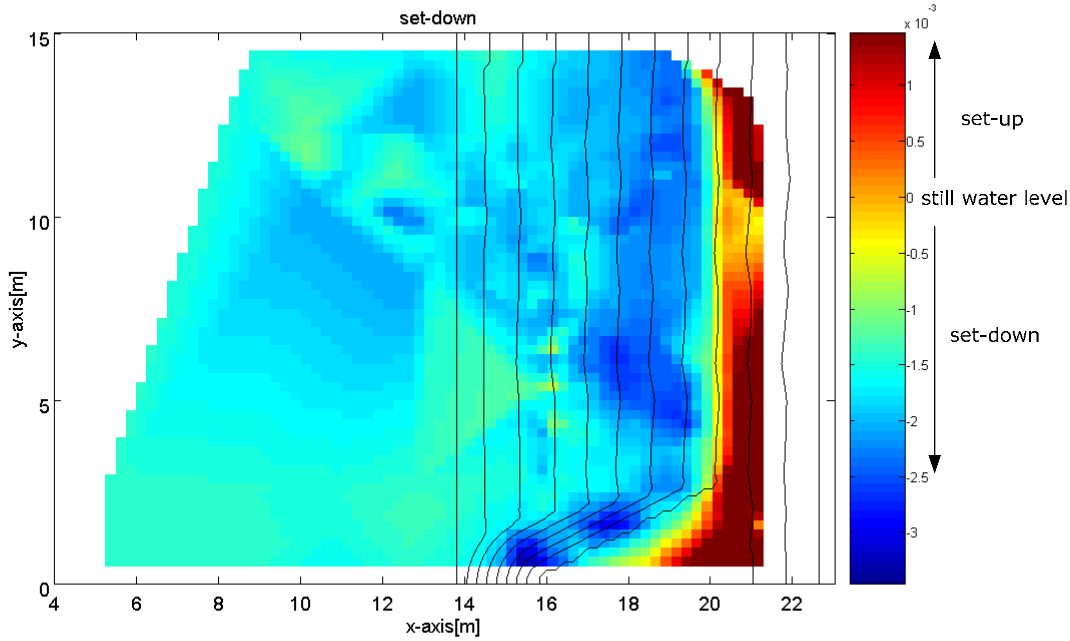

Figure 5-7: Interpolated in situ data showing set-down (blue) and set-up (red) due to wave shoaling and breaking. The locations of the measurement data are given in Figure 5-9.

The highest longshore gradient in water level is observed in two areas:

- At the reef-side at (x,y) ≈ (21, ½) to (x,y) ≈ (20,3)
- At the reefless-side at x ≈ 21, y ≈ [7½ to 12]

These gradients determine the location and direction of the rip current and circulation patterns. The expected flow directions due to water level gradients are indicated by the arrows in Figure 5-8

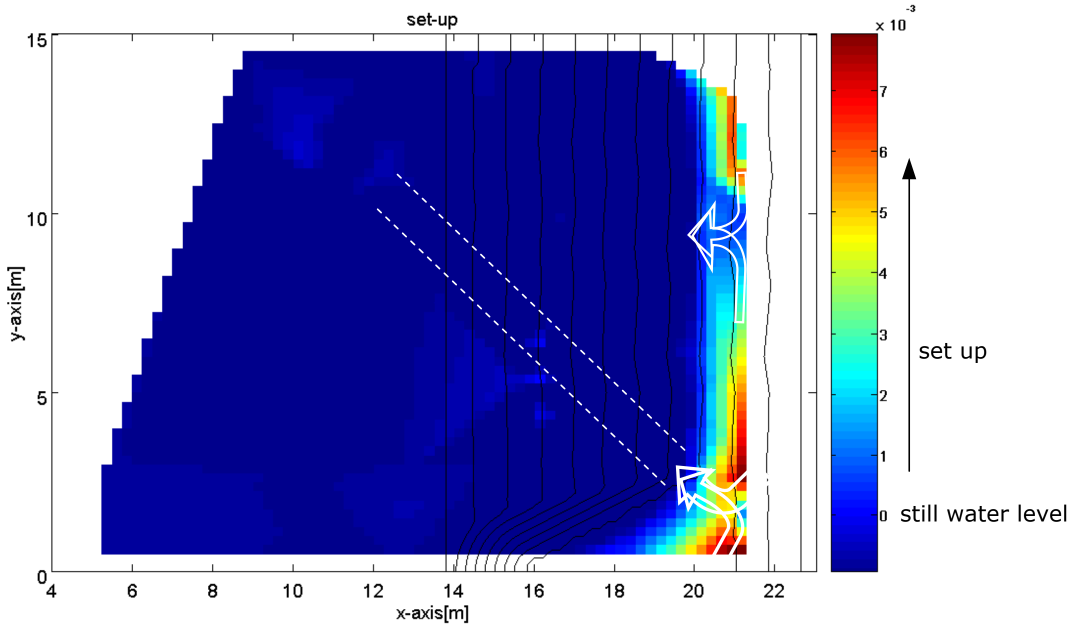

Figure 5-8: Interpolated in situ data showing set-up with adjusted colour scale; red=high, blue= low. The white arrows indicate set-up gradients. The white dashed line indicates the expected location of the rip.

After breaking (Figure 5-5 and Figure 5-6), the radiation stress is reduced, resulting in water level set-up (indicated by the red-yellow zone in Figure 5-7 marked with set-up). In Figure 5-8 the set-up is better visualized by adjusting the colour-axis.

The arrows point out the direction in which the current is expected to flow due to the convergence of the alongshore pressure-gradient-driven flow from the highest set-up to the lowest set-up.

5.5 Distribution of mean flow-velocity

As mentioned before, breaking-wave height and wave set-up are directly related; thus a longshore variation in wave height causes a longshore variation in set-up. The longshore gradient in set-up generates longshore flows from the position of highest waves and set-up toward the position of the lowest waves and set-up (Coastal Engineering Manual, 2006).

The momentum equation couples wave set-up gradients through radiation stress to currents (see section 3.3). The presented wave-induced mean flow-velocity distribution shows the development of the rip current. A top view of the mean sub-surface-velocity obtained with the EMF's is shown in Figure 5-9.

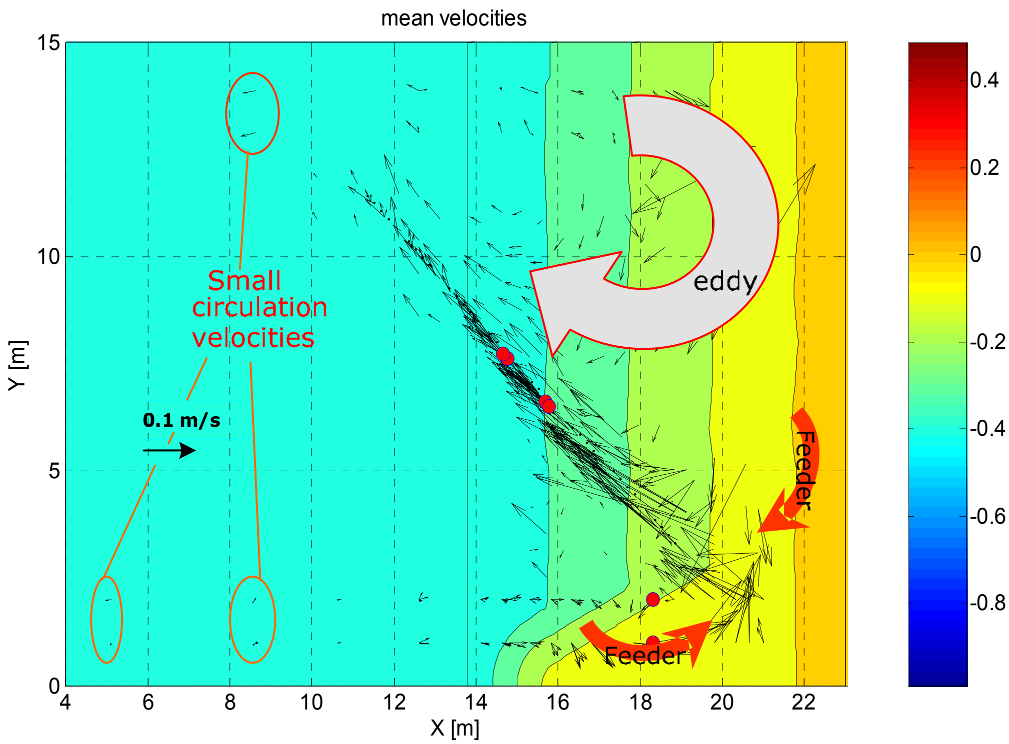

Figure 5-9: Mean velocity: the colour scale on the right represents the bed-level in meters, relative to the still water level. The velocity is depicted by the black arrows, where the length of the arrows corresponds to the velocity magnitude; the reference arrow for scaling is shown on the left: 0.1 [m/s]. The eddy and feeder currents are indicated by white and orange arrows.

In order to make sure that rip current velocities are measured and not circulation patterns of the basin, a series of velocity measurements close to the wave generator have been made (section 2.5). Circulation patterns of the basin can be regarded negligible when these velocities are very small, if observed (see 'small circulation velocities' in Figure 5-9).

The set-up induced longshore currents (Figure 5-8) manifests itself in the feeders and eddy circulation. Offshore, before approaching the reef, the velocities are almost zero. Entering the reef, the mean velocity increases and changes direction from onshore to offshore into a rip current. On the slope at the reefless-side similar mechanisms result in an eddy circulation. The development of the eddy is related to the influence of the rip current on the wave pattern (subject of section 5.6).

5.6 Influence of the rip current on the wave pattern

The bottom geometry in combination with the generated waves ultimately result in the generation of the rip current circulation which in its turn affects the wave pattern through wave-current interaction. Wave heights, current velocities, shoaling effects and refraction are complex interdependent processes which only can be solved iterative. The in-situ measurements have been analyzed, focusing on theoretically expected refraction and shoaling (section 3.1) for the given bathymetry and occurring currents.

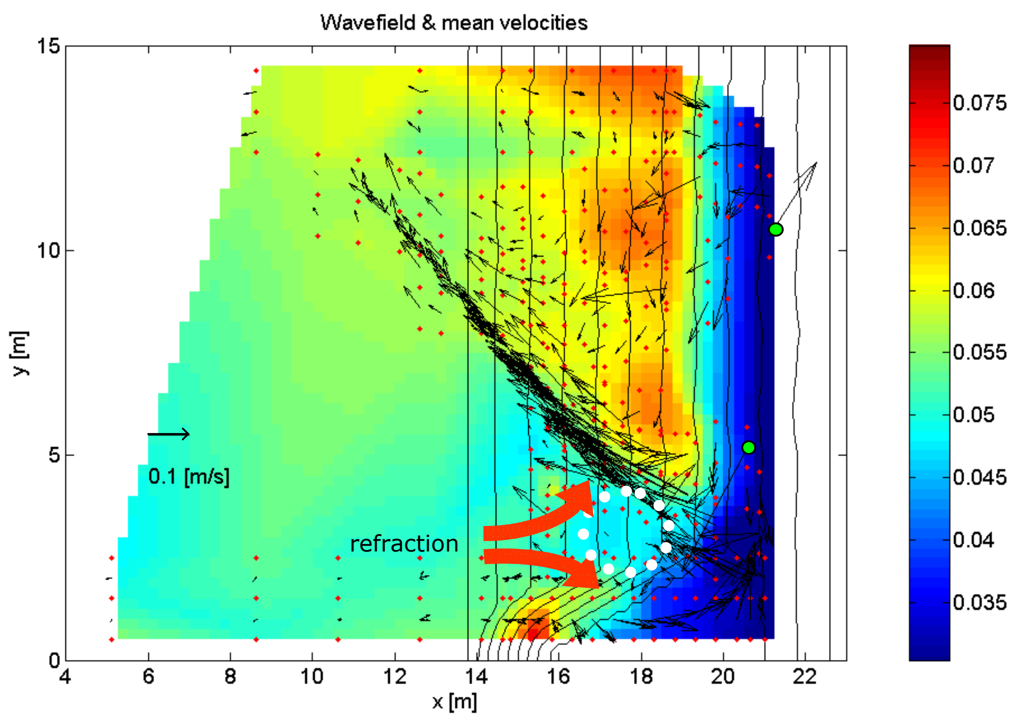

Figure 5-10: Wave height distribution (colour scale) and mean velocities (black arrows). In the indicated white-dotted area, refraction (red arrows) is dominant over shoaling. Wave heights [m] are indicated by the colour bar on the right; velocity scale is depicted in the figure by the black arrow; green arrows indicate unreliable measurements due to limited water depth at the EMF's; red dots indicate locations of the WHM's.

Next to the rip, indicated by the white dotted circle in Figure 5-10, the wave height is reduced due to refraction caused by the strong rip current and bathymetry of the reef. Therefore, the effect of refraction is stronger than the effect of shoaling (which would result in a higher wave height).

The flow velocity next to the reef ($x \approx 14$-17 m; $y \approx 2.5$ m) is minimal. Here waves and flow have the same direction and don't influence each other. At the reefless-side, next to the rip current ($x \approx 18$-19 m; $y \approx 5$-6 m), a complexity of shoaling and refraction effects takes place resulting in higher waves. The contribution of current refraction focuses waves. In combination with shoaling due to both the bathymetry and the rip current (at its maximum velocity area) this results in high waves. At the top of the reef ($x=14$ m; $y=0.5$ m), refraction focuses waves and results in high waves (indicated by the red colour Figure 5-10).

5.7 Repeatability of the rip current

The generation of the rip current in a given area has been presented in previous sections. The scope of this section is to examine if there is a repeatable pattern in time and space of the meandering of the rip current. Close to the reef the path of the rip current is restricted and farther away the meandering increases and is less predictable.

The location of the rip current meandering is shown by means of the variance of the low-pass filtered, time-averaged local velocities (VLF-velocities), obtained from all sequential in-situ measurements. The present analysis of in-situ measurements does not provide information about the spatial evolution of the current velocities.

Magnitude and direction of the VLF-velocities of the rip cannot be derived from the in-situ measurements because of limitations in the experimental set-up; velocities cannot be measured instantaneously at all locations of the basin. Therefore additional particle image velocity (PTV) measurements are used to identify both the direction and the magnitude of the rip-current meandering in time and space.

In-situ as well as PTV measurements are used to analyze the repeatability of the pattern of the rip current. In-situ and PTV data were obtained under comparable conditions, but not during the same measurement and are therefore not identical. The actual comparison between PTV and EMF measurements will be discussed in section 5.8.

To analyse the rip-current behaviour, the measured flow velocities have been low pass filtered at 0.03 Hz for both in-situ and PTV measurements. To identify the meandering of the rip current, all frequencies above f_lob, corresponding to half the group frequency, have been removed. By de-trending the very-low-frequency velocities, the mean circulation in the basin has been eliminated retaining the rip-current meandering effect only. The frequency of the meandering of the rip current is represented by f_loo. A scheme of the applied filters is presented in Figure 5-11.

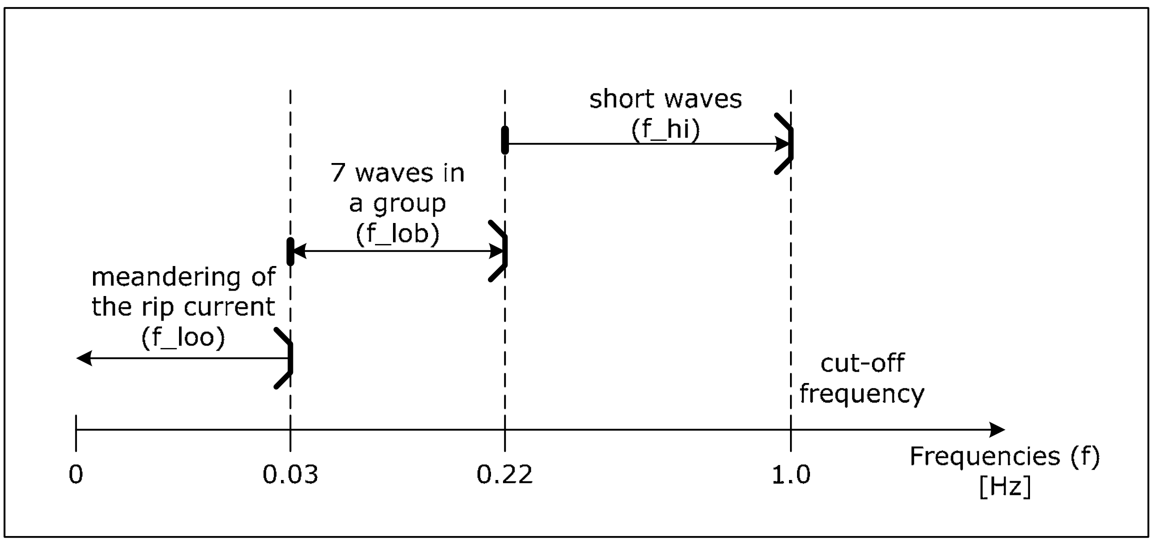

Figure 5-11: Schematic representation of the applied filters

Figure 5-12 presents the VLF component (filtered at 0.03 Hz) of the current velocity field. For this analysis, the same dataset as for the mean velocities (section 5.5), has been used.

Near the reef, the VLF-velocities of the rip are at a maximum, decreasing in offshore direction of the rip current. The horizontal excursion of the meandering rip-current increases with decreasing VLF-velocities, covering a larger area (see Figure 5-12).

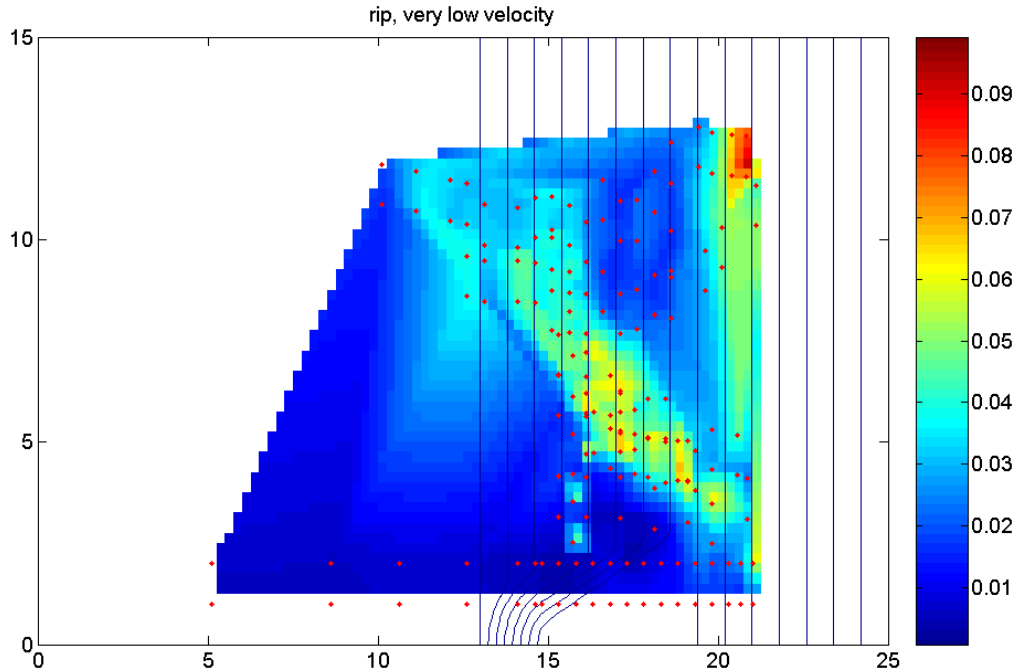

Figure 5-12: Top view of the wave basin with meandering rip-current velocities, filtered at 0.03Hz. The colour bar indicates the VLF-velocity ($\sqrt{U_{rms\_loo}{}^{2} + V_{rms\_loo}{}^{2}}$ [m/s]). The red dots indicate the locations of the EMF's

Initially, near the reef, the direction of the rip current is dominated by the high mean velocities. The rip current is forced in one certain direction, limiting the development of oscillations to a narrow path. In the mean direction of the rip current the meandering increases, ultimately disappearing where the rip-current velocities are no longer detectable.

No clear pattern of the meandering of the rip current can be derived from the in-situ VLF-velocity analysis (see Figure 5-12), indicating that the meandering of the rip current does not develop through a repeatable path, confirming the previously stated assumption.

The direction and magnitude of the rip-current meandering in time and space have been visualized by PTV measurements. At three stages of the measurement, snap shots are taken. Between snapshots a 15 seconds interval was applied, taking into account the time frame of the meandering of the rip current. Both VLF-velocities only and the mean velocity in combination with the VLF-velocities are presented (see Figure 5-13).

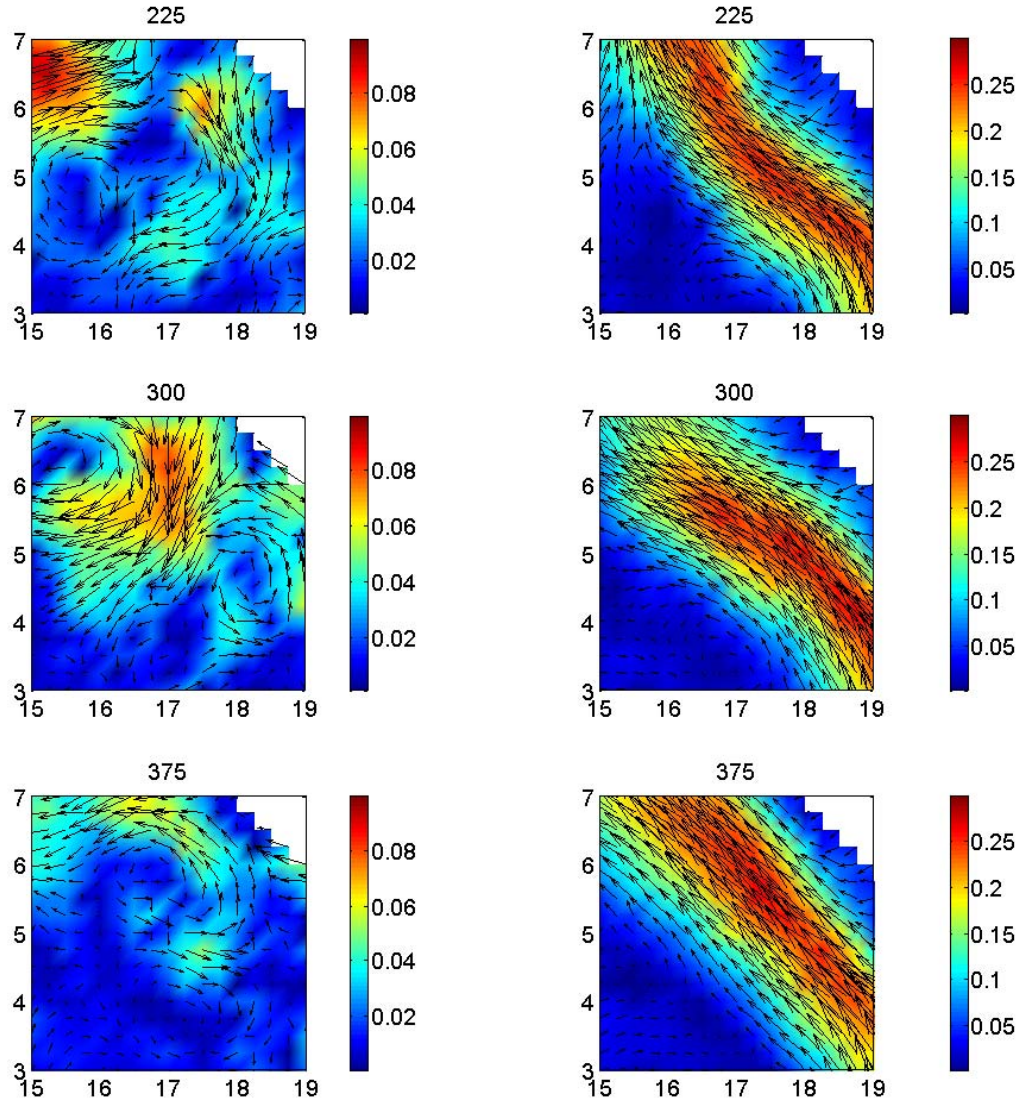

Figure 5-13: Rip current (PTV) filtered at 0.03 Hz (zoomed in) for three time increments (time interval equals 15 seconds). Left panel shows the VLF-velocity; right panel shows VLF-velocity, superposed on the mean velocity

Comparing the magnitude of the VLF-velocity to the VLF-velocity superposed on the mean velocity shows that the mean velocity is approximately three times the VLF-velocity, dominating the overall velocity picture.

Comparison of the three snap shots of the VLF-velocities shows the generation and disappearance of an eddy. The impact of this eddy on the mean flow is clearly visible (Figure 5-13), and determines the development and directions of the rip current.

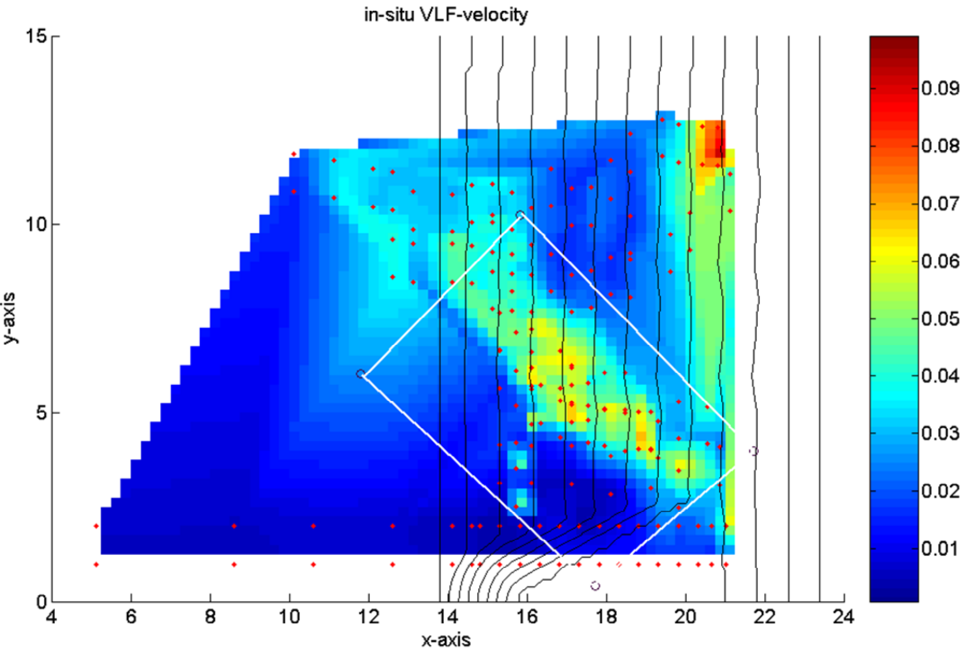
in-situ VLF-velocity
y-axis
x-axis
15
10
5
0
4
6
8
10
12
14
16
18
20
22
24
0.09
0.08
0.07
0.06
0.05
0.04
0.03
0.02
0.01

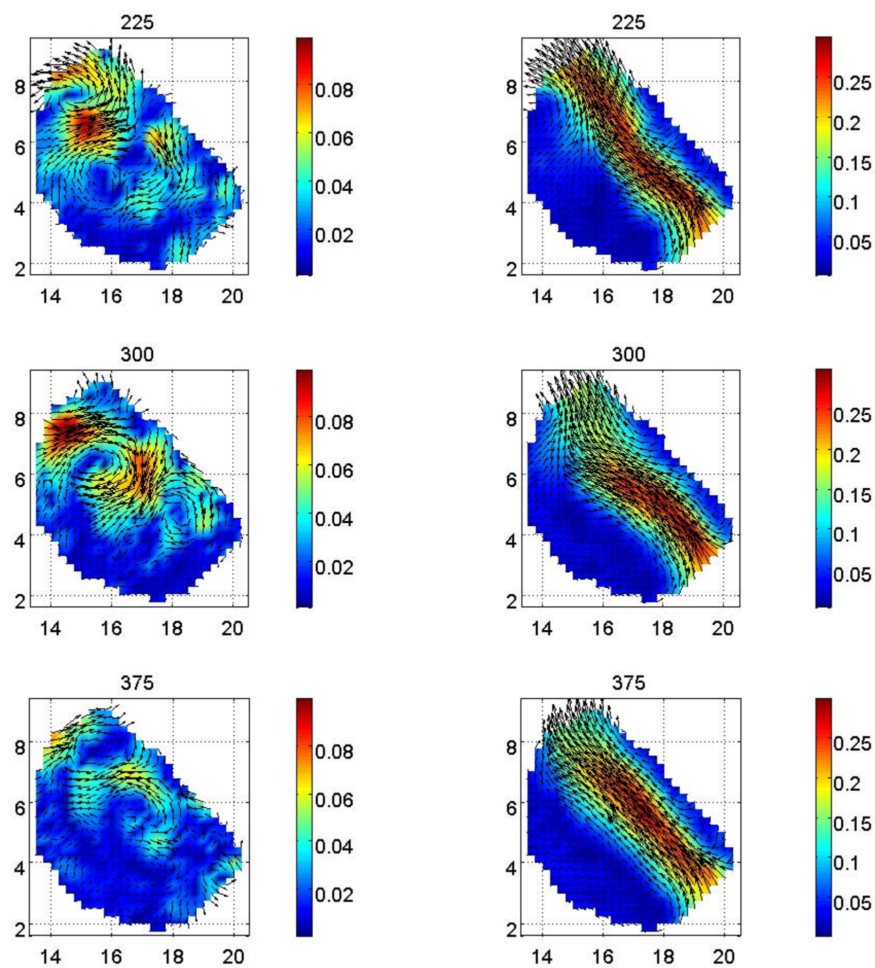
225
225
300
300
375
375
14
16
18
20
2
4
6
8
0.08
0.06
0.04
0.02
0.25
0.2
0.15
0.1
0.05

Figure 5-14 (previous page): Rip current (top panel in-situ, six bottom panels PTV) filtered at 0.03 Hz for three time increments (PTV, time interval equals 15 seconds). Left panels show the VLF-velocity; right panels show VLF-velocity, superposed on the mean velocity

It is observed that the in-situ VLF-velocity is lower than the PTV. The difference between the in-situ VLF-velocity magnitude compared with the PTV measurements is explained by the fact that the PTV-results are instantaneous velocities, whereas the in-situ measurements are presented as root-mean-square velocities. Visual inspection of the PTV-estimated velocity field shows that the meandering has a stochastic character consistent with the generation of eddies in the rip-current flow.

5.8 Correlation between PTV and in-situ measurements

Both in-situ measurements and PTV measurements indicate a stochastic character of the meandering of the rip current (section 5.7), only regarding VLF-velocities. In this section it is analysed to what extent velocities measured in the rip current (in-situ) correlate to surface velocity measurements (PTV) for higher frequency velocities (HF). Furthermore, magnitude and directions of the mean velocities of both PTV and in-situ measurements are compared.

The HF-velocities of the in-situ measurements are obtained near the bottom (at 1/3 h). In order to be able to compare in-situ to PTV measurements, in-situ measurements are transferred to velocities at the surface using the dispersion relation. The presence of a mean current implies a Doppler shift which has been taken into account in the transformation of the in-situ orbital velocities to the surface through the general dispersion relation ($\omega' = \omega + kU_{//}$) .

The stochastic character of the rip current requires the need to classify the mean velocity magnitude to be able to compare the in-situ measured data with the PTV measurements (Figure 5-15). The coordinates in the basin for the presented PTV and in-situ data are identical (Figure 5-15).

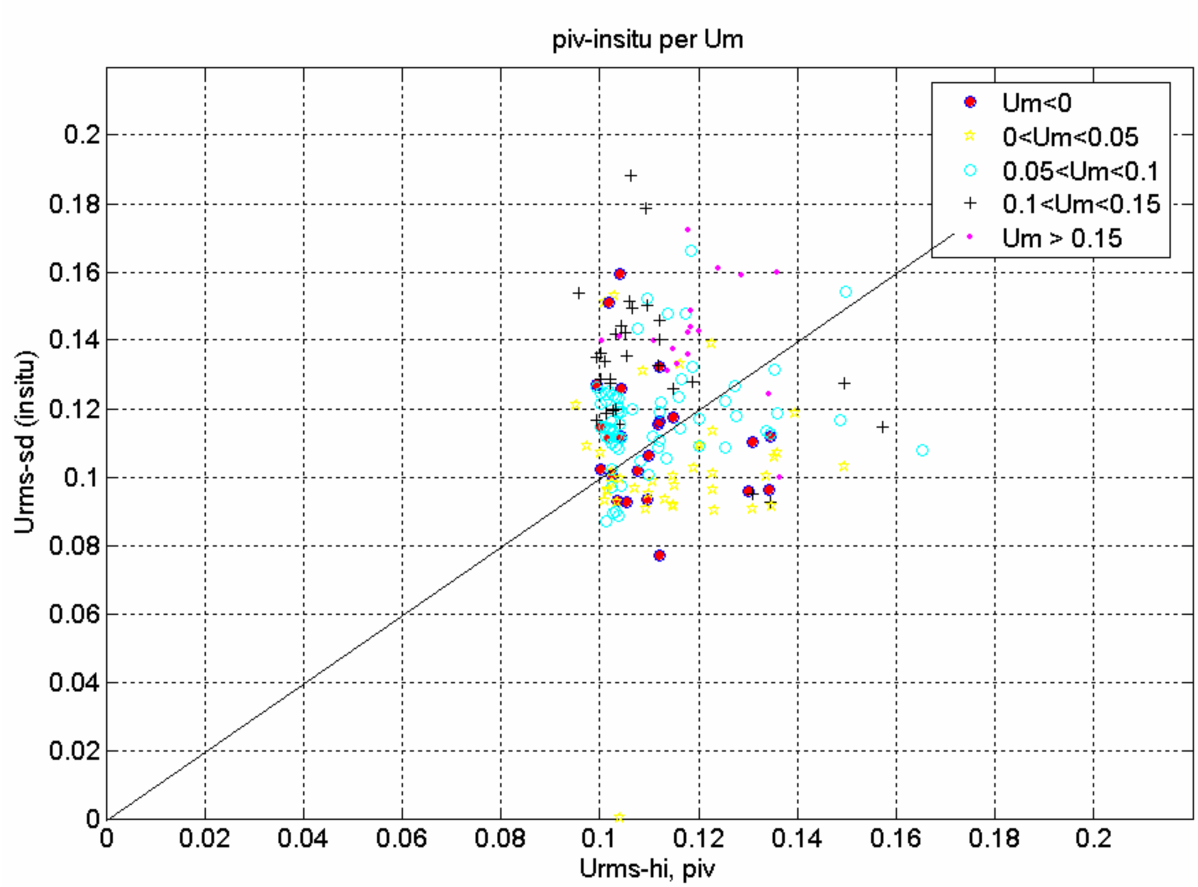

Figure 5-15: PTV velocities versus in-situ velocities, transferred to the surface, classified for varying mean velocities. Um<0 represents the mean velocity in offshore direction. Perfect agreement of Urms-sd (in-situ) with Urms-hi PTV is displayed by the black line. Velocities are in [m/s]

The presented PTV rms-velocities vary from 0.1 m/s to 0.16 m/s. The transferred in-situ measurements vary from 0.08 m/s to 0.18 m/s. Both PTV and transferred in-situ measurements indicate a comparable range of HF-velocities at the surface (Figure 5-15). Comparing PTV rms-velocities to in-situ rms-velocities leads to the observation that they do not correlate well and show a large amount of scatter.

For Um>0.15 m/s corresponding to strong mean rip-current velocities, in-situ rms-velocities are substantial larger than the PTV rms-velocities. Similar behaviour is observed for the mean velocities in the range 0.1 m/s < Um < 0.15 m/s. For small mean velocities, 0 m/s < Um < 0.05 m/s, in general in-situ rms-velocities are underestimated, relative to the PTV rms-velocities.

Although for mean velocities Um<0 m/s the PTV and in-situ rms-velocities do not show a clear relationship, where the observed differences between in-situ and PTV rms-velocities are evenly distributed. For mean velocities ranging from 0.05 m/s to 0.1 m/s, the PTV and in-situ rms-velocities are also evenly distributed around the line of perfect agreement. For several data points, PTV rms-velocities match the in-situ rms-velocities fairly well (Figure 5-15).

In general, for lower mean velocities the in-situ rms-velocities tend to be overestimated compared to PTV rms-velocities, higher mean velocities underrate the in-situ rms-velocities, relative to the PTV rms-velocities (Figure 5-15). Possible reason for this might be that meandering effects of the rip current in the vertical, registered by the EMF sensors, cannot be observed by surface velocity measurements (PTV). This indicates that the transformation from bottom velocities into surface velocities requires further investigation (see section 5.9).

Mean velocities obtained from PTV measurements and in-situ measurements are plotted together (Figure 5-16) in order to compare direction and magnitude. Previously (section 5.5), mean velocities derived from in-situ measurements were already presented (Figure 5-9. Mean velocities from PTV measurements represent surface flows and are measured synoptically. Mean velocities from the in-situ measurements are averaged in time for individual coordinates in the basin.

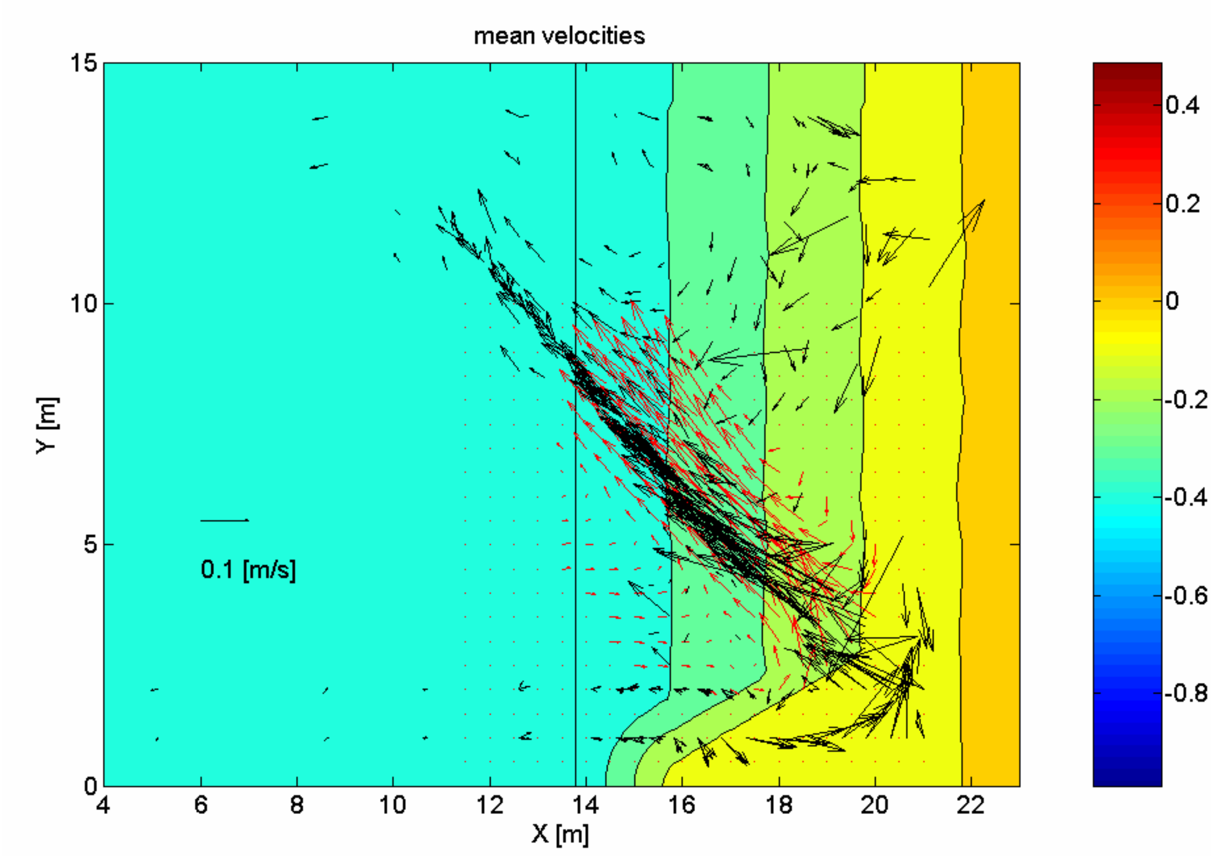

Figure 5-16: Mean velocities, obtained from PTV measurements (red arrows, include Stokes drift) and in-situ measurements (black arrows).

Similar to the HF-velocities (Figure 5-15), the mean velocities obtained from PTV and in-situ measurements are of the same order of magnitude. In the rip current, high mean velocities were found with both in-situ measurements and with PTV measurements. Offshore and approaching the reef, both PTV and in-situ measurements indicate very low mean velocities.

Next to the rip current, at the reef-side of the rip, in-situ measurements and PTV measurements indicate slightly different velocities, both in direction and magnitude. Possible explanation for this difference is the vertical structure of the velocity profile, incorporated in the in-situ based mean-velocities and not taken into account for PTV measurements. Also the Stokes drift which affects the PTV-estimated mean velocities will result in differences from the in-situ measurements.

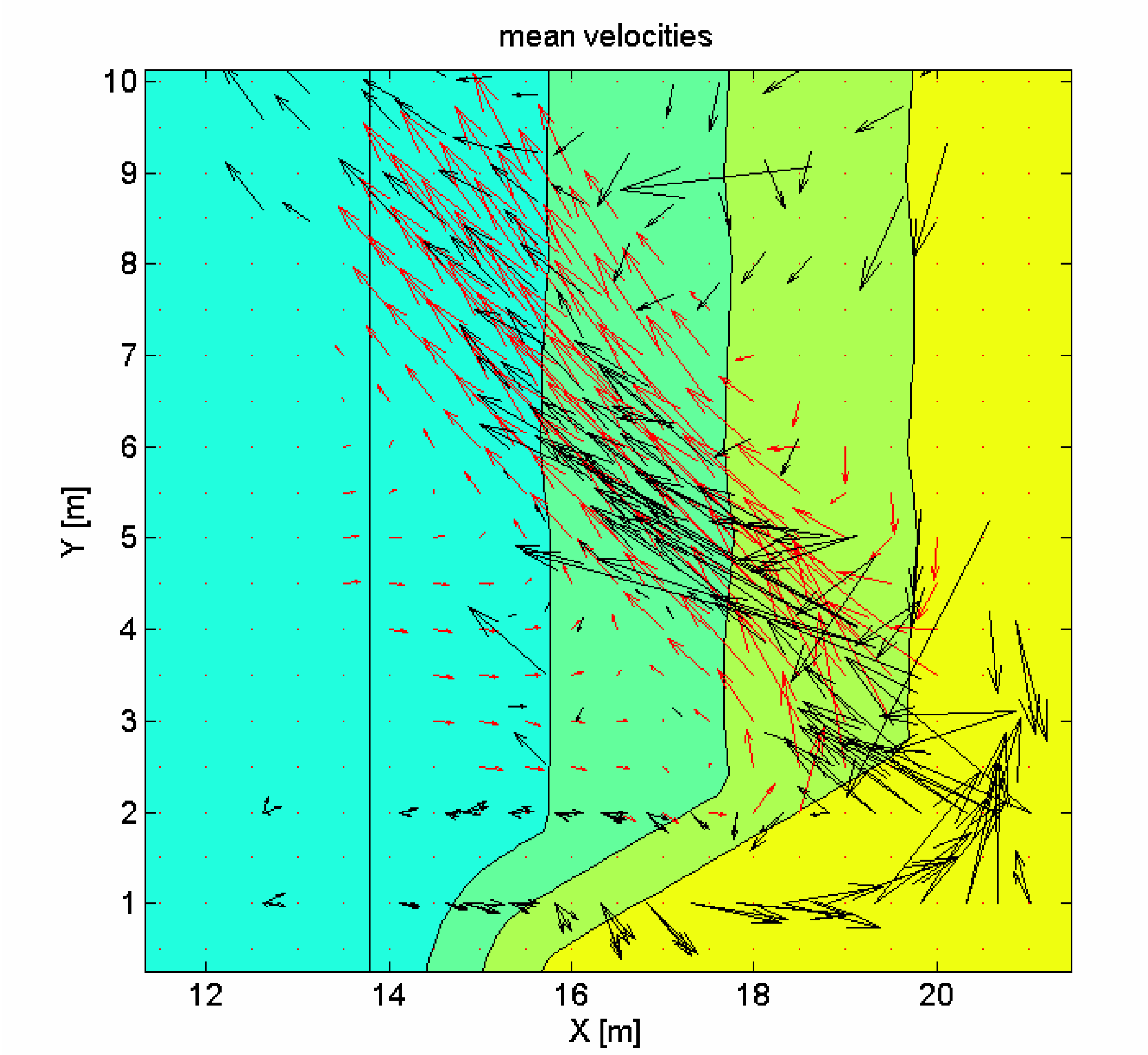

Figure 5-17: Detail of mean velocities, obtained from PTV measurements (red arrows) and in-situ measurements (black arrows). Presented PTV velocities are not corrected for Stokes drift.

Examining the mean PTV-based velocities in detail in the direction of the rip current (Figure 5-17), the persistent shift in direction towards the beach compared to the in-situ observations is expected to be due to the Stokes drift. Surfing behaviour of the floats on the waves was observed as well, potentially partially responsible for the persistent shift.

Mean velocities obtained from in-situ and PTV measurements show a good correlation, both in magnitude and direction. Observed minor differences are expected to be caused by the Stokes drift and the possible influence of the vertical structure of the velocity profile, which affects the in-situ based mean-velocities and are not taken into account for PTV measurements. In section 5.9 measurements on the vertical structure of the velocity profile will be presented.

5.9 Vertical structure of velocity distribution in the rip current

As stated with the research issues (section 2.4), moving into the direction of the rip, it is assumed that the highest velocities occur in the upper part of the rip, near the surface (Haas et al., 2002). To examine this, velocity measurements at different distances from the bottom, following the flow of the rip current, see Figure 5-18, were performed. Different methods have been applied to determine the vertical velocity profile of the rip current.

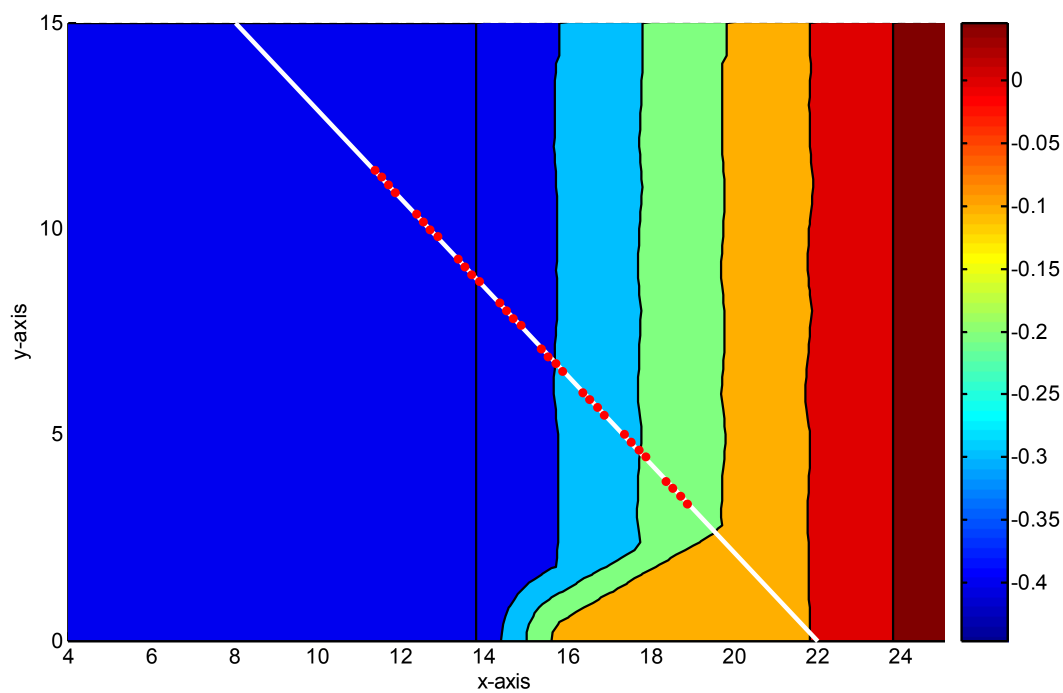

Figure 5-18: Deployment of measurements in the rip current. The white line indicates the expected path of the rip current. Red markers indicate positions of the EMF's. The colour scale on the right shows the position of the bottom [m].

Measurements in the vertical should ideally be taken simultaneously per position, given the stochastic character of the rip current. Experimental boundary conditions (section 2.5) require that the velocity measurement instruments (EMF's) have a minimal distance between them of 25 cm in order to obtain reliable data.

Consequence of this experimental requirement is that measurements cannot be taken simultaneously at the same position given the limited water depth.

Initially, the EMF's were positioned as indicated in Figure 5-19, to prevent slip stream effects (denoted arrangement HL in the following). Disadvantage of the HL arrangement is that in the direction of the rip current, the velocity is expected to decrease because of the increasing water depth, frictional effects and dispersion in the measurement direction. Arrangement LH (left image in Figure 5-19 is only applied to determine the decreasing effect of the rip current velocity and to verify the magnitude of slip stream effects.

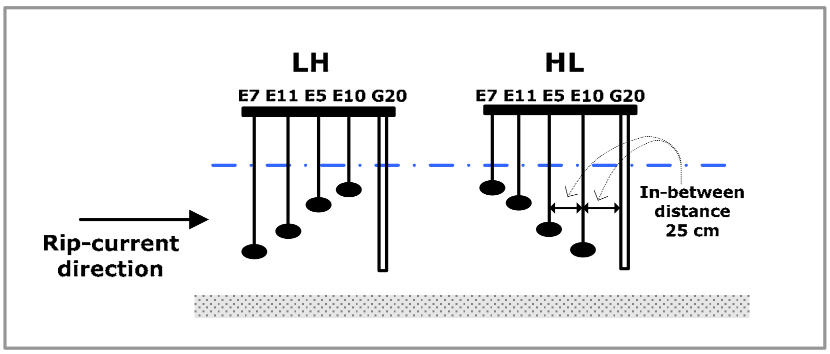

Figure 5-19: Arrangement of EMF's in the mobile frame relative to the rip current direction. Position of the instruments, relative to the bottom: at ¼, $^{1}/_{3}$, ½, ¾ times h, from low to high (LH) left image, from high to low (HL) right image.

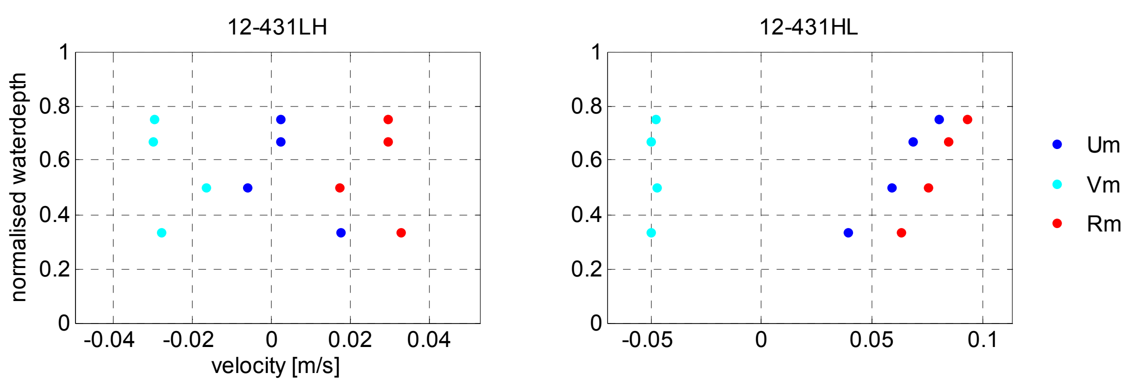

Figure 5-20: Vertical structure of mean flow velocity offshore with LH arrangement (left panel) and HL arrangement, consistent with expectations (right panel)

Measurements with the LH-arrangement show a high level of disturbance probably due to slip-stream effects, confirming the assumption stated before (left panel Figure 5-20). The vertical flow-velocity structure obtained with the HL-arrangement corresponds to the expected vertical distribution with higher velocities at the surface (right panel Figure 5-20).

It is observed that close to the reef, the velocity distribution is more uniform over the depth and in the offshore direction of the rip current; the highest velocities appear in the upper part of the vertical. However, it is unclear whether this effect is due to decreasing flow velocities of the rip current itself or due to the vertical distribution of the flow velocity in the rip current.

To overcome this, a third method is applied (Figure 5-22). For this, the condition that measurements should be taken simultaneously was abandoned. At fixed positions, sequential measurements were performed at 1/3rd, ½ and 2/3rd of the water depth.

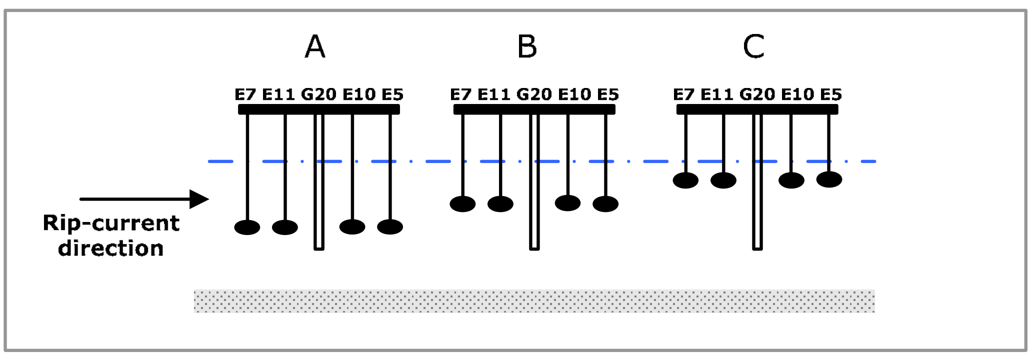

Figure 5-21: Arrangement of EMF's in the mobile frame parallel to the rip current direction.

Results from section 5.8 indicate that the vertical-velocity distribution in rip currents is expected to vary in x; y direction as well due to the stochastic rip-current behaviour. To account for this effect the local coordinate system is adjusted such that the upstream current-meter is aligned with the rip-current flow direction.

The EMF-frame was positioned in the flow direction of the rip current. The upstream EMF on the frame determines the local axes for all EMF's in that specific measurement. Ultimately, this results in a velocity component in the direction of the rip current and a component perpendicular to the local rip-current direction.

The magnitudes of the resultants of the parallel and perpendicular velocities ($r = \sqrt{u^2 + v^2}$) are compared for different positions in the vertical (Figure 5-22).

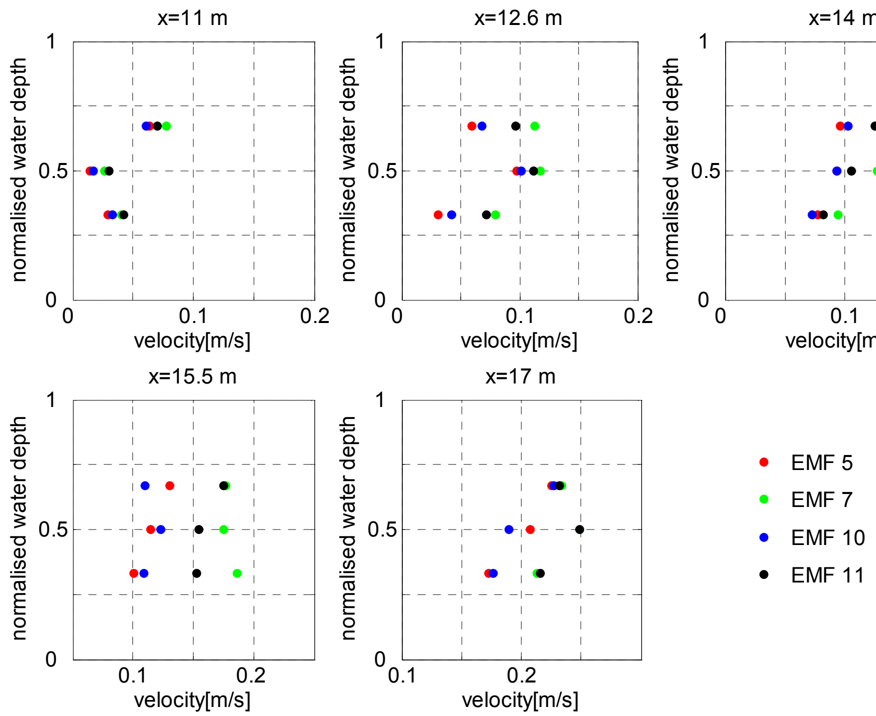

Figure 5-22: Vertical velocity distribution in the rip-current velocity for sequential in-situ measurements for x coordinates: x=11 m; x=12.6 m; x=14 m; x=15.5 m; x=17 m. The legend presents the codes for the EMF's. EMF 5 is the upstream EMF.

Per vertical position, four mean velocities are presented. All velocities presented have been transformed to the direction of the rip current as observed by r7. A variation in the vertical velocity distribution could be due to the fact that the assumption of a local axis system for the frame is not valid. It can be observed that the average velocities decrease in offshore direction.

At the most offshore located positions (x=11 m), at all vertical positions, the observed transformed velocities overlap. This indicates that the EMF-frame experiences comparable circumstances during the measurements. It is interpreted that due to the relatively large oscillation of the rip current offshore (section 5.7), all instruments on the EMF-frame observe comparable conditions.

Close to the reef (x=17 m), at the lower vertical positions (z=0.033; z=0.05) the EMF's present a strong variation in velocity, indicating that the EMF-frame was not fully covered by the rip current spatially (non-uniform conditions for the EMF's)(see section 5.7). Probably the bathymetry concentrates the currents closer to the bottom rather than at the surface, resulting in a larger rip-current area near the surface than near the bottom. With the size effects of the EMF-frame, this might give an explanation why the largest variation in velocities is observed near the bottom.

In the intermediate zone, between 'close to the reef' and 'far offshore', (x=12.6 m; x=14 m) the general trend is that velocities near the bottom tend to be smaller than velocities near the surface. Velocities from the in-between sensor deviate from the trend between bottom and surface velocity. From the large variation of the measured velocities, it is concluded that the instruments on the EMF-frame did not observe comparable conditions.

At (x=17), the surface velocities match, at (x=14) the bottom velocities match. Interpretation of the observed vertical velocity distribution at (x=15.5 m) is that a transition takes place from behaviour near the reef to behaviour in the intermediate zone.

The effect of the size of the EMF-frame relative to the size of the studied rip-current effects observed in the sequential vertical velocity measurements is expected to be valid for the HL-arrangement of the EMF's as well. However, vertical velocity distributions, measured by this latter method do not show this effect due to single measurement points. This emphasizes the necessity, as stated before, to measure vertical velocity distribution in rip currents simultaneously over the vertical.

6 DISCUSSION AND FUTURE DIRECTIONS

The primary objective of this research is to analyse wave and rip-current characteristics in the presence of a submerged reef. In literature (MacMahan et al., 2006) few quantitative field and laboratory measurements have been reported. An additional objective of this study is to provide a suitable dataset to validate a computer-based rip-current model.

In this experiment, the assumption is that close to the reef the path of the rip current is restricted and farther away the meandering increases and is less predictable. Furthermore, the correlation between velocities at the bottom and the water surface is studied. In detail, aspects of the repeatability of the rip current and the vertical velocity distribution have been studied.

The submerged reef was designed for generating surfable waves in Dutch coastal circumstances. The anticipated surf wave height in the field varied from 0.8 to 1.6 m in combination with a period ranging from 6 to 10 seconds (Henriquez, 2005). Comprehensive measurements in a laboratory wave-basin were performed. An extensive dataset on PTV and in-situ measurements has been collected. Complying the selected field conditions resulted in application of a bi-chromatic wave height of 8 cm and a mean wave period of 2.26 s.

Applying the dimensionless relationship between the rip-current mean velocity, deep-water wave height and the local water depth (MacMahan et al, 2005) on the measured wave heights (6 cm) and rip-current velocities (10 to 25 cm/s), indicate a field wave height of 0.8 m as expected by Henriquez (Henriquez, 2005). Converting the measured mean velocities in the wave basin to field conditions would result in rip-current velocities up to 2 m/s. Field observations (MacMahan et al, 2006) report substantially lower mean rip-current velocities (~0.45 m/s) and comparable maximum rip-current velocities. The continuous driving force for the development of the rip current and the fixed bathymetry in the wave basin might be the explanation for this difference.

To determine the repeatability of the generated waves, a reference gauge was placed just in front of the wave maker. The repeatability has been assessed by inter-comparing the offshore wave heights for different sets of tests. Because of the bi-chromatic character of the generated waves, the standard deviation of the wave-group envelope, responsible for the forcing of the long waves, has to be taken into account. The overall conclusion on the repeatability of the wave generation is that the generated waves are comparable for different sets.

It was observed that the waves on the reef break differently from those on the slope adjacent to the reef. This difference in wave breaking in combination with the wave (de)focusing due to refraction, results in a water level set-up gradient, the driving force for the development of the current. Water level set-up and set-down measurements indicate the expected locations of the feeder currents. Mean velocity measurements are performed to locate the rip current.

The rip-current meandering is shown by means of the variance of the low pass filtered time-averaged local velocities, obtained from sequential in-situ measurements. No clear pattern of the meandering of the rip current can be derived from the in-situ VLF-velocity analysis. Visual inspection of the PTV-estimated velocity field shows that the meandering has a stochastic character consistent with the generation of eddies in the rip-current flow.

Vertical-velocity measurements were done by simultaneous measurements at different locations and by sequential measurements at identical locations. The available instruments prohibited synoptical measurements. In both cases the rip current could not be detected by all the instruments, probably due to the size of the EMF-frame relative to the size of the rip current.

In the rip channel, the velocity distribution is more uniform over the depth, and in the offshore direction of the rip current the highest velocities appear in the upper part of the vertical. However, it is unclear whether this effect is due to decreasing flow velocities of the rip current itself or due to the vertical distribution of the flow velocity in the rip current.

In laboratory research on the vertical structure of the velocity distribution, Drønen (Drønen et al, 2002) reported that off-shore directed rip-currents have the tendency to show maximum velocities near the bottom. Haas and Svendsen (Haas et al, 2002) report off-shore rapidly twisting velocity profiles over the depth with much stronger velocities near the surface, corresponding to the presented measurements in this report. Drønen's model lay-out (Drønen et al, 2002) with a fixed position of the rip current, prohibiting meandering, might be the cause of the contradicting observations.

The results emphasize the necessity, as stated before, to measure the vertical velocity distribution in rip currents simultaneously over the vertical. It is recommended to perform this type of measurements with instruments, capable of measuring the vertical velocity distribution. These future results can be compared with a HL-distribution of the EMF's as presented in this report.

For this experiment both in-situ measurements and video observations have been collected. The focus of this research was on the analysis of the in-situ measurements; only a limited portion of the video observations was regarded. The obtained video observations are available for further analysis.

7 REFERENCES

Battjes, J.A., 1974. Surf Similarity. Proc. of the 14th International Coastal Conference, Am. Soc. of Civil Eng., Copenhagen, pp.467-479.

Battjes, J.A., 1986. Collegehandleiding b76, Korte Golven. Delft University of Technology, Faculty of Civil Engineering and Geosciences..

Bellotti, G., 2004. A simplified model of rip currents systems around discontinuous submerged barriers. Coast. Eng. 51, 323-335.

Cáceres, I., Le Hai Trung, van Ettinger, E., Reniers, A.J.H.M., Uijttewaal, W.S.J., 2007. Wave and flow response to an Artificial Surf Reef. Laboratory measurements. *In press*.

Chen, Q., Dalrymple, R.A., Kirby, J.T., Kennedy, A.B., Haller, M.C., 1999. Boussinesq modelling of a rip current system. J. Geophys. Res., 104.

Coastal Engineering Manual 1110-2-1100 (2006), Part II, Washington DC, USA.

Dean, R.G., Dalrymple, R.A., 1984. Water wave mechanics for engineers and scientists. World Scientific Publishing Co., Singapore.

Drønen, N., Karunarathna, H., Fredshoe, J., Sumer, B.M., Deigaard, R., 2002. An experimental study of rip channel flow. Coast. Eng. 45 (3-4), 223-238.

Dyhr-Nielsen, M., Sørensen, T., 1970. Some sand transport phenomena on coasts with bars. Proceedings of the 12th International Conference on Coastal Engineering. ASCE, New York. pp 855-866.

Fredsøe, J., Deigaard, R., 1992. Mechanics of Coastal Sediment Transport. World Scientific Publishing Co., Singapore.

Haas, K.A., Svendsen, I.A., 2002. Laboratory measurements of the vertical structure of rip currents. J. Geophys. Res., 107. doi:10.1029/2001JC000911

Haas, K.A., Svendsen, I.A., Haller, M.C., Qun Zhao., 2003. Quasi-three-dimensional modelling of rip current systems. J. Geophys. Res., 108. doi:10.1029/2002JC001355

Haller, M.C., Dalrymple, R.A., 1999. Rip current dynamics and nearshore circulation. University of Delaware, Ocean Eng. Lab., Research report No. CACR-99-05

Haller, M.C., Dalrymple, R.A., 2001. Rip current instabilities. J. Fluid Mech. 433, 161-192.

Haller, M.C., Dalrymple, R.A., Svendsen, I.A., 2002. Experimental study of nearshore dynamics on barred beach with channels. J. Geophys. Res. 107 (14), 1-21.

Haslett, S.K., 2000. Coastal Systems. Routledge Taylor and Francis Group, USA.

Henriquez, M., 2005. Artificial surf reefs. Thesis report, Delft University of Technology, Faculty of Civil Engineering and Geosciences.

Kennedy, A.B., Thomas, D., 2004. Drifter measurements in a laboratory rip current. J. Geophys. Res. 109, C08005. doi:10.1029/2003JC001927.

Komar, P.D., 1976. Beach processes and sedimentation. Englewood Cliffs, New Jersey, Prentice-Hall Inc. pp.343-350.

MacMahan, J.H., Thornton, E.B., Stanton, T.P., Reniers, A.J.H.M, 2005. RIPEX: Observations of a rip current system. Marine Geology 218, pp.113-134.

MacMahan, J.H., Thornton, E.B., Reniers, A.J.H.M., 2006. Rip current review. Coast. Eng. 53, 191-208.

Park, Koo-Yong, Borthwick, A.G.L., 2001, Quadtree grid numerical model of nearshore wave-current interaction. Coast. Eng. 42, 219-239.

Phillips, O.M., 1977. The Dynamics of the Upper Ocean. 2nd ed. Cambridge University Press, New York.

Reniers, A.J.H.M., MacMahan, J.H., Thornton, E.B., Stanton, T.P., 2006. Modelling infragravity motions on a rip-channel beach. Coast. Eng. 53, 209-222.

Rijn, L.C. van, 1990. Principles of Fluid Flow and Surface Waves in Rivers, Estuaries, Seas and Oceans. Aqua Publications, The Netherlands.

Smith, J.A., Largier, J.L., 1995. Observations of nearshore circulation: Rip currents. J. Geophys. Res. 100. pp 10,967-10,975.

Svendsen, I.A., 1984. Mass flux and undertow in a surf zone. Coast. Eng. 8, 347-365.

Zou, Q., Hay, A.E., Bowen, A.J., 2003. Vertical structure of surface gravity waves propagating over a sloping seabed: Theory and field measurements. J. Geophys. Res. 108, 3265. doi.1029/2002JC001432.

Internet reference:

(1) http://www.actuelewaterdata.nl/golfgegevens

(2) http://www.coastal.udel.edu/faculty/rad/wavetheory.html

(3) http://www.sea.uct.ac.za/sea2002s/waves/wavemaker.html

ANNEX 1 : DEPLOYMENT OF THE GAUGES

breaking of the waves on the slope takes place at 19[m]/ 19.5[m] / 20 [m] / 20.5[m] (depends on which wave in the wavegroup)

Measurements at the 'rifless side'
duration measurements is 10 minutes
doormeting *(= measurement without waiting until the waterlevel is still again)* after at least **10** min.of wavemaking =>i.e.doormeting(**10**)

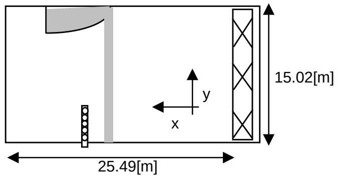

Wavegauges are placed 3 a 4 cm under the waterlevel, just free from the bottom
pressure-meters are placed as high as possible, at a fixed distance from the surface
EMS:needs a free space around of about 5 cm, 3 cm is the limit

during all the measurements the position of G18 does not change

position G18:	x-axis	y-axis	waterdepth	distance from the bottom
	1,5	5	0,4	0,03

distance to the side	G 21	EMS 10	G 20	EMS 11	G 19
Rifside	0,5	1,005	1,505	1,995	2,5
Rifless-side	0,637	1,142	1,642	2,132	2,637

Week 30	ascifile	distance from ref.point	x-axis position G21 E10 G20 E11 G19	G21 y	E10 y	G20 y	E11 y	G19 y	Water depth at the gauges [m]:	distance from the bottom G21	distance from the bottom E10	distance from the bottom G20	distance from the bottom E11	distance from the bottom G19
'waterdepth filled up to 0,40 [m], gauges are cleaned														
	7bc_ma1	12,5	12,62	0,637	1,142	1,642	2,132	2,637	0,4	0,03	0,13	0,03	0,13	0,03
	7bc1_ma1	12,5	12,62	0,637	1,142	1,642	2,132	2,637	0,4	0,03	0,13	0,03	0,13	0,03
	7bc_ma2	8,5	8,62	0,637	1,142	1,642	2,132	2,637	0,4	0,03	0,13	0,03	0,13	0,03
doormeting(15)	7bc0_ma2	8,5	8,62	0,637	1,142	1,642	2,132	2,637	0,4	0,03	0,13	0,03	0,13	0,03
	7bc_ma3	14,5	14,62	0,637	1,142	1,642	2,132	2,637	0,335	0,03	0,11	0,03	0,11	0,03
	7bc_di2	15,2	15,32	0,637	1,142	1,642	2,132	2,637	0,3	0,03	0,1	0,03	0,1	0,03
	7bc1_di2	15,2	15,32	0,637	1,142	1,642	2,132	2,637	0,3	0,03	0,1	0,03	0,1	0,03
waterdepth filled up to 0.4[m], gauges are cleaned														
	7bc_wo1	16,2	16,32	0,637	1,142	1,642	2,132	2,637	0,25	0,03	0,08	0,03	0,08	0,03
doormeting(10)	7bc1_wo1	16,2	16,32	0,637	1,142	1,642	2,132	2,637	0,25	0,03	0,08	0,03	0,08	0,03
	7bc2_wo1	16,2	16,32	0,637	1,142	1,642	2,132	2,637	0,25	0,03	0,08	0,03	0,08	0,03
	7bc_wo2	17,2	17,32	0,637	1,142	1,642	2,132	2,637	0,2	0,03	0,07	0,03	0,07	0,03
	7bc1_wo2	17,2	17,32	0,637	1,142	1,642	2,132	2,637	0,2	0,03	0,07	0,03	0,07	0,03
	7bc_wo3	18,2	18,32	0,637	1,142	1,642	2,132	2,637	0,15	0,03	0,03	0,03	0,03	0,03
	7bc1_wo3	18,2	18,32	0,637	1,142	1,642	2,132	2,637	0,15	0,03	0,03	0,03	0,03	0,03
waterdepth filled up to 0.4[m], gauges are cleaned														
	7bc_do1	18,5	18,62	0,637	1,142	1,642	2,132	2,637	0,135	0,03	0,03	0,03	0,03	0,03
	7bc1_do1	18,5	18,62	0,637	1,142	1,642	2,132	2,637	0,135	0,03	0,03	0,03	0,03	0,03
	7bc_do2	18,675	18,795	0,637	1,142	1,642	2,132	2,637	0,12	0,03	0,03	0,03	0,03	0,03
	7bc1_do2	18,675	18,795	0,637	1,142	1,642	2,132	2,637	0,12	0,03	0,03	0,03	0,03	0,03

2nd series: Measurements at the reef-side

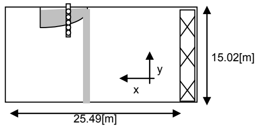

Callibration before measuring:

	ΔV [Volt]	Δx [cm]	ΔV/Δx	ρ
G19	3,08	7	0,44	ρ 80
	2,21	5	0,442	
G20	2,08	5	0,416	ρ 80
	2,9	7	0,414	
G21	2,08	5	0,416	ρ 71
	2,91	7	0,416	
G18	1,28	3,1	0,413	ρ 71

width of the bassin	15,02

distance to the side	G 21	EMS 10	G 20	EMS 11	G 19
Reefside	0,5	1,005	1,505	1,995	2,5
Reefless-side	0,637	1,142	1,642	2,132	2,637

Week 37	ascifile	distance from ref.point	x-axis position G21 E10 G20 E11 G19	y-axis position G21	y-axis position E10	y-axis position G20	y-axis position E11	y-axis position G19	water depth at G21	water depth at E10	water depth at G20	water depth at E11	water depth at G19	distance from the bottom G21	distance from the bottom E10	distance from the bottom G20	distance from the bottom E11	distance from the bottom G19
new water, gauges are cleaned																		
	7bc_50	5	5,12	14,52	14,015	13,515	13,025	12,52	0,4	0,4	0,4	0,4	0,4	0,03	0,1	0,03	0,1	0,03
	7bc_85	8,5	8,62	14,52	14,015	13,515	13,025	12,52	0,4	0,4	0,4	0,4	0,4	0,03	0,1	0,03	0,1	0,03
15min.meting	7bc1_85	8,5	8,62	14,52	14,015	13,515	13,025	12,52	0,4	0,4	0,4	0,4	0,4	0,03	0,1	0,03	0,1	0,03
	7bc2_85	8,5	8,62	14,52	14,015	13,515	13,025	12,52	0,4	0,4	0,4	0,4	0,4	0,03	0,1	0,03	0,1	0,03
	7bc_105	10,5	10,62	14,52	14,015	13,515	13,025	12,52	0,4	0,4	0,4	0,4	0,4	0,03	0,1	0,03	0,1	0,03
	7bc1_105	10,5	10,62	14,52	14,015	13,515	13,025	12,52	0,4	0,4	0,4	0,4	0,4	0,03	0,1	0,03	0,1	0,03
	7bc_125	12,5	12,62	14,52	14,015	13,515	13,025	12,52	0,4	0,4	0,4	0,4	0,4	0,03	0,1	0,03	0,1	0,03
	7bc1_125	12,5	12,62	14,52	14,015	13,515	13,025	12,52	0,4	0,4	0,4	0,4	0,4	0,03	0,1	0,03	0,1	0,03
hotstart(10)	7bc2_125	12,5	12,62	14,52	14,015	13,515	13,025	12,52	0,4	0,4	0,4	0,4	0,4	0,03	0,1	0,03	0,1	0,03
water filled up to 40 [cm]																		
	7bcN_125	12,5	12,62	14,52	14,015	13,515	13,025	12,52	0,4	0,4	0,4	0,4	0,4	0,03	0,1	0,03	0,1	0,03
	7bcN1_125	12,5	12,62	14,52	14,015	13,515	13,025	12,52	0,4	0,4	0,4	0,4	0,4	0,03	0,1	0,03	0,1	0,03

Callibration at 12.5m afterwards

	ΔV [Volt]	Δx [cm]	ΔV/Δx	ρ
G19	2,77	7	0,396	ρ 80
	2,07	5	0,414	
G20	2,1	5	0,42	ρ 80
	2,85	7	0,407	
G21	2,19	5	0,438	ρ 71
	3,07	7	0,439	

Week 37	ascifile	distance from ref.point	x-axis position G21 E10 G20 E11 G19	y-axis position G21	y-axis position E10	y-axis position G20	y-axis position E11	y-axis position G19	water depth at G21	water depth at E10	water depth at G20	water depth at E11	water depth at G19	distance from the bottom G21	distance from the bottom E10	distance from the bottom G20	distance from the bottom E11	distance from the bottom G19
	7bc_140	14	14,12	14,52	14,015	13,515	13,025	12,52	0,295	0,32	0,36	0,365	0,367	0,03	0,11	0,03	0,12	0,03
	7bc1_140	14	14,12	14,52	14,015	13,515	13,025	12,52	0,295	0,32	0,36	0,365	0,367	0,03	0,11	0,03	0,12	0,03
hotstart (14)	7bc1d_140	14	14,12	14,52	14,015	13,515	13,025	12,52	0,295	0,32	0,36	0,365	0,367	0,03	0,11	0,03	0,12	0,03
	7bc2_140	14	14,12	14,52	14,015	13,515	13,025	12,52	0,295	0,32	0,36	0,365	0,367	0,03	0,11	0,03	0,12	0,03
	7bc3_140	14	14,12	14,52	14,015	13,515	13,025	12,52	0,295	0,32	0,36	0,365	0,367	0,03	0,11	0,03	0,12	0,03
	7bc_145	14,5	14,62	14,52	14,015	13,515	13,025	12,52	0,22	0,25	0,3	0,338	0,34	0,03	0,08	0,03	0,11	0,03

Week38 (includes pressuremeters) From now on 11 channels
4 wavegauges: G18,G19,G20,G21
two velocitymeters:E10x,E10y,E11x,E11y
Two pressuremeters: pressure10y,pressure11R
one wavemaker:F77

channel	gauge	channel	gauge	channel	gauge
1	G18	5	E10x	9	F77
2	G19	6	E10y	10	pressure10 yellow (connected to EMS10)
3	G20	7	E11x	11	pressure11red (connected to EMS 11)
4	G21	8	E11y		

water filled up to 40[cm]

Week 38	ascifile	distance from ref.point	x-axis position G21 E10 G20 E11 G19	G21 y	E10 y	G20 y	E11 y	G19 y	water depth at G21	water depth at E10	water depth at G20	water depth at E11	water depth at G19	distance from the bottom G21	distance from the bottom E10	distance from the bottom G20	distance from the bottom E11	distance from the bottom G19
	7bc_145	14,5	14,62	14,52	14,015	13,515	13,025	12,52	0,22	0,25	0,3	0,338	0,34	0,03	0,08	0,03	0,12	0,03
	7bc1_145	14,5	14,62	14,52	14,015	13,515	13,025	12,52	0,22	0,25	0,3	0,338	0,34	0,03	0,08	0,03	0,12	0,03
hotstart(18)	7bc2_145	14,5	14,62	14,52	14,015	13,515	13,025	12,52	0,22	0,25	0,3	0,338	0,34	0,03	0,08	0,03	0,12	0,03
	7bc3_145	14,5	14,62	14,52	14,015	13,515	13,025	12,52	0,22	0,25	0,3	0,338	0,34	0,03	0,08	0,03	0,12	0,03
	7bc_147	14,7	14,82	14,52	14,015	13,515	13,025	12,52	0,185	0,22	0,28	0,328	0,325	0,03	0,07	0,03	0,11	0,03
hotstart(40)	7bc2d_147	14,7	14,82	14,52	14,015	13,515	13,025	12,52	0,185	0,22	0,28	0,328	0,325	0,03	0,07	0,03	0,11	0,03
	7bc1_147	14,7	14,82	14,52	14,015	13,515	13,025	12,52	0,185	0,22	0,28	0,328	0,325	0,03	0,07	0,03	0,11	0,03
	7bc3_147	14,7	14,82	14,52	14,015	13,515	13,025	12,52	0,185	0,22	0,28	0,328	0,325	0,03	0,07	0,03	0,11	0,03
waterdepth filled up to 0.4[m], gauges are cleaned																		
	7bc_152	15,2	15,32	14,52	14,015	13,515	13,025	12,52	0,105	0,16	0,23	0,3	0,305	0,03	0,06	0,03	0,1	0,03
	7bc1_152	15,2	15,32	14,52	14,015	13,515	13,025	12,52	0,105	0,16	0,23	0,3	0,305	0,03	0,06	0,03	0,1	0,03
	7bc2_152	15,2	15,32	14,52	14,015	13,515	13,025	12,52	0,105	0,16	0,23	0,3	0,305	0,03	0,06	0,03	0,1	0,03
hotstart(29)	7bc3d_152	15,2	15,32	14,52	14,015	13,515	13,025	12,52	0,105	0,16	0,23	0,3	0,305	0,03	0,06	0,03	0,1	0,03

Week 38	ascifile	distance from ref.point	x-axis position G21 E10 G20 E11 G19	G21 y	E10 y	G20 y	E11 y	G19 y	water depth at G21	water depth at E10	water depth at G20	water depth at E11	water depth at G19	distance from the bottom G21	distance from the bottom E10	distance from the bottom G20	distance from the bottom E11	distance from the bottom G19
	7bc_157	15,7	15,82	14,52	14,015	13,515	13,025	12,52	0,08	0,12	0,195	0,26	0,28	0,03	0,05	0,04	0,08	0,025
hotstart(20)	7bc1d_157	15,7	15,82	14,52	14,015	13,515	13,025	12,52	0,08	0,12	0,195	0,26	0,28	0,03	0,05	0,04	0,08	0,025
	7bc2_157	15,7	15,82	14,52	14,015	13,515	13,025	12,52	0,08	0,12	0,195	0,26	0,28	0,03	0,05	0,04	0,08	0,025
	7bc3_157	15,7	15,82	14,52	14,015	13,515	13,025	12,52	0,08	0,12	0,195	0,26	0,28	0,03	0,05	0,04	0,08	0,025
waterdepth filled up to 0.4[m], gauges are cleaned																		
	7bc_162	16,2	16,32	14,52	14,015	13,515	13,025	12,52	0,08	0,08	0,155	0,22	0,255	0,03	0,07	0,03	0,02	0,03
hotstart(20)	7bcd_162	16,2	16,32	14,52	14,015	13,515	13,025	12,52	0,08	0,08	0,155	0,22	0,255	0,03	0,07	0,03	0,02	0,03
	7bc1_162	16,2	16,32	14,52	14,015	13,515	13,025	12,52	0,08	0,08	0,155	0,22	0,255	0,03	0,07	0,03	0,02	0,03
	7bc2_162	16,2	16,32	14,52	14,015	13,515	13,025	12,52	0,08	0,08	0,155	0,22	0,255	0,03	0,07	0,03	0,02	0,03
	7bc3_162	16,2	16,32	14,52	14,015	13,515	13,025	12,52	0,08	0,08	0,155	0,22	0,255	0,03	0,07	0,03	0,02	0,03
	7bc_167	16,7	16,82	14,52	14,015	13,515	13,025	12,52	0,08	0,08	0,12	0,188	0,235	0,03	0,04	0,03	0,04	0,03
hotstart(33)	7bc1d_167	16,7	16,82	14,52	14,015	13,515	13,025	12,52	0,08	0,08	0,12	0,188	0,235	0,03	0,04	0,03	0,04	0,03

G19	ρ=209
G20	ρ=419
G21	ρ=488

Week 39																		
	_167	16,7	16,82	14,52	14,015	13,515	13,025	12,52	0,08	0,08	0,12	0,188	0,235	0,03	0,04	0,03	0,04	0,03
	7bc1_167	16,7	16,82	14,52	14,015	13,515	13,025	12,52	0,08	0,08	0,12	0,188	0,235	0,03	0,04	0,03	0,04	0,03
	7bc_172	17,2	17,32	14,52	14,015	13,515	13,025	12,52	0,08	0,08	0,08	0,145	0,21	0,03	0,03	0,03	0,05	0,03
hotstart(18)	7bcd_172	17,2	17,32	14,52	14,015	13,515	13,025	12,52	0,08	0,08	0,08	0,145	0,21	0,03	0,03	0,03	0,05	0,03
	7bc1_172	17,2	17,32	14,52	14,015	13,515	13,025	12,52	0,08	0,08	0,08	0,145	0,21	0,03	0,03	0,03	0,05	0,03

water bijgevuld

Week 40	ascifile	distance from ref.point	x-axis position G21 E10 G20 E11 G19	G21 y	E10 y	G20 y	E11 y	G19 y	water depth at G21	water depth at E10	water depth at G20	water depth at E11	water depth at G19	distance from the bottom G21	distance from the bottom E10	distance from the bottom G20	distance from the bottom E11	distance from the bottom G19
	7bc_177	17,7	17,82	14,52	14,015	13,515	13,025	12,52	0,09	0,085	0,09	0,105	0,18	0,03	0,03	0,03	0,03	0,03
hotstart(23)	7bcd_177	17,7	17,82	14,52	14,015	13,515	13,025	12,52	0,09	0,085	0,09	0,105	0,18	0,03	0,03	0,03	0,03	0,03
	7bc1_177	17,7	17,82	14,52	14,015	13,515	13,025	12,52	0,09	0,085	0,09	0,105	0,18	0,03	0,03	0,03	0,03	0,03
measurements with and without(**z**) pressuremeters to investigate if they effect EMS11 and EMS12																		
	7bc1z_177	17,7	17,82	14,52	14,015	13,515	13,025	12,52	0,09	0,085	0,09	0,105	0,18	0,03	0,03	0,03	0,03	0,03
	7bcg(10_11)z_177		changing EMS11&EMS10		13,025		14,015											
	7bcz1_177	17,7	17,82	14,52	14,015	13,515	13,025	12,52	0,09	0,085	0,09	0,105	0,18	0,03	0,03	0,03	0,03	0,03
	7bc_182	18,2	18,32	14,52	14,015	13,515	13,025	12,52	0,087	0,085	0,09	0,085	0,135	0,03	0,055	0,03	0,045	0,03
	7bc1_182	18,2	18,32	14,52	14,015	13,515	13,025	12,52	0,087	0,085	0,09	0,085	0,135	0,03	0,055	0,03	0,045	0,03
	7bcz_182	18,2	18,32	14,52	14,015	13,515	13,025	12,52	0,087	0,085	0,09	0,085	0,135	0,03	0,055	0,03	0,045	0,03
hotstart(27)	7bczd_182	18,2	18,32	14,52	14,015	13,515	13,025	12,52	0,087	0,085	0,09	0,085	0,135	0,03	0,055	0,03	0,045	0,03
	7bczc_182	18,2	18,32	14,52	14,015	13,515	13,025	12,52	0,087	0,085	0,09	0,085	0,135	0,03	0,055	0,03	0,045	0,03
EMS11 is placed closer to the bottom (to invesigate influence nearness bottom)																		
	7bcz_187	18,7	18,82	14,52	14,015	13,515	13,025	12,52	0,09	0,09	0,09	0,09	0,1	0,03	0,07	0,03	0,07	0,03
	7bcz1_187	18,7	18,82	14,52	14,015	13,515	13,025	12,52	0,09	0,09	0,09	0,09	0,1	0,03	0,07	0,03	0,07	0,03

water bijgevuld

Week 43	ascifile	distance from ref.point	x-axis position G21 E10 G20 E11 G19	G21 y	E10 y	G20 y	E11 y	G19 y	water depth at G21	water depth at E10	water depth at G20	water depth at E11	water depth at G19	distance from the bottom G21	distance from the bottom E10	distance from the bottom G20	distance from the bottom E11	distance from the bottom G19
	7bcz_187	18,7	18,82	14,52	14,015	13,515	13,025	12,52	0,09	0,09	0,09	0,09	0,1	0,03	0,07	0,03	0,07	0,03
	7bcz1_187	18,7	18,82	14,52	14,015	13,515	13,025	12,52	0,09	0,09	0,09	0,09	0,1	0,03	0,07	0,03	0,07	0,03
gauges are cleaned																		
	7bcz_192	19,2	19,32	14,52	14,015	13,515	13,025	12,52	0,09	0,087	0,087	0,087	0,09	0,03	0,07	0,03	0,07	0,03
	7bcz1_192	19,2	19,32	14,52	14,015	13,515	13,025	12,52	0,09	0,087	0,087	0,087	0,09	0,03	0,07	0,03	0,07	0,03
	7bc1_192	19,2	19,32	14,52	14,015	13,515	13,025	12,52	0,09	0,087	0,087	0,087	0,09	0,03	0,07	0,03	0,07	0,03
	7bc_197	19,7	19,82	14,52	14,015	13,515	13,025	12,52	0,08	0,08	0,08	0,08	0,08	0,03	0,07	0,03	0,07	0,03
	7bc1_197	19,7	19,82	14,52	14,015	13,515	13,025	12,52	0,08	0,08	0,08	0,08	0,08	0,03	0,07	0,03	0,07	0,03
	7bcz_197	19,7	19,82	14,52	14,015	13,515	13,025	12,52	0,08	0,08	0,08	0,08	0,08	0,03	0,07	0,03	0,07	0,03
	7bcz1_197	19,7	19,82	14,52	14,015	13,515	13,025	12,52	0,08	0,08	0,08	0,08	0,08	0,03	0,07	0,03	0,07	0,03
	7bcz1_202	20,2	20,32	14,52	14,015	13,515	13,025	12,52	0,06	0,06	0,06	0,06	0,06	0,03	0,05	0,03	0,05	0,03
	7bc_202	20,2	20,32	14,52	14,015	13,515	13,025	12,52	0,06	0,06	0,06	0,06	0,06	0,03	0,05	0,03	0,05	0,03
	7bc1_202	20,2	20,32	14,52	14,015	13,515	13,025	12,52	0,06	0,06	0,06	0,06	0,06	0,03	0,05	0,03	0,05	0,03
unreliable area, wavegauges are very near to the bottom, there is not enough water above the gauges																		
	7bc_2055	20,55	20,67	14,52	14,015	13,515	13,025	12,52	0,043	0,043	0,043	0,043	0,043	0,02	0,033	0,02	0,033	0,02
	7bc1_2055	20,55	20,67	14,52	14,015	13,515	13,025	12,52	0,043	0,043	0,043	0,043	0,043	0,02	0,033	0,02	0,033	0,02
	7bc_209	20,9	21,02	14,52	14,015	13,515	13,025	12,52	0,03	0,03	0,03	0,03	0,03	0,01	0,01	0,01	0,01	0,01
	7bc1_209	20,9	21,02	14,52	14,015	13,515	13,025	12,52	0,03	0,03	0,03	0,03	0,03	0,01	0,01	0,01	0,01	0,01
Measurement to investigate the reliability of the pressuremeters																		
	val_1053	10,53	10,65	14,52	14,015	13,515	13,025	12,52	0,4	0,4	0,4	0,4	0,4	>0.03	0,13	>0.03	0,13	>0.03
	val1_1053	10,53	10,65	14,52	14,015	13,515	13,025	12,52	0,4	0,4	0,4	0,4	0,4	>0.03	0,13	>0.03	0,13	>0.03
	val2_1053	10,53	10,65	14,52	14,015	13,515	13,025	12,52	0,4	0,4	0,4	0,4	0,4	>0.03	0,13	>0.03	0,13	>0.03

nents, all through the bassin

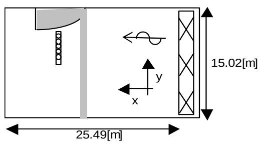

G18	ρ=71
G19	ρ=500
G20	ρ=500
G21	ρ=500

pressuremeters are always placed 6[cm] below waterlevel

(range: 50)

gauge number	G21	E10	G20	E11	G19
y-distance from measurementpoint	0,577	1,082	1,582	2,0715	2,577

d1835_411 *pressure 10y got loose*

waterdepth filled up to 0,40 [m], gauges are cleaned

Week 44	ascifile	x-distance staging from ref.point	y-distance staging from rifside	y-distance staging from ref.point	x-axis position G21 E10 G20 E11 G19	y-axis position G21	y-axis position E10	y-axis position G20	y-axis position E11	y-axis position G19	water depth at G21	water depth at E10	water depth at G20	water depth at E11	water depth at G19	distance from the bottom G21	distance from the bottom E10	distance from the bottom G20	distance from the bottom E11	distance from the bottom G19
	7bc1_197	19,7	3,24	11,78	19,82	11,203	10,698	10,198	9,7085	9,203	0.08	0,08	0,08	0,08	0,08	0,03	0,04	0,03	0,04	0,03
	7bc2_197	19,7	3,24	11,78	19,82	11,203	10,698	10,198	9,7085	9,203	0,08	0,08	0,08	0,08	0,08	0,03	0,05	0,03	0,05	0,03
hotstart(46)	7bcd_197	19,7	3,24	11,78	19,82	11,203	10,698	10,198	9,7085	9,203	0,08	0,08	0,08	0,08	0,08	0,03	0,04	0,03	0,04	0,03
	7bc14_197	19,7	1,4	13,62	19,82	13,043	12,538	12,038	11,5485	11,043	0,08	0,08	0,08	0,08	0,08	0,03	0,04	0,03	0,04	0,03
hotstart(27)	7bc14d_197	19,7	1,4	13,62	19,82	13,043	12,538	12,038	11,5485	11,043	0,08	0,08	0,08	0,08	0,08	0,03	0,04	0,03	0,04	0,03
	a2075_202	20,75	2,02	13	20,87	12,423	11,918	11,418	10,9285	10,423	0,035	0,035	0,035	0,035	0,035	0,01	0,01	0,01	0,01	0,01
hotstart(22)	d2075_202	20,75	2,02	13	20,87	12,423	11,918	11,418	10,9285	10,423	0,035	0,035	0,035	0,035	0,035	0,01	0,01	0,01	0,01	0,01
	c2075_202	20,75	2,02	13	20,87	12,423	11,918	11,418	10,9285	10,423	0,035	0,035	0,035	0,035	0,035	0,01	0,01	0,01	0,01	0,01
	a2045_311	20,45	3,11	11,91	20,57	11,333	10,828	10,328	9,8385	9,333	0,055	0,055	0,055	0,055	0,055	0,01	0,01	0,01	0,01	0,01
hotstart(16)	d2045_311	20,45	3,11	11,91	20,57	11,333	10,828	10,328	9,8385	9,333	0,055	0,055	0,055	0,055	0,055	0,01	0,01	0,01	0,01	0,01
	a192_2725	19,2	2,725	12,295	19,32	11,718	11,213	10,713	10,2235	9,718	0,115	0,115	0,115	0,115	0,115	0,03	0,07	0,03	0,07	0,03
waterdepth filled up to 0,40 [m], gauges are cleaned																				
	b192_2725	19,2	2,725	12,295	19,32	11,718	11,213	10,713	10,2235	9,718	0,115	0,115	0,115	0,115	0,115	0,03	0,05	0,03	0,05	0,03
hotstart(26)	d192_2725	19,2	2,725	12,295	19,32	11,718	11,213	10,713	10,2235	9,718	0,115	0,115	0,115	0,115	0,115	0,03	0,05	0,03	0,05	0,03
	a19_2955	19	2,955	12,065	19,12	11,488	10,983	10,483	9,9935	9,488	0,125	0,125	0,125	0,125	0,125	0,03	0,07	0,03	0,07	0,03
hotstart(23)	d19_2955	19	2,955	12,065	19,12	11,488	10,983	10,483	9,9935	9,488	0,125	0,125	0,125	0,125	0,125	0,03	0,07	0,03	0,07	0,03
	b19_2955	19	2,955	12,065	19,12	11,488	10,983	10,483	9,9935	9,488	0,125	0,125	0,125	0,125	0,125	0,03	0,07	0,03	0,07	0,03
	a187_2955	18,7	2,955	12,065	18,82	11,488	10,983	10,483	9,9935	9,488	0,14	0,14	0,14	0,14	0,14	0,03	0,07	0,03	0,07	0,03

waterdepth filled up to 0,40 [m]

Week 45	ascifile	x-distance staging from ref.point	y-distance staging from rifside	y-distance staging from ref.point	x-axis position G21 E10 G20 E11 G19	y-axis position G21	y-axis position E10	y-axis position G20	y-axis position E11	y-axis position G19	water depth at G21	water depth at E10	water depth at G20	water depth at E11	water depth at G19	distance from the bottom G21	distance from the bottom E10	distance from the bottom G20	distance from the bottom E11	distance from the bottom G19
	b187_2955	18,7	2,955	12,065	18,82	11,488	10,983	10,483	9,9935	9,488	0,14	0,14	0,14	0,14	0,14	0,03	0,07	0,03	0,07	0,03
hotstart(35)	d187_2955	18,7	2,955	12,065	18,82	11,488	10,983	10,483	9,9935	9,488	0,14	0,14	0,14	0,14	0,14	0,03	0,07	0,03	0,07	0,03
	a1835_302	18,35	2,92	12,1	18,47	11,523	11,018	10,518	10,0285	9,523	0,15	0,15	0,15	0,15	0,15	0,03	0,07	0,03	0,07	0,03
hotstart(29)	d1835_302	18,35	2,92	12,1	18,47	11,523	11,018	10,518	10,0285	9,523	0,15	0,15	0,15	0,15	0,15	0,03	0,07	0,03	0,07	0,03
	a1835_411	18,35	4,01	11,01	18,47	10,433	9,928	9,428	8,9385	8,433	0,15	0,15	0,15	0,15	0,15	0,03	0,07	0,03	0,07	0,03
hotstart(25)	d1835_411	18,35	4,01	11,01	18,47	10,433	9,928	9,428	8,9385	8,433	0,15	0,15	0,15	0,15	0,15	0,03	0,07	0,03	0,07	0,03
	a1783_411	17,83	4,01	11,01	17,95	10,433	9,928	9,428	8,9385	8,433	0,18	0,18	0,18	0,18	0,18	0,03	0,07	0,03	0,07	0,03
hotstart(31)	d1783_411	17,83	4,01	11,01	17,95	10,433	9,928	9,428	8,9385	8,433	0,18	0,18	0,18	0,18	0,18	0,03	0,07	0,03	0,07	0,03
	a1783_315	17,83	3,05	11,97	17,95	11,393	10,888	10,388	9,8985	9,393	0,18	0,18	0,18	0,18	0,18	0,03	0,07	0,03	0,07	0,03
hotstart(17)	d1783_315	17,83	3,05	11,97	17,95	11,393	10,888	10,388	9,8985	9,393	0,18	0,18	0,18	0,18	0,18	0,03	0,07	0,03	0,07	0,03
waterdepth filled up to 0,40 [m]																				
	b1783_315	17,83	3,05	11,97	17,95	11,393	10,888	10,388	9,8985	9,393	0,18	0,18	0,18	0,18	0,18	0,03	0,07	0,03	0,07	0,03
				15,02																
	a1743_323	17,43	3,13	11,89	17,55	11,313	10,808	10,308	9,8185	9,313	0,2	0,2	0,2	0,2	0,2	0,03	0,07	0,03	0,07	0,03
hotstart(27)	d1743_323	17,43	3,13	11,89	17,55	11,313	10,808	10,308	9,8185	9,313	0,2	0,2	0,2	0,2	0,2	0,03	0,07	0,03	0,07	0,03
	a1743_382	17,43	3,72	11,3	17,55	10,723	10,218	9,718	9,2285	8,723	0,2	0,2	0,2	0,2	0,2	0,03	0,07	0,03	0,07	0,03
hotstart(44)	d1743_382	17,43	3,72	11,3	17,55	10,723	10,218	9,718	9,2285	8,723	0,2	0,2	0,2	0,2	0,2	0,03	0,07	0,03	0,07	0,03
	a170_377	17	3,67	11,35	17,12	10,773	10,268	9,768	9,2785	8,773	0,22	0,22	0,22	0,22	0,22	0,03	0,07	0,03	0,07	0,03
hotstart(26)	d170_377	17	3,67	11,35	17,12	10,773	10,268	9,768	9,2785	8,773	0,22	0,22	0,22	0,22	0,22	0,03	0,07	0,03	0,07	0,03
																0,03	0,07	0,03	0,07	0,03
	a170_434	17	4,14	10,88	17,12	10,303	9,798	9,298	8,8085	8,303	0,22	0,22	0,22	0,22	0,22	0,03	0,07	0,03	0,07	0,03
hotstart(25)	d170_434	17	4,14	10,88	17,12	10,303	9,798	9,298	8,8085	8,303	0,22	0,22	0,22	0,22	0,22	0,03	0,07	0,03	0,07	0,03
From here on: duration measurement takes 30 minutes																				
	l170_434	17	4,14	10,88	17,12	10,303	9,798	9,298	8,8085	8,303	0,22	0,22	0,22	0,22	0,22	0,03	0,07	0,03	0,07	0,03
																0,03	0,07	0,03	0,07	0,03
	l170_440	17	4,2	10,82	17,12	10,243	9,738	9,238	8,7485	8,243	0,22	0,22	0,22	0,22	0,22	0,03	0,07	0,03	0,07	0,03
	l1672_478	16,72	4,58	10,44	16,84	9,863	9,358	8,858	8,3685	7,863	0,235	0,235	0,235	0,235	0,235	0,03	0,08	0,03	0,08	0,03
	l1672_336	16,72	3,26	11,76	16,84	11,183	10,678	10,178	9,6885	9,183	0,235	0,235	0,235	0,235	0,235	0,03	0,08	0,03	0,08	0,03
	l1622_376	16,22	3,66	11,36	16,34	10,783	10,278	9,778	9,2885	8,783										

G19	ρ=500	(from 160_475 on)	G19	ρ=200 (from 160_533 on)
G20	ρ=500		G20	ρ=200
G21	ρ=200		G21	ρ=200

Week 46	ascifile	x-distance staging from ref.point	y-distance staging from rifside	y-distance staging from ref.point	x-axis position G21 E10 G20 E11 G19	y-axis position G21	y-axis position E10	y-axis position G20	y-axis position E11	y-axis position G19	water depth at G21	water depth at E10	water depth at G20	water depth at E11	water depth at G19	distance from the bottom G21	distance from the bottom E10	distance from the bottom G20	distance from the bottom E11	distance from the bottom G19
	160_373	16	3,63	11,39	16,12	10,813	10,308	9,808	9,3185	8,813	0,27	0,27	0,27	0,27	0,27	0,03	0,09	0,03	0,09	0,03
	160_475	16	4,55	10,47	16,12	9,893	9,388	8,888	8,3985	7,893	0,27	0,27	0,27	0,27	0,27	0,03	0,09	0,03	0,09	0,03
	160_533	16	5,13	9,89	16,12	9,313	8,808	8,308	7,8185	7,313	0,27	0,27	0,27	0,27	0,27	0,03	0,09	0,03	0,09	0,03
	156_525	15,6	5,05	9,97	15,72	9,393	8,888	8,388	7,8985	7,393	0,28	0,28	0,28	0,28	0,28	0,03	0,09	0,03	0,09	0,03
	156_465	15,6	4,45	10,57	15,72	9,993	9,488	8,988	8,4985	7,993	0,28	0,28	0,28	0,28	0,28	0,03	0,09	0,03	0,09	0,03
	156_322	15,6	3,12	11,9	15,72	11,323	10,818	10,318	9,8285	9,323	0,28	0,28	0,28	0,28	0,28	0,03	0,09	0,03	0,09	0,03
	152_578	15,2	5,58	9,44	15,32	8,863	8,358	7,858	7,3685	6,863	0,31	0,31	0,31	0,31	0,31	0,03	0,1	0,03	0,1	0,03
	152_477	15,2	4,57	10,45	15,32	9,873	9,368	8,868	8,3785	7,873	0,31	0,31	0,31	0,31	0,31	0,03	0,105	0,03	0,105	0,03
waterdepth filled up to 0,40 [m]																				
	152_208	15,2	2,08	12,94	15,32	12,363	11,858	11,358	10,8685	10,363	0,31	0,31	0,31	0,31	0,31	0,03	0,105	0,03	0,105	0,03
	16_216	16	2,06	12,96	16,12	12,383	11,878	11,378	10,8885	10,383	0,27	0,27	0,27	0,27	0,27	0,03	0,09	0,03	0,09	0,03
	17_205	17	2,05	12,97	17,12	12,393	11,888	11,388	10,8985	10,393	0,22	0,22	0,22	0,22	0,22	0,03	0,07	0,03	0,07	0,03
	18_178	18	1,78	13,24	18,12	12,663	12,158	11,658	11,1685	10,663	0,17	0,17	0,17	0,17	0,17	0,03	0,07	0,03	0,07	0,03
	19_w	19	1,94	13,08	19,12	12,503	11,998	11,498	11,0085	10,503										

From here on: Measurements are taken from the rifless side

gauges are cleaned

	H19_388	19	irrelevant	3,88	19,12	4,457	4,962	5,462	5,9515	6,457										

Week 47	ascifile	x-distance staging from ref.point	y-distance staging from rifside	y-distance staging from ref.point	x-axis position G21 E10 G20 E11 G19	y-axis position G21	y-axis position E10	y-axis position G20	y-axis position E11	y-axis position G19	water depth at G21	water depth at E10	water depth at G20	water depth at E11	water depth at G19	distance from the bottom G21	distance from the bottom E10	distance from the bottom G20	distance from the bottom E11	distance from the bottom G19
	H185_372	18,5	irrelevant	3,72	18,62	4,297	4,802	5,302	5,7915	6,297	0,145	0,145	0,145	0,145	0,145	0,03	0,07	0,03	0,07	0,03
	H185_155	18,5	irrelevant	1,55	18,62	2,127	2,632	3,132	3,6215	4,127	0,145	0,145	0,145	0,145	0,145	0,03	0,07	0,03	0,07	0,03
	H185_488	18,5	irrelevant	4,88	18,62	5,457	5,962	6,462	6,9515	7,457	0,145	0,145	0,145	0,145	0,145	0,03	0,07	0,03	0,07	0,03
	H175_516	17,5	irrelevant	5,16	17,62	5,737	6,242	6,742	7,2315	7,737	0,19	0,19	0,19	0,19	0,19	0,03	0,08	0,03	0,08	0,03
	H175_297	17,5	irrelevant	2,97	17,62	3,547	4,052	4,552	5,0415	5,547	0,19	0,19	0,19	0,19	0,19	0,03	0,08	0,03	0,08	0,03
	H17_298	17	irrelevant	2,98	17,12	3,557	4,062	4,562	5,0515	5,557	0,22	0,22	0,22	0,22	0,22	0,03	0,08	0,03	0,08	0,03
	H17_528	17	irrelevant	5,28	17,12	5,857	6,362	6,862	7,3515	7,857	0,22	0,22	0,22	0,22	0,22	0,03	0,08	0,03	0,08	0,03
	H16_527	16	irrelevant	5,27	16,12	5,847	6,352	6,852	7,3415	7,847	0,27	0,27	0,27	0,27	0,27	0,03	0,09	0,03	0,09	0,03
	H16_35		irrelevant	3,5	0,12	4,077	4,582	5,082	5,5715	6,077	0,27	0,27	0,27	0,27	0,27	0,03	0,09	0,03	0,09	0,03
	H155_31	15,5	irrelevant	3,1	15,62	3,677	4,182	4,682	5,1715	5,677	0,29	0,29	0,29	0,29	0,29	0,03	0,1	0,03	0,1	0,03
	H155_472	15,5	irrelevant	4,72	15,62	5,297	5,802	6,302	6,7915	7,297	0,29	0,29	0,29	0,29	0,29	0,03	0,1	0,03	0,1	0,03
	H155_525	15,5	irrelevant	5,25	15,62	5,827	6,332	6,832	7,3215	7,827	0,29	0,29	0,29	0,29	0,29	0,03	0,1	0,03	0,1	0,03
	H15_52	15	irrelevant	5,2	15,12	5,777	6,282	6,782	7,2715	7,777	0,32	0,32	0,32	0,32	0,32	0,03	0,11	0,03	0,11	0,03
	H15_369	15	irrelevant	3,69	15,12	4,267	4,772	5,272	5,7615	6,267	0,32	0,32	0,32	0,32	0,32	0,03	0,11	0,03	0,11	0,03
	H15_289	15	irrelevant	2,89	15,12	3,467	3,972	4,472	4,9615	5,467	0,32	0,32	0,32	0,32	0,32	0,03	0,11	0,03	0,11	0,03
	H145_29	14,5	irrelevant	2,9	14,62	3,477	3,982	4,482	4,9715	5,477						0,03		0,03		0,03
	H145_452	14,5	irrelevant	4,52	14,62	5,097	5,602	6,102	6,5915	7,097						0,03		0,03		0,03

waterdepth filled up to 0,40 [m]

Week 48	ascifile	x-distance staging from ref.point	y-distance staging from rifside	y-distance staging from ref.point	x-axis position G21 E10 G20 E11 G19	y-axis position G21	y-axis position E10	y-axis position G20	y-axis position E11	y-axis position G19	water depth at G21	water depth at E10	water depth at G20	water depth at E11	water depth at G19	distance from the bottom G21	distance from the bottom E10	distance from the bottom G20	distance from the bottom E11	distance from the bottom G19
	H14_447	14	irrelevant	4,47	14,12	5,047	5,552	6,052	6,5415	7,047										
	H14_315	14	irrelevant	3,15	14,12	3,727	4,232	4,732	5,2215	5,727										
	HV13_308	13	irrelevant	3,08	13,12	3,657	4,162	4,662	5,1515	5,657	0,4	0,4	0,4	0,4	0,4	0,03	0,13	0,03	0,13	0,03
	HV13_447	13	irrelevant	4,47	13,12	5,047	5,552	6,052	6,5415	7,047	0,4	0,4	0,4	0,4	0,4	0,03	0,13	0,03	0,13	0,03
	HV125_435	12,5	irrelevant	4,35	12,62	4,927	5,432	5,932	6,4215	6,927	0,4	0,4	0,4	0,4	0,4	0,03	0,13	0,03	0,13	0,03
	HV125_256	12,5	irrelevant	2,56	12,62	3,137	3,642	4,142	4,6315	5,137	0,4	0,4	0,4	0,4	0,4	0,03	0,13	0,03	0,13	0,03
	HV12_248	12	irrelevant	2,48	12,12	3,057	3,562	4,062	4,5515	5,057	0,4	0,4	0,4	0,4	0,4	0,03	0,13	0,03	0,13	0,03
	HV11_225	11	irrelevant	2,25	11,12	2,827	3,332	3,832	4,3215	4,827	0,4	0,4	0,4	0,4	0,4	0,03	0,13	0,03	0,13	0,03
	HV10_209	10	irrelevant	2,09	10,12	2,667	3,172	3,672	4,1615	4,667	0,4	0,4	0,4	0,4	0,4	0,03	0,13	0,03	0,13	0,03
		G19	ρ=500																	
		G20	ρ=500																	
gauges are cleaned		G21	ρ=500																	

Week 48	ascifile	x-distance staging from ref.point	y-distance staging from rifside	y-distance staging from ref.point	x-axis position G21 E10 G20 E11 G19	y-axis position G21	y-axis position E10	y-axis position G20	y-axis position E11	y-axis position G19	water depth at G21	water depth at E10	water depth at G20	water depth at E11	water depth at G19	distance from the bottom G21	distance from the bottom E10	distance from the bottom G20	distance from the bottom E11	distance from the bottom G19
	H21_261	21	irrelevant	2,61	21,12	3,187	3,692	4,192	4,6815	5,187	0,025	0,025	0,025	0,025	0,025					
	H20_363	20	irrelevant	3,63	20,12	4,207	4,712	5,212	5,7015	6,207										
	H195_421	19,5	irrelevant	4,21	19,62	4,787	5,292	5,792	6,2815	6,787										
	H18_481	18	irrelevant	4,81	18,12	5,387	5,892	6,392	6,8815	7,387										
	H18_226	18	irrelevant	2,26	18,12	2,837	3,342	3,842	4,3315	4,837										
G19	ρ=200																			
G20	ρ=200																			
G21	ρ=200																			
	H165_247	16,5	irrelevant	2,47	16,62	3,047	3,552	4,052	4,5415	5,047										
	H165_473	16,5	irrelevant	4,73	16,62	5,307	5,812	6,312	6,8015	7,307										

waterdepth filled up to 0,40 [m]

Week 49	ascifile	x-distance staging from ref.point	y-distance staging from rifside	y-distance staging from ref.point	x-axis position G21 E10 G20 E11	y-axis position G21	y-axis position E10	y-axis position G20	y-axis position E11	y-axis position G19	water depth at G21	water depth at E10	water depth at G20	water depth at E11	water depth at G19	distance from the bottom G21	distance from the bottom E10	distance from the bottom G20	distance from the bottom E11	distance from the bottom G19
	H193_115	19,3	irrelevant	1,15	19,42	1,727	2,232	2,732	3,2215	3,727										
G19	ρ=500																			
G20	ρ=500																			
G21	ρ=500																			
	H207_139	20,7	irrelevant	1,39	20,82	1,967	2,472	2,972	3,4615	3,967										
	H203_136	20,3	irrelevant	1,36	20,42	1,937	2,442	2,942	3,4315	3,937										
	H197_131	19,7	irrelevant	1,31	19,82	1,887	2,392	2,892	3,3815	3,887										

Velocity-measurements in the rip-current

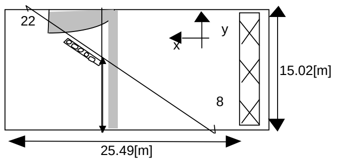

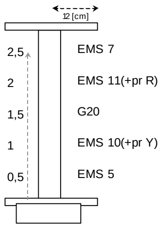

	gages placed at:
a	1/3 from the bottom
b	1/2 waterdepth
c	2/3 from the bottom
w	0.04[m] beneath waterlevel

velocitygauges: EMS 5,7,10,11
wave-gauge: G20
pressure: 10Y, 11R

distance between the gauges=0.5[m]

channel	gaugenr.
1	G18
2	pr 10y
3	G20
4	pr 11r
5	E10x
6	E10y
7	E11x
8	E11y
9	F77
10	E7x
11	E7y
12	E5x
13	E5y

a	1/3 from the bottom	#VALUE!	0	#VALUE!	#VALUE!	0
b	1/2 waterdepth	#VALUE!	0	#VALUE!	#VALUE!	0
c	2/3 from the bottom	#VALUE!	0	#VALUE!	#VALUE!	0
w	0.04[m] beneath waterlevel	#VALUE!	-0,04	#VALUE!	#VALUE!	-0,04

waterdepth filled up to 0,40 [m], gauges are cleaned

Week 51	ascifile	x-distance staging from ref.point	y-distance staging from ref.point	x-axis position EMS 5	x-axis position EMS 10	x-axis position G 20	x-axis position EMS 11	x-axis position EMS 7	y-axis position EMS 5	y-axis position EMS 10	y-axis position G 20	y-axis position EMS 11	y-axis position EMS 7	water depth at EMS 7	water depth at EMS 11	water depth at G20	water depth at EMS 10	water depth at EMS 5	distance from the bottom EMS 7	distance from the bottom EMS 11	distance from the bottom G20	distance from the bottom EMS 10	distance from the bottom EMS 5
	mui11_328a	11	3,28	11,53	11,67	11,79	11,88	11,96	3,46	3,61	3,72	3,81	3,9	1	1	1	1	1	0,33	0,33	0,33	0,33	0,33
	mui11_328b	11	3,28	11,53	11,67	11,79	11,88	11,96	3,46	3,61	3,72	3,81	3,9	1	1	1	1	1	0,5	0,5	0,5	0,5	0,5
hotstart(46)	mui11_328cd	11	3,28	11,53	11,67	11,79	11,88	11,96	3,46	3,61	3,72	3,81	3,9	1	1	1	1	1	0,67	0,67	0,67	0,67	0,67
	mui11_328c	11	3,28	11,53	11,67	11,79	11,88	11,96	3,46	3,61	3,72	3,81	3,9	1	1	1	1	1	0,67	0,67	0,67	0,67	0,67
E10+G20 above the sill !				0,53	0,67	0,79	0,88	0,96	0,18	0,33	0,44	0,53	0,62										
	mui126_502a	12,6	5,02	13,13	13,27	13,39	13,48	13,56	5,2	5,35	5,46	5,55	5,64	1	1	1	1	1	0,33	0,33	0,33	0,33	0,33
	mui126_502b	12,6	5,02	13,13	13,27	13,39	13,48	13,56	5,2	5,35	5,46	5,55	5,64	1	1	1	1	1	0,5	0,5	0,5	0,5	0,5

waterdepth filled up to 0,40 [m]

Week 52	ascifile	x-distance staging from ref.point	y-distance staging from ref.point	x-axis position EMS 5	x-axis position EMS 10	x-axis position G 20	x-axis position EMS 11	x-axis position EMS 7	y-axis position EMS 5	y-axis position EMS 10	y-axis position G 20	y-axis position EMS 11	y-axis position EMS 7	water depth at EMS 7	water depth at EMS 11	water depth at G20	water depth at EMS 10	water depth at EMS 5	distance from the bottom EMS 7	distance from the bottom EMS 11	distance from the bottom G20	distance from the bottom EMS 10	distance from the bottom EMS 5
E10+G20 above the sill !																							
	mui126_502c	12,6	5,02	13,13	13,27	13,39	13,48	13,56	5,2	5,35	5,46	5,55	5,64	1	1	1	1	1	0,67	0,67	0,67	0,67	0,67
	mui126_502W	12,6	5,02	13,13	13,27	13,39	13,48	13,56	5,2	5,35	5,46	5,55	5,64	1	1	1	1	1	0,96	0,96	0,33	0,96	0,96
measurements at rifside (duration measurement: 10 minutes**)**																							
	muir14_658w	14	6,58	14,53	14,67	14,79	14,88	14,96	6,76	6,91	7,02	7,11	7,2	1	1	1	1	1	0,96	0,96	0,33	0,96	0,96
	muir14_658c	14	6,58	14,53	14,67	14,79	14,88	14,96	6,76	6,91	7,02	7,11	7,2	1	1	1	1	1	0,67	0,67	0,67	0,67	0,67
	muir14_658b	14	6,58	14,53	14,67	14,79	14,88	14,96	6,76	6,91	7,02	7,11	7,2	1	1	1	1	1	0,5	0,5	0,5	0,5	0,5
	muir14_658a	14	6,58	14,53	14,67	14,79	14,88	14,96	6,76	6,91	7,02	7,11	7,2	1	1	1	1	1	0,33	0,33	0,33	0,33	0,33
from here on: duration measurement takes 30 minutes																							
	muir155_825a	15,5	8,25	16,03	16,17	16,29	16,38	16,46	8,43	8,58	8,69	8,78	8,87	1	1	1	1	1	0,33	0,33	0,33	0,33	0,33
	muir155_825b	15,5	8,25	16,03	16,17	16,29	16,38	16,46	8,43	8,58	8,69	8,78	8,87	1	1	1	1	1	0,5	0,5	0,5	0,5	0,5
	muir155_825c	15,5	8,25	16,03	16,17	16,29	16,38	16,46	8,43	8,58	8,69	8,78	8,87	1	1	1	1	1	0,67	0,67	0,67	0,67	0,67
	muir17_98c	17	9,8	17,53	17,67	17,79	17,88	17,96	9,98	10,13	10,24	10,33	10,42	1	1	1	1	1	0,67	0,67	0,67	0,67	0,67
	muir17_98b	17	9,8	17,53	17,67	17,79	17,88	17,96	9,98	10,13	10,24	10,33	10,42	1	1	1	1	1	0,5	0,5	0,5	0,5	0,5
	muir17_98b2	17	9,8	17,53	17,67	17,79	17,88	17,96	9,98	10,13	10,24	10,33	10,42	1	1	1	1	1	0,5	0,5	0,5	0,5	0,5
measurement to see if situations are comparable/ repeatable																							
	muir17_98a	17	9,8	17,53	17,67	17,79	17,88	17,96	9,98	10,13	10,24	10,33	10,42	1	1	1	1	1	0,33	0,33	0,33	0,33	0,33
	muir14_66a	14	6,6	14,53	14,67	14,79	14,88	14,96	6,78	6,93	7,04	7,13	7,22	1	1	1	1	1	0,33	0,33	0,33	0,33	0,33
	muir14_66b	14	6,6	14,53	14,67	14,79	14,88	14,96	6,78	6,93	7,04	7,13	7,22	1	1	1	1	1	0,5	0,5	0,5	0,5	0,5
	muir14_66c	14	6,6	14,53	14,67	14,79	14,88	14,96	6,78	6,93	7,04	7,13	7,22	1	1	1	1	1	0,67	0,67	0,67	0,67	0,67

new staging: gauges placed with only 0.15[m] in between at different hights at the same time

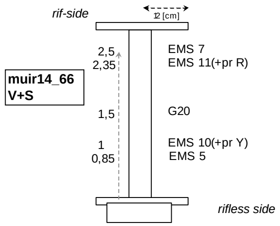

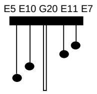

new staging: gauges placed with 0.25[m] in between at the same depth(G), or at different depths (S1,2,3,4,5) during one measurement

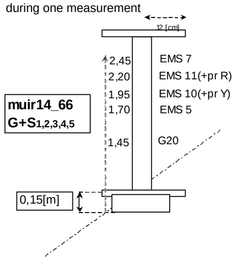

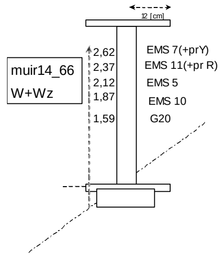

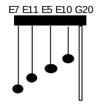

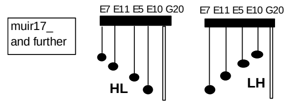

Week 52	ascifile	x-distance staging from ref.point	y-distance staging from ref.point	x-axis position EMS 5	x-axis position EMS 10	x-axis position G 20	x-axis position EMS 11	x-axis position EMS 7	y-axis position EMS 5	y-axis position EMS 10	y-axis position G 20	y-axis position EMS 11	y-axis position EMS 7	water depth at EMS 7	water depth at EMS 11	water depth at G20	water depth at EMS 10	water depth at EMS 5	distance from the bottom EMS 7	distance from the bottom EMS 11	distance from the bottom G20	distance from the bottom EMS 10	distance from the bottom EMS 5
	muir14_66V	14	6,6	14,63	14,67	14,79	14,94	14,96	6,89	6,93	7,04	7,19	7,22	1	1	1	1	1	0,33	0,67	0,33	0,67	0,33
	muir14_66S	14	6,6	14,63	14,67	14,79	14,94	14,96	6,89	6,93	7,04	7,19	7,22	1	1	1	1	1	0,33	0,67	0,33	0,67	0,33

Week 52	ascifile	x-distance staging from ref.point	y-distance staging from ref.point	x-axis position G 20	x-axis position EMS 5	x-axis position EMS 10	x-axis position EMS 11	x-axis position EMS 7	y-axis position G 20	y-axis position EMS 5	y-axis position EMS 10	y-axis position EMS 11	y-axis position EMS 7	water depth at G20	water depth at EMS 5	water depth at EMS 10	water depth at EMS 11	water depth at EMS 7	distance from the bottom G20	distance from the bottom EMS 5	distance from the bottom EMS 10	distance from the bottom EMS 11	distance from the bottom EMS 7
	muir14_66G	14	6,6	14,81	14,85	14,9	14,94	14,98	7,06	7,11	7,15	7,19	7,23	0,3	0,3	0,29	0,29	0,28	0,1	0,1	0,1	0,1	0,09
	muir14_66S1	14	6,6	14,81	14,85	14,9	14,94	14,98	7,06	7,11	7,15	7,19	7,23	0,3	0,3	0,29	0,29	0,28	0,1	0,1	0,15	0,19	0,21
	muir14_66S2	14	6,6	14,81	14,85	14,9	14,94	14,98	7,06	7,11	7,15	7,19	7,23	0,3	0,3	0,29	0,29	0,28	0,1	0,23	0,19	0,15	0,09
	muir14_66S3	14	6,6	14,81	14,85	14,9	14,94	14,98	7,06	7,11	7,15	7,19	7,23	0,3	0,3	0,29	0,29	0,28	0,1	0,23	0,19	0,15	0,09
repeating S2	muir14_66S4	14	6,6	14,81	14,85	14,9	14,94	14,98	7,06	7,11	7,15	7,19	7,23	0,3	0,3	0,29	0,29	0,28	0,1	0,23	0,19	0,15	0,09
	muir14_66S5	14	6,6	14,81	14,85	14,9	14,94	14,98	7,06	7,11	7,15	7,19	7,23	0,3	0,3	0,29	0,29	0,28	0,1	0,23	0,19	0,15	0,09

changing E10 and E5

Week 52	ascifile	x-distance staging from ref.point	y-distance staging from ref.point	x-axis position G 20	x-axis position EMS 10	x-axis position EMS 5	x-axis position EMS 11	x-axis position EMS 7	y-axis position G 20	y-axis position EMS 10	y-axis position EMS 5	y-axis position EMS 11	y-axis position EMS 7	water depth at G20	water depth at EMS 10	water depth at EMS 5	water depth at EMS 11	water depth at EMS 7	distance from the bottom G20	distance from the bottom EMS 10	distance from the bottom EMS 5	distance from the bottom EMS 11	distance from the bottom EMS 7
	muir14_66W	14	6,49	14,8	14,86	14,9	14,94	14,98	6,95	7	7,04	7,09	7,13	0,3	0,3	0,29	0,29	0,28	0,1	0,23	0,2	0,15	0,09
from here on: without pressuremeters																							
	muir14_66Wz	14	6,49	14,8	14,86	14,9	14,94	14,98	6,95	7	7,04	7,09	7,13	0,3	0,3	0,29	0,29	0,28	0,1	0,23	0,2	0,15	0,09
	muir17_97HL	17	9,7	17,77	17,83	17,87	17,92	17,96	10,12	10,18	10,23	10,27	10,31	1	1	1	1	1	0,33	0,33	0,5	0,67	0,8
	muir17_97LH2	17	9,7	17,77	17,83	17,87	17,92	17,96	10,12	10,18	10,23	10,27	10,31	1	1	1	1	1	0,33	0,75	0,67	0,5	0,33
waterlevel filled up to: 40.3 cm																							
	muir17_97HL2	17	9,7	17,77	17,83	17,87	17,92	17,96	10,12	10,18	10,23	10,27	10,31	1	1	1	1	1	0,33	0,33	0,5	0,67	0,8
	muir16_857HL	16	8,57	16,78	16,83	16,87	16,91	16,96	9	9,05	9,1	9,14	9,18	1	1	1	1	1	0,33	0,75	0,67	0,5	0,33
	muir16_857LH	16	8,57	16,78	16,83	16,87	16,91	16,96	9	9,05	9,1	9,14	9,18	1	1	1	1	1	0,33	0,33	0,5	0,67	0,75
	muir15_755LH	15	7,55	15,78	15,83	15,87	15,91	15,96	7,98	8,03	8,08	8,12	8,16	1	1	1	1	1	0,33	0,33	0,5	0,67	0,75
	muir15_755HL	15	7,55	15,78	15,83	15,87	15,91	15,96	7,98	8,03	8,08	8,12	8,16	1	1	1	1	1	0,33	0,75	0,67	0,5	0,33
waterlevel: 0.4[m]																							
	mui13_538LH	13	5,38	13,79	13,84	13,88	13,93	13,97	5,82	5,87	5,92	5,96	6	1	1	1	1	1	0,33	0,33	0,5	0,67	0,75
	mui13_538HL	13	5,38	13,79	13,84	13,88	13,93	13,97	5,82	5,87	5,92	5,96	6	1	1	1	1	1	0,33	0,75	0,67	0,5	0,33
gauges are standing above the sill!!!																							
	mui12_431HL	12	4,31	12,79	12,84	12,88	12,93	12,97	4,75	4,8	4,85	4,89	4,93	1	1	1	1	1	0,33	0,75	0,67	0,5	0,33
	mui12_431LH	12	4,31	12,79	12,84	12,88	12,93	12,97	4,75	4,8	4,85	4,89	4,93	1	1	1	1	1	0,33	0,33	0,5	0,67	0,75
	mui11_322LH	11	3,22	11,8	11,85	11,89	11,93	11,97	3,67	3,72	3,77	3,81	3,85	1	1	1	1	1	0,33	0,33	0,5	0,67	0,75
	mui11_322HL	11	3,22	11,79	11,84	11,88	11,93	11,97	3,67	3,72	3,77	3,81	3,85	1	1	1	1	1	0,33	0,75	0,67	0,5	0,33
	mui10_215HL	10	2,15	10,79	10,84	10,88	10,93	10,97	2,59	2,64	2,69	2,73	2,77	1	1	1	1	1	0,33	0,75	0,67	0,5	0,33
	mui10_215LH	10	2,15	10,79	10,84	10,88	10,93	10,97	2,59	2,64	2,69	2,73	2,77	1	1	1	1	1	0,33	0,33	0,5	0,67	0,75

ANNEX 2 : PTV OBSERVATION

Overview video images

Images were taken in the rip current area, following the rip-current path as determined in previous in-situ measurements. First a calibration was performed for the two film area's. For this, the available film-frame was indicated by five markers, four at the outer corners and one in the centre of the area. These markers were also used to determine the magnitude of distortion of the image. Specifications of the camera and lens, provided by the supplier, indicated no significant distortion effects. The local coordinates of the markers were used to translate pixel location into world coordinates.

The recordings were divided into two series (one for each recording area). For each series there are three specific time scenarios:

- recording starts simultaneously with the wave generator (to see the evolution of the rip-current)
- recording starts after five minutes of generating waves
- recording starts twenty minutes after generating waves

For operational purposes, the recording area in the basin was indicated by ropes. Before recording, the recording area was seeded with particles. During recording, additional seeding was done from outside the recording area in such way that the particles floated into the recording area. With this method enough particles were present at all times during the experiments. Furthermore, disturbance of the video observations by particles thrown through the recording area was prevented.

Reference recording area 1 for particle tracking with five markers

Figure 1 gives the position of recording area 1 relative to the wave basin by means of the five markers.

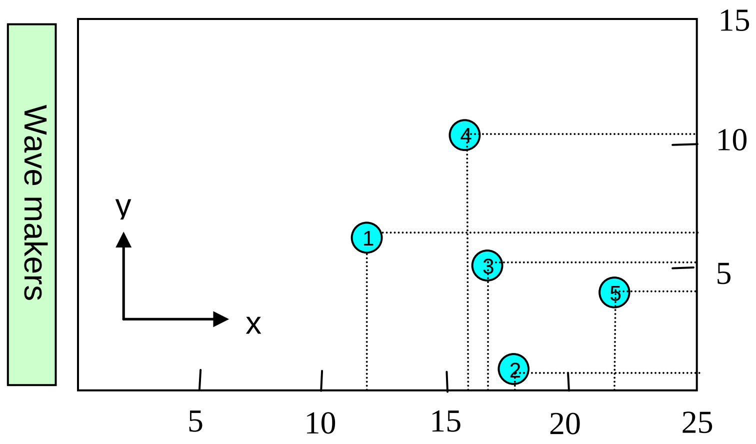

Figure 1: Wave basin with recording area 1

Figure 2 presents the reference image with the five markers in it. Note the applied local coordinate system for the reference recording (Figure 2).

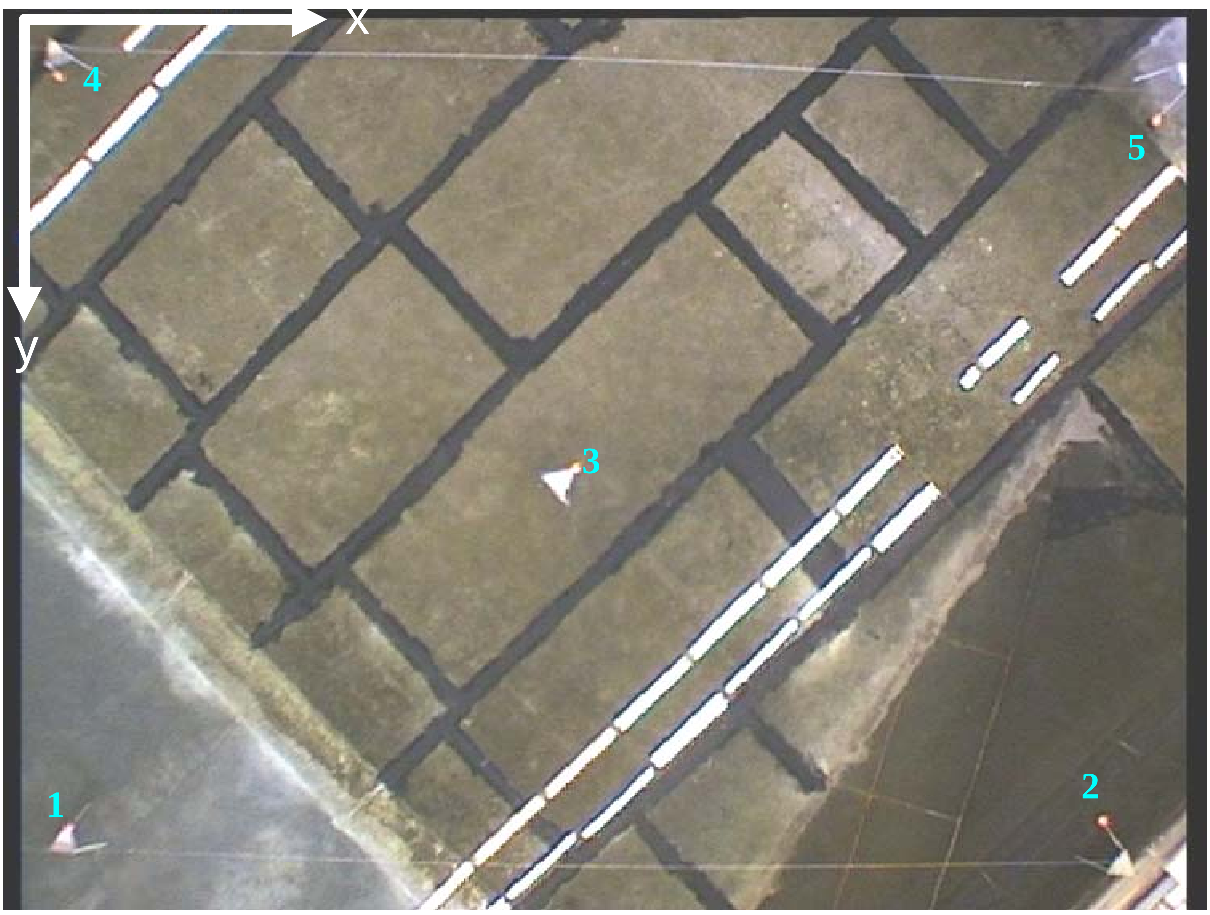

Figure 2: Reference recording area 1 with coordinate system and five markers

The correlation between recording coordinate system and the wave basin coordinate system for the five markers is given in Table 1.

Table 1: Correlation between pixel coordinate system and wave basin coordinate system for markers in reference recording area 1

Reference	Pixel x	Pixel y	Wave basin coordinates	
Mark 1	42	521	X = 11.81	Y = 6.03
Mark 2	702	518	X = 17.74	Y = 0.43
Mark 3	365	293	X = 16.66	Y = 5.25
Mark 4	35	43	X = 15.84	Y = 10.25
Mark 5	736	71	X = 21.72	Y = 4.00

Lab report and notes for recordings in area 1

Recordings were performed with particles (bulbshaped candles) in the wave basin for the indicated area.

Recording 1:

Recording starts at still water situation

(Development rip current during first 5 minutes)

Recording 2:

Recording starts at still water situation

Recording 3:

Recording starts at still water situation

Recording 4:

Recording starts approximately 5 minutes after start wave makers.

(development rip current after 5 minutes)

Recording 5:

Recording starts approximately 5 minutes after start wave makers.

Recording 6:

Recording starts approximately 20 minutes after start wave makers.

(it is expected that wave basin induced effects become substantial at this timescale; potentially circulation effects in the wave basin as driving force for the rip current are no longer negligible)

Recording 7:

Recording starts approximately 20 minutes after start wave makers.

Reference recording area 2 for particle tracking with five markers

Figure 3 gives the position of recording area 1 relative to the wave basin by means of the five markers.

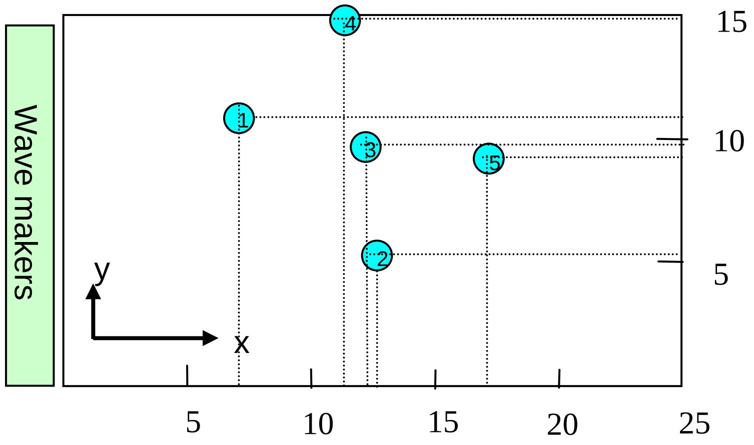

Figure 3: Wave basin with recording area 2

Figure 4 presents the reference image with the five markers in it. Note the applied local coordinate system for the reference recording.

Figure 4: Reference recording area 2 with coordinate system and five markers

The correlation between recording coordinate system and the wave basin coordinate system for the five markers is given in Table 2.

Table 2: Correlation between pixel coordinate system and wave basin coordinate system for markers in reference recording area 2

Reference	Pixel x	Pixel y	Wave basin coordinates	
Mark 1	40	537	X = 7.16	Y = 10.95
Mark 2	698	534	X = 12.87	Y = 5.12
Mark 3	401	296	X = 12.41	Y = 9.74
Mark 4	41	48	X = 11.42	Y = 14.97
Mark 5	706	53	X = 17.05	Y = 9.15

Lab report and notes for recordings in area 2

Recordings were performed with particles (bulbshaped candles) in the wave basin for the indicated area.

<u>Recording 8:</u>

Recording starts approximately 5 minutes after start wave makers.

(14.02 start wave maker, 14.08 start recording, 14.14 accumulation of particles in the wave maker: end of recording)

<u>Recording 9:</u>

Recording starts approximately 5 minutes after start wave makers.

<u>Recording 10:</u> (Wednesday February 2 2005)

Recording starts approximately 20 minutes after start wave makers.

10.29 reference recording still water situation

10.43 start wave makers

11.03 / 04 start recording (bandje voor de lens)

11.09 end of recording (accumulation of particles in the wave maker: end of recording; run out of particles; circulation effects in wave basin)

<u>Recording 11:</u>

Recording starts approximately 20 minutes after start wave makers.

11.50 reference recording still water situation

11.55 start wave makers

12.18 start recording

12.24 end of recording (run out of particles)

Recording 12: (Thursday February 3 2005)
Recording starts at still water situation
11.09 start wave makers, start recording
11.17 end of recording

Recording 13:
Recording starts at still water situation
14.05 start recording
14.18 end of recording

Annex 3 :

Total overview of vertical distribution measurements

Total result of measurements in the rip current with deployment HL LH

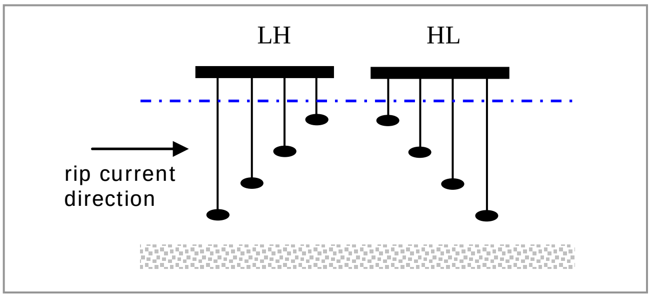

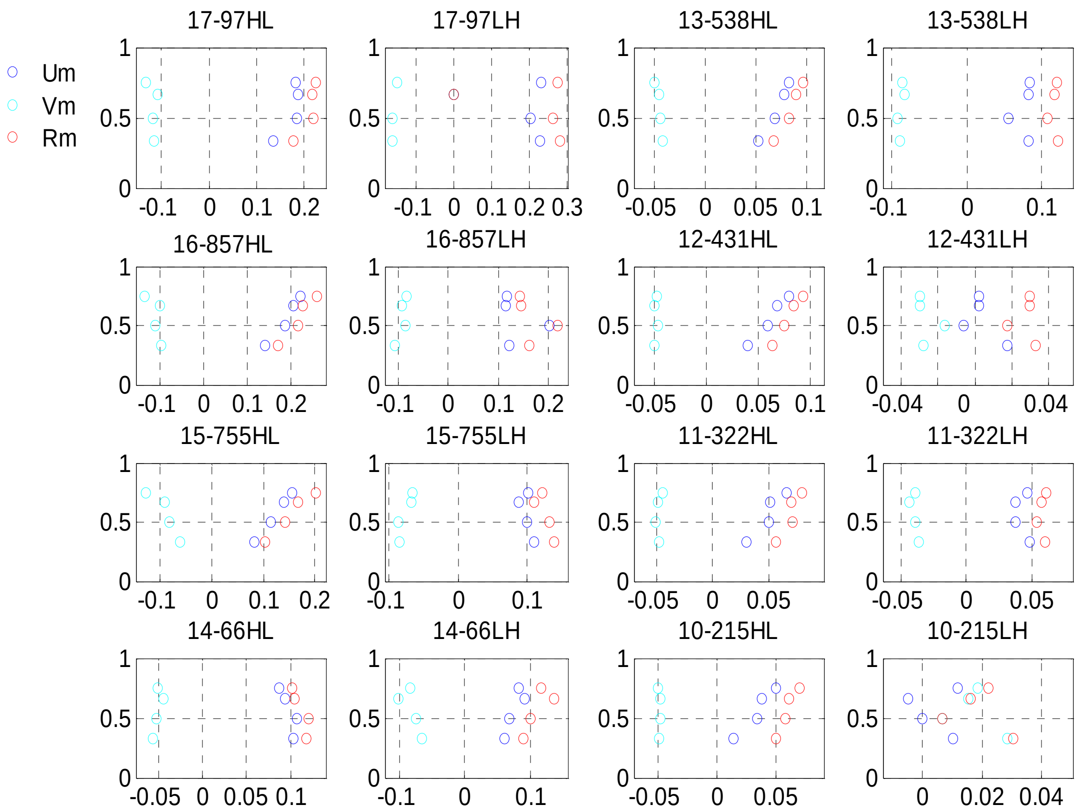

Total result of measurements in the rip current with deployment A B C